



POLITECNICO DI TORINO

Department of Electronics and Telecommunications
Master's Degree in Electronic Engineering

Master's degree thesis

Automatic Test Equipment for Plant Microbial Fuel Cells for Energy Harvesting

Supervisor:

Prof. Crovetto Paolo Stefano

Author:

Alessandro Rizzo

Co-Supervisor:

Prof. Comino Elena

Prof. Musolino Francesco

ACADEMIC YEAR 2018/2019

Abstract

Nowadays the Internet has become essential for everyone. Smartphones and laptops are just few examples but also remote sensors cover a good slice of the devices connected to the network able to exchange information. These sensors are spread in the most disparate environments making their maintenance increasingly difficult and the cost too high. As a consequence, supplying energy to all these devices has become one of the most important and expensive part of their design.

A new possibility to reduce maintenance and to reduce the use of environment dangerous batteries can be to replace them with an alternative sustainable energy source present in situ. One of the most interesting, attractive and fascinating is a bioelectrochemical source that produces energy from the living plants without burn them named Plant Microbial Fuel Cell (P-MFC).

The objective of the thesis is to design an automatic test equipment able to perform an electrical characterization of P-MFCs. This process is fundamental to understand how they works but also to optimize their energy production and extraction through the design of a dedicated energy harvester. It has been carried out in its entirety in DIATI department at the Politecnico di Torino using a system based on Raspberry Pi board. The main challenges are the circuit design and the management due to the very low current and voltage values.

A preliminary analysis involves a quick literature review of the P-MFC state-of-art regarding its structure and its internal mechanisms, and the high-level block scheme definition of the sensing system. Then a complete description of each block is provided also for their design. Afterwards, the sensing system is realized in practice on a PCB and the calibration and verification operations are carried out in order to test its correct behavior. Finally, it is connected to the P-MFC and, performing different analysis, an electric model of the energy source can be extracted.

The C language is used to program the Raspberry Pi board. The software used for the management is MATLAB®, although LTSpiceIV® is exploited as well in the design phase.

Ringraziamenti

Davvero molte persone hanno permesso il completamento di questo lavoro con il loro supporto morale e tecnico e, anche se vorrei menzionarli tutti, sicuramente dimenticherò qualcuno nella lista. Tuttavia, desidero esprimere la mia sincera gratitudine in particolare:

- alla mia famiglia, a mio padre Bruno, a mia madre Marina e a mia nonna Cesira, per il loro supporto e per aver creduto in me incondizionatamente durante tutta la mia carriera universitaria. Grazie davvero;
- ad una persona molto speciale, Veronica, per essere stata la luce nei momenti più duri e bui dei miei studi universitari e soprattutto della vita;
- ai miei migliori amici Giglio e Marco con i quali ho condiviso gioie, dubbi e dolori sin da quando eravamo bambini;
- ai miei professori Prof. Stefano Crovetto e Prof. Francesco Musolino, per la loro costante guida durante questo progetto complesso ma allo stesso tempo anche molto stimolante;
- alla professoressa Prof. Elena Comino per avermi proposto questo interessante argomento di tesi dal quale ho imparato molto e inoltre per il continuo supporto non soltanto tecnico ma anche morale durante le difficoltà;
- a tutti i ricercatori del dipartimento DIATI, in particolare a Giada, Laura e Paolo, per aver condiviso questi mesi a stretto contatto giornalmente durante il mio lavoro.

Contents

1	Introduction	1
1.1	Problem statement	1
1.1.1	Replace batteries with plant microbial fuel cells	2
1.1.2	Current and prospective applications of P-MFC as energy source of IoT nodes	3
1.2	Research objectives, methodology	5
1.2.1	P-MFC characterization	6
1.2.2	P-MFC energy harvester	7
1.3	Thesis outline	9
2	State of art of P-MFC	11
2.1	Bioelectrochemical systems hierarchy	12
2.1.1	Microbial electrolysis cell	13
2.1.2	Microbial fuel cells	13
2.1.3	Microbial solar cells	14
2.2	Plant Microbial Fuel Cell	15
2.2.1	Structure of a P-MFC	16
2.2.2	Internal mechanisms of a P-MFC	17
2.2.3	Losses in a P-MFC	19
2.3	Environmental parameters	20
2.3.1	Temperature	21
2.3.2	Humidity	21
2.3.3	Light intensity	22
2.4	Analysis of a P-MFC	22
2.4.1	Static analysis	22
2.4.2	Dynamic analysis	24
3	Ad-hoc automatized sensing system: hardware	29
3.1	Electronic load and design	32
3.1.1	Constant current source with operational amplifier	32
3.1.2	Constant current source without operational amplifier	33

3.1.3	Constant current source with parallel resistances	35
3.1.4	Constant current source with series resistances	37
3.2	Temperature sensing and design	48
3.2.1	DHT22 - Air temperature and humidity sensors	48
3.2.2	LM335 - Temperature sensors	49
3.2.3	LM35 - Temperature sensors	49
3.3	Humidity sensing and design	51
3.4	Light intensity sensing and design	54
4	Ad-hoc automatized sensing system: software and test	59
4.1	Raspberry Pi interface	60
4.2	Firmware on the Raspberry Pi	63
4.2.1	Measurement algorithm	64
4.3	User interface application	70
4.3.1	Use of the application	71
4.3.2	Calibration	76
4.4	Test of the sensing system	81
4.4.1	Circuit design	81
4.4.2	Static analysis	84
4.4.3	Dynamic analysis	85
5	P-MFC in practice	93
5.0.1	PCB of the electronic load board	93
5.0.2	System connections	95
5.0.3	Moisture sensor problem	97
5.0.4	Plant description	97
5.1	Carex Morrowii - Gregory	99
5.1.1	Plant structure	99
5.1.2	Open circuit voltage measurements	100
5.2	Carex Hachijoensis - James and Jason	103
5.2.1	Plant structure	103
5.2.2	Open circuit voltage measurements	104
5.2.3	The absence of the membrane	104
5.2.4	Waterlogged condition	105
5.3	Carex Hachijoensis - Loria	110
5.3.1	Plant structure	110
5.3.2	Negative voltages with electronic load board	111
5.3.3	Current range identification	112
5.3.4	Environment influence	113
5.3.5	Static analysis	114
5.3.6	Dynamic analysis	116

5.3.7	The need of the plant	117
6	Conclusions	123
6.1	Summary	123
6.2	Results	125
6.3	Future prospective and applications	126
6.3.1	Possible future P-MFC researches	126
6.3.2	Electronic circuit improvements	127
6.4	Applications	130
A	Schematic, PCB layers, 3D viewer and prototype	133
B	User interface application and Raspberry Pi algorithm: code	137
B.1	User interface application: main functions	137
B.2	Raspberry Pi algorithm: main function	146
	Bibliography	151

Introduction

1.1 Problem statement

Nowadays, one of the most interesting engineering technology fields is the Internet of Things (IoT). *"I'm fairly sure the phrase "Internet of Things" started life as the title of a presentation I made at Procter & Gamble (P&G) in 1999"*: this was the sentence pronounced by Kevin Ashton in 2009 for RFID Journal [1] where he explains where this name comes from. The IoT is a neologism used to name real objects connected to the internet. The definition is quite tricky because they have been defined in several different ways so far. With the Internet of Things, one indicates a set of technologies that allows to connect to the Internet any type of electronic device. The purpose is essentially to monitor, control, transfer information from the physical world and then carry out consequent actions.

Final user is able to receive information on a device connected to Internet through the gateways (or concentrators) from some sensors which monitor the physical world (Figure 1.1). The connection between the external world and gateways is the IoT node. IoT nodes are devices able to perform sensing and interact with the world. The most attractive aspect is that

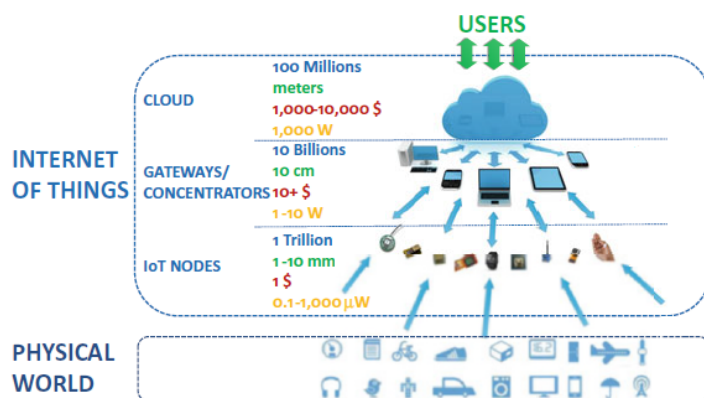


Figure 1.1: A simplified architecture of the IoT [2]

they can be used anywhere for whatever application [2, p.20]: from agriculture to consumer products, automotive, healthcare either also in manufacturing or supply chain (e.g. Industry 4.0), smart environments from homes to buildings thanks to the extreme miniaturization of the integrated systems (expected form factor in the scale of millimeters). Other important characteristics are their autonomy in functionality and energy with very low cost (cost target in 1 \$ range). They usually have a very long lifetime e.g. decades using small batteries.

1.1.1 Replace batteries with plant microbial fuel cells

The idea is to replace batteries using an alternative sustainable energy that does not damage the environment. In 2008 in the sub-department of Environmental Technology at Wageningen University [3] it was demonstrated the possibility to produce non destructive and sustainable bio-electricity with the so called Plant Microbial Fuel Cell (P-MFC) [4] [5]. P-MFC (Figure 1.2) is a system based on Microbial Fuel Cell concept employing plants and bacteria to produce energy. It differs from the others bioelectrochemical systems since the majority of the organic matter is actively produced by the system itself, in situ.

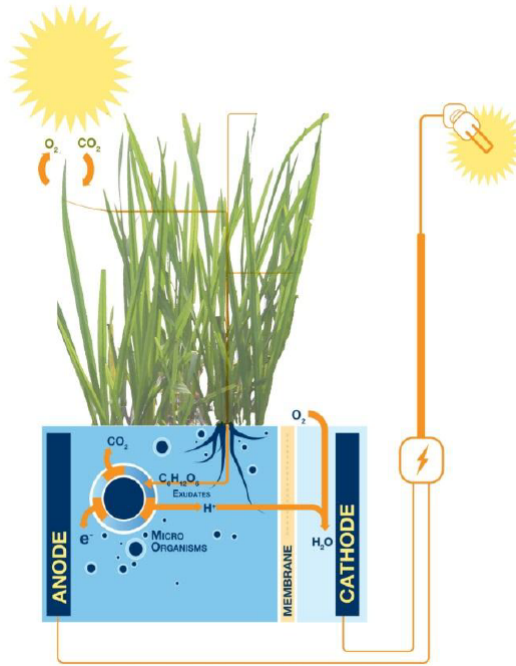


Figure 1.2: Basic structure of P-MFC [6]

The IoT nodes can be self-powered by the energy harvested from the plant without using any kind of external battery. They have the possibility to be placed where

it is difficult to get there so the fact that they are self-powered create an huge advantage in maintenance. It is not a limited technology because several species of plants can be used such as reed sweetgrass, cordgrass, rice, tomatoes, lupines, algae and so on.

1.1.2 Current and prospective applications of P-MFC as energy source of IoT nodes

With the increasing of the pollution during the last decades, governments start to invest in green energy even inside the cities: the Senseable City Lab of the MIT in Boston developed Treepedia [7] that is a website to compute the Green View Index in the big cities of the planet. In the elaborated ranking, the only Italian city present is Turin (Figure 1.3).

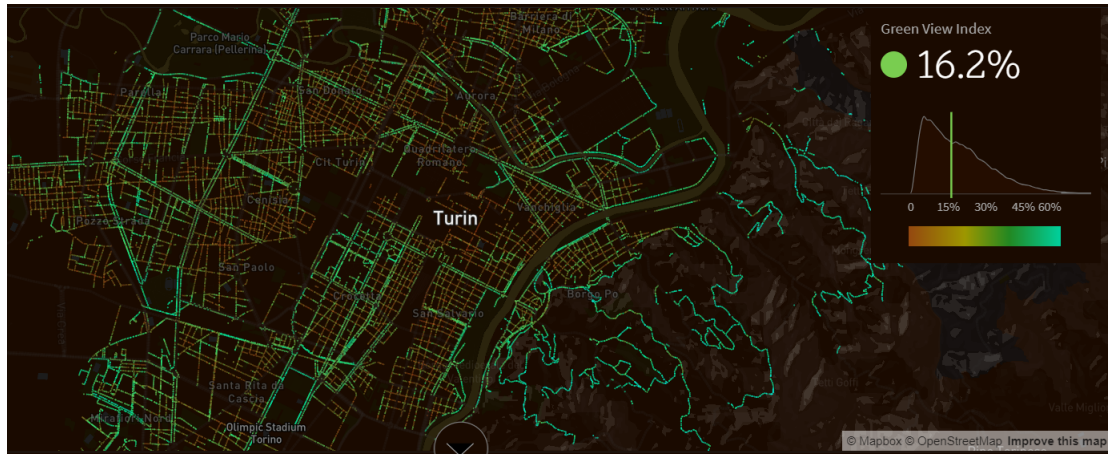


Figure 1.3: Green View Index of Turin in February 2019 [7]

Exploit all this green area not only to improve the air quality but also to provide energy to some device could be a smart idea. The electrical energy produced can be harvested to feed several kind of IoT nodes. The use of the P-MFC to feed sensors can be applied in several fields: agriculture, woods, smart cities and so on (Figure 1.4).

According to the California Department of Forestry and Fire Protection, the 2018 was the most destructive wildfire season on California with a total of 8527 fires burning an area of 1 893 913 acres which has caused more than \$3.5 billion in damages [8]. They broke out mostly during the warmer and drier periods of the year and also due to the strong wind, the fire continues to spread very quickly. To prevent or at least limit the damages, the idea is a continuous monitoring of that area by using sensors feed by these natural plants. The plants provides

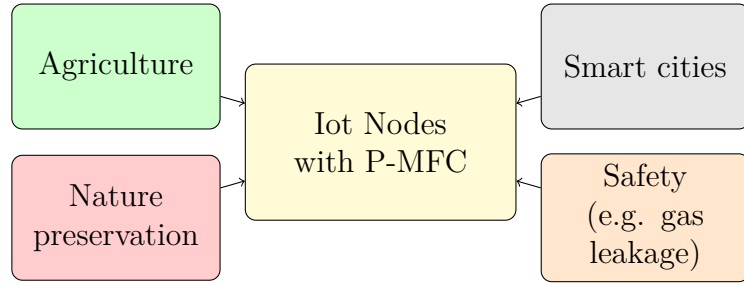


Figure 1.4: Possible fields application for the use of IoT with P-MFC

energy for their whole life therefore avoiding the need to replace the discharged batteries. They can monitor in real-time the presence of fire through some sensors scattered in areas most at risk and notice helping to intervene immediately alerted. Prevention is essential. In the areas of wildlife and nature preservation, their use can be important to monitor also the quality of available natural resources (e.g. water), their level pollution, earthquake early detection and counteraction of illegal activities against wildlife [2].

Another example could be in the agriculture sector. The north of Italy is full of rice and corn fields. The banks of the rivers are full of plants which are useful from the structural point of view as well. Why they can not be used also to harvest energy for sensors that monitor air pollution, the need to irrigate a field and so on. In the last decades, the technologies has entered forcefully in agriculture and the use of these sensors spread on the countryside can further improve their management. The IoT can monitor the quality, the actual usage and the availability of resources for better management (e.g. irrigation) and storage (e.g. avoid waste of feed and fertilizing). Monitoring the environmental conditions permits to support growth of animal and plants (e.g. aquaculture).

Remaining in Italy, the Alps are full of beautiful woods. They can produce energy that can be harvested to connect several sensors to monitor for instance the temperatures and the climate changes but also to monitor the earth vibration that can cause avalanches.

Inside houses there are a lot of small ornamental plants which can have double duty: not only decorative but also safety monitoring water or gas leakage so minimizing the human and material losses in case of emergency. Another home use can be the sensing of the solar light and adjusting automatically the light spread in the garden. Gardens needs to be irrigated periodically and, with this technology, this process can be automatized not only periodically but also when it needs: a humidity sensor can monitor the presence of water in the soil and decide when irrigate it. The maintenance of a fancy and health garden could be easier.

In an office or in a university, the maintenance of the green could be simplified

in this way. An interesting example is the University of Wageningen using plants to produce green electrical energy [9]. On campus the roof of the NIOO-KNAW building [10] can both store water and regulate the temperature of the building below and can even supply electricity through the plants on the roof (Figure 1.5).



Figure 1.5: Wageningen university, campus NIOO-KNAW building roof [10]

1.2 Research objectives, methodology

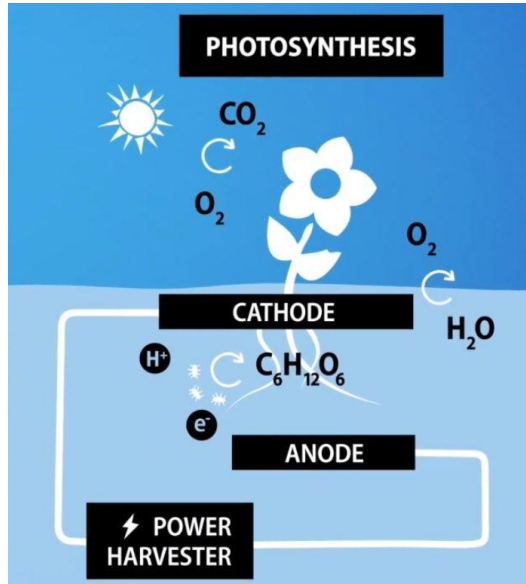


Figure 1.6: Schematic overview of a Plant Microbial Fuel Cell [11, p.93]

The IoT nodes are preferred to operate autonomously mainly for reliability, maintenance and cost aspects. The use of an ambient environmental energy source such as the P-MFC reduces the system volume whereas batteries can be too bulky for them. In addition, a battery can only store a limited amount of energy and thus requires frequent recharge. Due to aging effect, after a certain number of recharges, a battery has to be replaced. With countless nodes in the network, maintenance cost can be formidably high. The harvesting of renewable energy eliminates battery replacement cost and is environment friendly. The technology studied is the P-MFC. The Figure 1.6 shows the structure of a P-MFC system. The system is composed by two electrodes

(cathode and anode) separated by a membrane [4]. Anode and cathode are the P-MFC terminals to connect some external devices. During its life cycle, the plant releases through the radical system in the soil organic compounds such as sugar and amino acids. The electroactive microorganisms present naturally in the soil, oxidize them producing electrons, protons and CO_2 . The microorganisms, under anaerobic condition, are the responsible for deliver the electrons into the anode surface. The electrons and protons reach the cathode where react together reducing the oxygen present at the cathode. The electrons pass through the external circuit while the proton through the membrane [5].

1.2.1 P-MFC characterization

Before to use them as a power source, they have to be characterized in order to better understand how they work and which are the effects related to internal phenomena [4]. The most interesting parameters are voltage and current provided by the P-MFC from which the power delivered can be computed. The electrical conditions can be set by connecting at the plant an electronic load [12] [13] and measures both voltage and current of the plant (Figure 1.7). The characterization

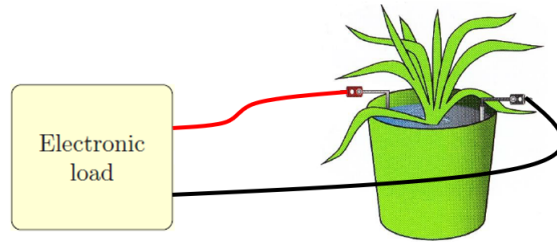


Figure 1.7: Connection of the electronic load to P-MFC

allows to find the conditions to maximize its output power so to increase the efficiency of the system. In contrast to a battery powered system, a self-powered device deals with a much unstable energy source that is sensitive to ambient environment so the characterization process has to take into account a lot of influence quantities like the temperature, soil humidity, solar light, health state of the plant and so on (Figure 1.8). These environmental parameters are often measured with different instruments. Voltage and current are strongly dependent from a lot of parameters: for example the solar light increase the power production due to the plant growth while a reduction of temperature can cause the decreasing of the available power [11, p.86].

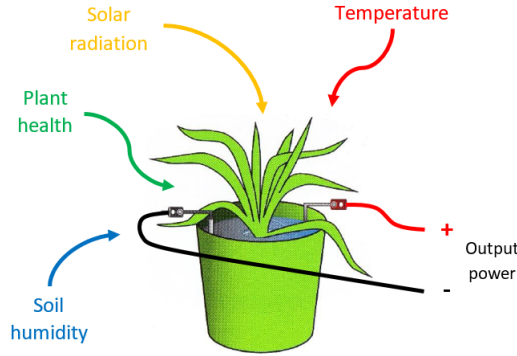


Figure 1.8: Environmental parameters acts like influence quantities on the P-MFC

1.2.2 P-MFC energy harvester

The load is never connected directly to the P-MFC but is added an power management system able to extract the energy from the renewable source and convert it into electronic format (Figure 1.9). The voltage of a single P-MFC is usually no

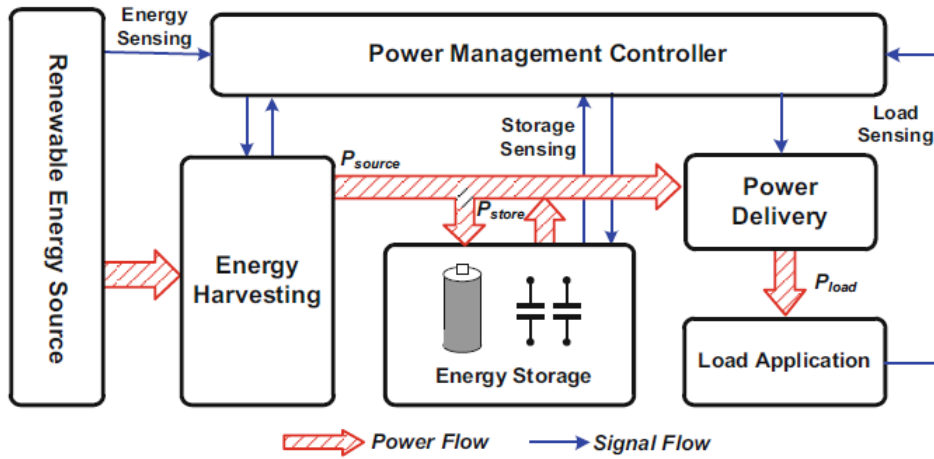


Figure 1.9: Power management system block diagram for self-powered device [2, p.288]

more than 1 V [6] [14, p.7] [15, p.4] [16, p.30] so the power management system has to increase the voltage up to a compatible one (boost converter is a possible implementation [14] [15]) for the sensors. Hence, an energy harvesting module becomes an essential part of power management system. The duty of the harvester is to collect the energy from the plant, store and then deliver it to power small sensors.

Since the the operation conditions of both energy source and load vary continuously, the energy storage is used as an energy buffer: when the harvested power is greater than the load power, the excessive power is stored for future use. Typical power density available from a plant microbial fuel cell is in the order of few $\frac{\mu\text{W}}{\text{cm}^2}$ (area referred to the electrodes one). A complete characterization allows to design the energy harvester making it works in the point of maximum production of energy MPP (Figure 1.10) increasing the efficiency and allowing so the connection of a wider range of IoT nodes. Because of the high diversity of energy forms and har-

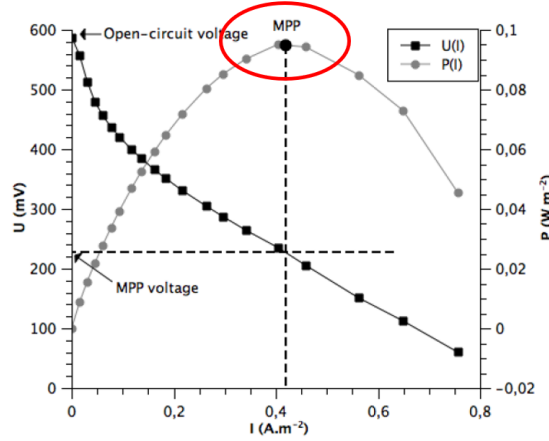


Figure 1.10: Example of experimental polarization and power density curves normalized to the cathode area of a P-MFC highlighting the maximum power point (MPP) of the system [16, p.30]

vesting transducers, harvesting methods can be different: maximum power point tracking (MPPT) techniques [17] are highly popular for photovoltaic solar energy harvesting, while resonant frequency and impedance matching schemes are common for piezoelectric energy harvesting [18]. The polarization and power curves are usually expressed in function of the current per area ($\frac{\text{A}}{\text{m}^2}$) and never absolute value. This allows the comparison between different graphs taking into account of the environmental conditions as well.

Duty cycling operation of IoT node

Meeting power budgets of few μW or below is feasible only if the IoT node actively performs tasks (e.g., sensing, processing) only infrequently. The power needs to be aggressively reduced by duty cycling the IoT node operation, alternating active tasks and long sleep periods with periodicity set by the wake-up cycle T_{wakeup} as shown in Figure 1.11. During the active phase, the IoT node works and consumes

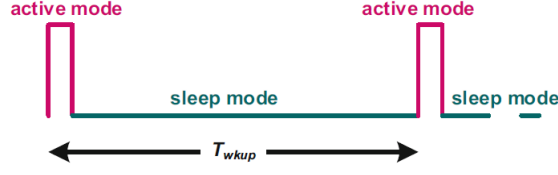


Figure 1.11: Usual schedule working of IoT nodes: short active mode and long sleep mode [2, p.10]

harvester power P_{IoT} while during the long sleep mode, the energy E_{SLEEP} is harvested from the P-MFC and the IoT nodes does not work. The average IoT node power \bar{P} can be computed in function of the wake-up cycle T_{wkup} :

$$\bar{P} = P_{\text{IoT}} + \frac{E_{\text{SLEEP}}}{T_{\text{wkup}}}$$

The complete characterization of the power source (i.e. P-MFC) helps to optimize the design of the energy harvester which allows to store the maximum electrical energy. Higher the energy, either larger could be the active mode or higher number of IoT nodes can be connected concurrently. The thesis is focused on how the characterization of the P-MFC can be performed with a low-cost automatized electronic device and with methods are used nowadays.

1.3 Thesis outline

The thesis starts (**Chapter 1 Introduction**) with a description of the system under test (P-MFC) and making different examples on the possible applications of this energy source connected to an IoT node. The P-MFC technology is explored pointing out the structure, which are the most interesting parameters for its characterization and how to connect the sensing system. Hereafter, the characterization will be useful to design the power management system able to extract energy from P-MFC to feed some IoT nodes. The node works infrequently due to the limited amount of power delivered by the P-MFC. The second chapter (**Chapter 2 State of art of P-MFC**) explains the derivation of the P-MFC in the bioelectrochemical systems hierarchy. The structure of P-MFC and the internal mechanisms are described in details. The P-MFC can be seen as a black box and in order to characterize the system, different analysis can be performed: study the steady state conditions (static analysis) but also understand how the system reacts to a change between steady states so study the transient characteristics (dynamic analysis). The static analysis fixes a limited number of point on the polarization curve to determine the static parameters while for the dynamic

one the electrochemical impedance spectroscopy with white noise is employed that allows to derive an equivalent electronic circuit (electrical model of the P-MFC). At the end of the chapter, a brief discussion is presented exhibiting the importance of the measurement of the environmental parameters for results comparison and to understand the internal mechanisms as well. The analysis are performed measuring the electrical parameters (voltage and current) of the plant. The third chapter (**Chapter 3 Ad-hoc automatized sensing system: hardware**) shows different electronic circuits to perform these analysis. A section shows also the passages to design the circuital solutions. The system is able also to measure the environmental parameters through sensors. The sections showing the sensors contain also the design procedure of each conditioning circuitry. The idea to make the use of the sensing system easier and automatized is to create an user interface. It is described in the detail in the fourth chapter (**Chapter 4 Ad-hoc automatized sensing system: software and test**). It describes the algorithm to manage the sensing system but also how to use the graphical interface. The sensing system has to be subjected to a calibration process initially but also periodically so when the calibration period is elapsed. The last part of this chapter shows how the whole sensing system is tested replacing the P-MFC with a known 1-time constant electronic circuit to evaluate the quality of the results. Once the correctness is verified, the P-MFC can be connected to the sensing system. The fifth chapter (**Chapter 5 Results of P-MFC measurements**) shows first the procedure to build the P-MFC trying also some experimental idea as for example the removal of the membrane. The rest of the chapter shows experimental results of static and dynamic analysis on different P-MFCs which contain the same type of plant. At the end of the thesis (**Chapter 6 Conclusions**), there are some considerations about the work done, the difference between the expected and the obtained results and the possible improvements applying also other kind of analysis to find out further results.

Chapter 2

State of art of P-MFC

This chapter describes in detail the state of art of a Plant Microbial Fuel Cell (P-MFC). It is important to understand its derivation starting from bioelectrochemical systems passing through the microbial fuel cells and the microbial solar cells as shown in Figure 2.1.

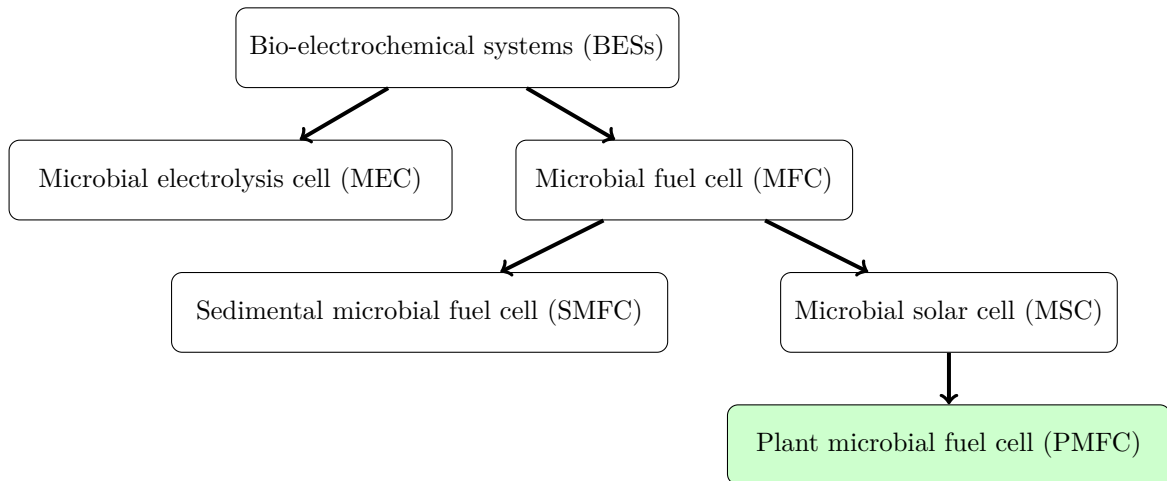


Figure 2.1: Basic scheme of the system

The P-MFC will be studied in details talking about its structure composed by the cathode, anode and membrane but also the mechanisms involved in energy production are interesting to be analyzed. The plant uses photosynthesis to produce organic carbon which are used by the microorganisms present in the soil to produce electrons and protons. Their presence allows the flow of an electrical current through an electrical load connected between cathode and anode. Figure 2.2 shows graphically this process. Further considerations must be done also related the environmental parameters e.g. the air temperature and the soil humidity and

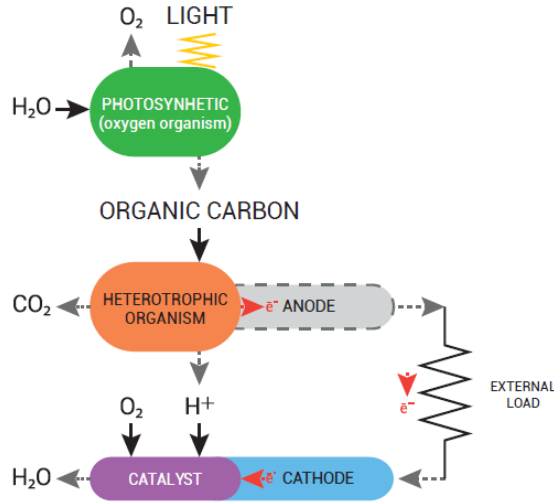


Figure 2.2: Illustrative diagram of P-MFC system [5]

which is their effect on the energy production of the P-MFC. Since the purpose of this thesis is the characterization of a P-MFC energy harvester, a section shows the state of art of different kind of analysis used to understand the behavior and which are the optimal conditions to increase the energy efficiency. Initially the P-MFC can be seen as a black box that is able to convert chemical into electrical energy (Figure 2.3) but after its characterization it can be model from an electrical point of view.



Figure 2.3: Schematic representation of energy conversion of a P-MFC

2.1 Bioelectrochemical systems hierarchy

Bioelectrochemical systems (BESs) are systems capable of converting chemical energy into electricity and viceversa while employing microbes as catalysts [5, pp. 18-19]. Microbes, inoculated or naturally present into the system, metabolise organic waste transforming it in electric current. The BESs are still technologies

under development and they are not use on a large-scale but they give the possibility to produce energy from the environment without affect it. The hierarchy of BESs is shown in Figure 2.1. BESs are divided in two main groups: microbial electrolysis cells and microbial fuel cells.

2.1.1 Microbial electrolysis cell

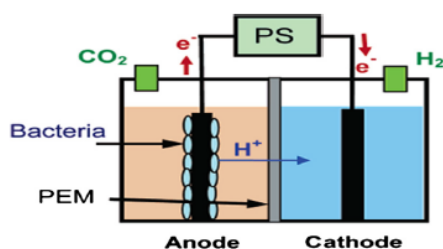


Figure 2.4: MEC schematic [19, p.430]

The microbial electrolysis cells (MECs) were discovered in 2005 by two independent research groups, one at Penn State University and the second at Wageningen University in the Netherlands [19]. They are a promising approach for hydrogen production from organic matter, including wastewater and other renewable resources. The production of hydrogen or methane is obtained applying electric current to an organic compound (Figure 2.4).

2.1.2 Microbial fuel cells

The microbial fuel cells (MFCs) are a particular fuel cell designed to extract energy from an organic compound present in the substrates by the help of microorganisms (Figure 2.5). The MFC setup is characterized by two electrode chambers separated by a proton exchange membrane (PEM [21]). The two chamber are named anodic and cathodic and are respectively the negative and the positive pole. The anodic chamber contains the electrochemical active bacteria that oxidase carbon or organic/inorganic matter and release protons and electrons. Both will go into the cathodic chamber with a different path: the protons pass through the membrane while the electrons through the external circuit driven by the electrical potential difference between the two poles. In the cathode chamber, protons

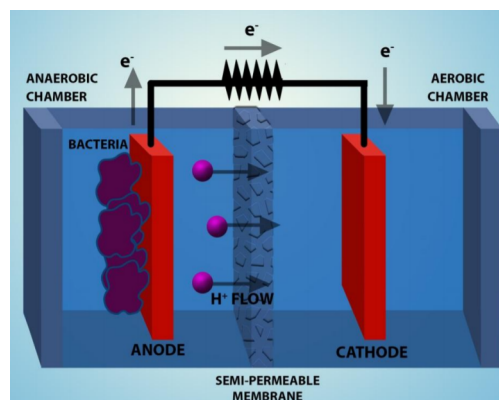


Figure 2.5: Time response to a load-resistance step for P-MFC [20, p.181]

and electrons react with the oxygen (present in the air) closing the electrical circuit and releasing water. Two subgroups of MFC are the sedimental microbial fuel cells and the microbial solar cell.

2.1.3 Microbial solar cells

The microbial solar cells (MSCs) [22] are the collective name for biotechnological systems that make use of phototrophic microbes or higher plants to entrap solar energy which is further utilized by electroactive bacteria to generate in situ electric current (Figure 2.6).

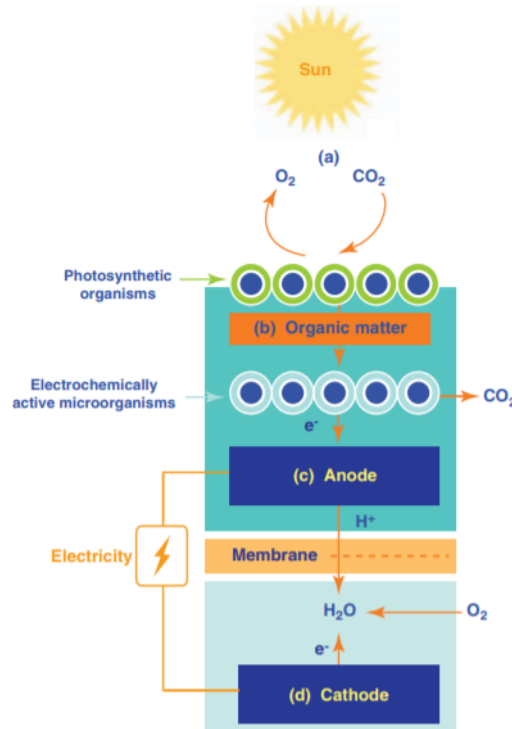


Figure 2.6: . Model of a microbial solar cell including the basic principles. [22, p.42]

Depending on the way the solar radiations are harvested and the organic compounds are transformed, it's possible to distinguish three kinds of MSCs: MSCs with phototrophic biofilms, MSCs photobioreactors [23] and Plant microbial fuel cell. The MSCs with phototrophic biofilms use a self-organizing biofilm on the anode surface of a fuel cell. The MSCs photobioreactors use photosynthetic organisms such algae to harvest the solar energy. The P-MFCs use higher plants to harvest the solar energy.

2.2 Plant Microbial Fuel Cell

The plant microbial fuel cells (P-MFCs) [24] are the most investigated between MSCs. They give the possibility to produce energy from living plants without burn them. P-MFC (Figure 2.7) aims to transform solar radiation into green electricity in a clean manner employing plants and bacteria to produce energy. Differently from the other BESs, the majority of the organic matter, from which the energy is generated, is actively produced by the system itself.

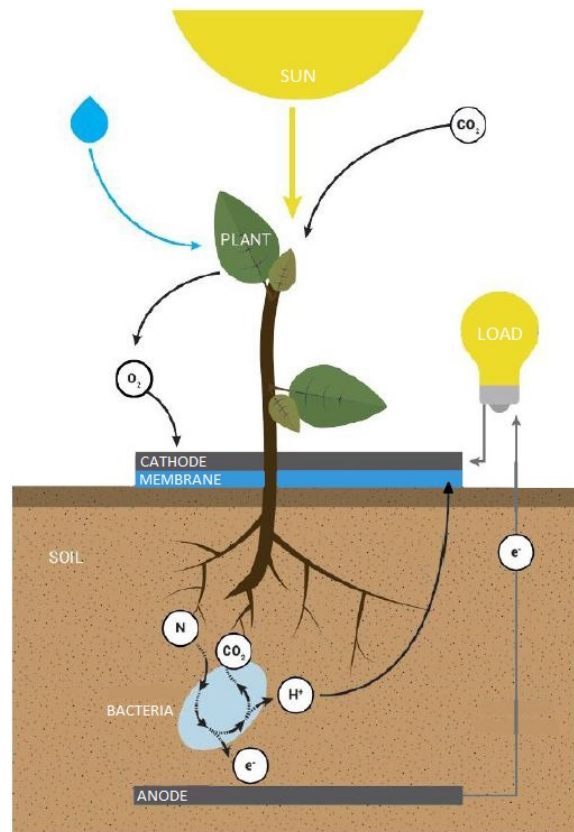


Figure 2.7: P-MFC structure

The main processes at the base of this technology are:

- photosynthesis
- transport of organic matter to anode compartment
- anodic oxidation of organic matter by electrochemically active bacteria
- cathodic reduction of oxygen

Photosynthesis allows to extract the nutrients that the plant needs to live. Not all the nutrients are used and part of these like sugar and amino acids are then expelled into the soil through the intact roots as exudates i.e. rhizodeposition. The electroactive microorganisms naturally present in the soil oxidize these substances by releasing electrons, protons and CO_2 . Under anaerobic condition, these microorganisms are responsible for deliver the electrons into the anode surface. Protons reach the cathode passing through the membrane. By connecting an electric load between electrodes, also the electrons reach the cathode and their presence allows the reduction of the oxygen present in it. These mechanisms lead to flow an electric current through the load. In what follows, all the components, the internal reactions and possible losses are explored in details.

2.2.1 Structure of a P-MFC

The P-MFC structure is composed by some main components: the plant and its roots, microorganisms (bacteria), electrodes (anode and cathode) and membrane as shown in Figure 2.7.

Plant and its roots. Usually, in the P-MFC are used plants can grow with their roots under waterlogged conditions: water avoids the oxygen intrusion from the air at the anode chamber. Presence of oxygen cause a lost of electricity production because electrons are directly used for oxygen reduction without arriving at the cathode.

Anode. The electrochemically active microorganisms have been found to be able to deliver electrons to a solid surface like a graphite electrode: the anode. The anode must work under anaerobic conditions and be made by a conductive, biocompatible and chemically stable material. Metal anodes consisting of noncorrosive stainless steel mesh can be utilized so copper is not useful due to the toxicity of even trace copper ions to bacteria. The most versatile electrode material is graphite since it is relatively inexpensive, easy to handle and have a defined surface area.

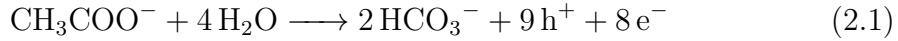
Cathode. The anode is coupled to a second electrode: the cathode. The microorganisms transport the protons at the cathode which are used to reduce oxygen or another compound. Usually, it is placed in contact with the air having to reduce oxygen. The choice of the cathode greatly affects performance so it can varied depending on application. Since the low cost, the cathode is made by graphite as well.

Membrane. The P-MFC requires the separation between the oxidation at the anode and the reduction at the cathode by a membrane. It is a semipermeable membrane designed to conduct only protons while acting as an electrons insulator and reactant barrier i.e. proton-exchange membrane (PEM). PEMs can be made

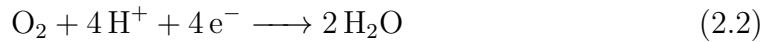
from either pure polymer membranes or from composite ones, where other materials are embedded in a polymer matrix. One of the most common and commercially available PEM materials is the fluoropolymer Nafion. This material is very expensive so other solutions are searched. In this thesis is used PET as membrane material given its low cost.

2.2.2 Internal mechanisms of a P-MFC

In the P-MFC plants can grow with their roots under the soil. The anode is placed under the roots to avoid oxygen intrusion from the air. The non-availability of oxygen at the anode would ensure that electrons will directly used for electricity production and not for oxygen reduction. In the soil the plant releases exudates. They are both rhizodeposits and dead cell material which will be used by the bacteria for electricity production. At the root soil interface organic matter is released by the plant and directly oxidized by the present bacteria. Microbial activity around the roots of a plant is more than 10 times higher than in the rest of the soil [25]. In the P-MFC bacteria break down the organic matter and release electrons. The substrate is composed by a complex mix so, only for explanation, one takes acetate as a model-substrate. The oxidation of acetate by bacteria is [11]:



The electrons released are donated to the anode. This happens naturally because bacteria can gain energy by donating electrons to another compound. Other electron acceptors can interfere with electricity production when it is energetically more attractive for the bacteria instead of the anode [26]. Some alternative electron-acceptors in the anode are oxygen, carbon dioxide, nitrate and sulphate. Oxygen can be by intrusion from the air or actively transported into the soil [27]. Nitrate and sulphate are normally present in plant-grown media for plant nutrition. The anode is coupling with the cathode. The cathode reaction would be oxygen reduction to water [11]:



This is preferably because oxygen is available and cheap. The anode voltage E_{an} can be computed from the Nernst formula [28]:

$$E_{\text{an}} = E_{\text{an}_0} - \frac{RT}{n_A F} \ln\left(\frac{[\text{CH}_3\text{COO}^-]}{[\text{H}^+]^9 [\text{HCO}_3^-]^2}\right) \quad (2.3)$$

where E_{an_0} is the standard anode potential at 0 °C, R the universal gas constant, T the temperature, n_A the number of electrons involved in the reaction, F the Faraday's constant and $[\cdot]$ contains the concentration of the element inside. Protons

reach the cathode by flowing across the membrane creating a net positive charge while the electrons pass through the external circuit creating a current flow. Since the electrons exiting through the anode arriving at the cathode, the current direction is considering positive from the cathode to the anode. The cathode voltage E_{cath} can be computed from the Nernst formula [28]:

$$E_{\text{cath}} = E_{\text{cath}_0} - \frac{RT}{n_C F} \ln\left(\frac{1}{p\text{O}_2 [\text{H}^+]^4}\right) \quad (2.4)$$

where E_{cath_0} is the standard anode potential at 0 °C, n_A the number of electrons involved in the reaction, $p\text{O}_2$ the partial oxygen pressure. The potential of the cell E_{cell} is the difference between the cathode E_{cath} and anode E_{an} potential:

$$E_{\text{cell}} = E_{\text{cath}} - E_{\text{an}} \quad (2.5)$$

The oxygen concentration at the cathode is limited due to the limitation of oxygen diffusion into the electrode. The electrode needs to be wet in order improve the transport of protons. The product between current I_{cell} and voltage E_{cell} leads to the output power P_{cell} of the P-MFC [5, pp. 47-48]:

$$P_{\text{cell}} = E_{\text{cell}} \cdot I_{\text{cell}} \quad (2.6)$$

The theoretical maximum cell potential is higher than the measured one due to the internal losses of the P-MFC due to the cathode, anode and membrane resistance and current dependent losses.

Numerical example.

To better understand some possible voltage and power ranges of a P-MFC, a numerical example with typical values is performed. The physical constants are the universal gas constant $R = 8.314 \frac{\text{J}}{\text{mol}\cdot\text{K}}$, the Faraday's constant $F = 9.65 \cdot 10^4 \frac{\text{C}}{\text{mol}}$. The number of electrons involved in the reaction at the anode is $n_A = 8$ (from reaction 2.1) while at the cathode is $n_C = 4$ (from reaction 2.2). The typical values are taken from [28, p. 452] with concentrations $[\text{CH}_3\text{COO}^-] = [\text{HCO}_3] = 10 \text{ mM}$ and $[\text{H}^+] = 1 \text{ mM}$, temperature $T = 25^\circ\text{C}$, partial oxygen pressure $p_{\text{O}_2} = 0.2 \text{ bar}$. From [28, p. 452] are taken the typical values of standard anode potential $E_{\text{an}_0} = -0.289 \text{ V}$ and standard cathode potential $E_{\text{cath}_0} = 0.805 \text{ V}$ with standard hydrogen electrode. Now it is possible to compute the anode potential from equation 2.3:

$$E_{\text{an}} = -0.289 \text{ V} - \frac{8.314 \frac{\text{J}}{\text{mol}\cdot\text{K}} \cdot 298.5 \text{ K}}{8 \cdot 9.65 \cdot 10^4 \frac{\text{C}}{\text{mol}}} \ln \left(\frac{10 \text{ mM}}{(1 \text{ mM})^9 \cdot (10 \text{ mM})^2} \right) = -0.504 \text{ V}$$

and the cathode potential from equation 2.4:

$$E_{\text{cath}} = 0.805 \text{ V} - \frac{8.314 \frac{\text{J}}{\text{mol}\cdot\text{K}} \cdot 298.5 \text{ K}}{4 \cdot 9.65 \cdot 10^4 \frac{\text{C}}{\text{mol}}} \ln \left(\frac{1}{0.2 \text{ bar} \cdot (1 \text{ mM})^4} \right) = 0.617 \text{ V}$$

The potential of the cell can be computed from equation 2.5

$$E_{\text{cell}} = 0.617 \text{ V} - (-0.504 \text{ V}) \approx 1.1 \text{ V}$$

Supposing to have a maximum current provided by the P-MFC $I_{\text{MAX}} = 500 \mu\text{A}$ [5, p.83], from the typical polarization curve of Figure 1.10 the MPP is approximately in the middle of the range for both current and voltage so the maximum power P can be computed from equation 2.6:

$$P_{\text{cell}} = \frac{1.1 \text{ V}}{2} \cdot \frac{500 \mu\text{A}}{2} = 275 \mu\text{W}$$

These considerations are made with an ideal case because the internal losses reduce the maximum output power of the system.

2.2.3 Losses in a P-MFC

Until this point, the P-MFC is described as an ideal system. Within a real P-MFC, a number of losses impede its proper operation. These can be divided into voltage drops and current drops as described in [29].

Voltage losses [16, p.33]

Bacteria capture a fraction of the energy content of the substrate for their growth and maintenance. This cause a voltage reduction because bacterias are activating the reaction at the anode i.e. activation drop, that also includes phenomena at the cathode. These are caused by the necessity to have a local potential difference, overcoming energy barriers, before a reaction takes place at the surface of both electrodes. A portion of the voltage generated is lost in initiating the chemical reactions that transfer the electron to or from the electrode. This voltage drop is highly non-linear. The ohmic drop is the linear resistance due to the flow of electrons through the material of the electrodes and the various interconnections. This voltage drop is essentially proportional to current density so it can be model as a resistance. The concentration drop results from the change in concentration of the reactants at the surface of the electrodes as the fuel is used. Concentration drops are amplified for high current densities, when the reactants are consumed at high rates at the surface of the electrodes.

Current losses [16, p.34]

In an ideal P-MFC, the anode is the unique electron acceptor available to bacteria for the oxidation of the substrate. In practice however, a fraction of electron may well migrate to the cathode through the membrane or react with alternative electron acceptors like oxygen and non-organic oxidants. In the absence of viable electron acceptor, some bacteria are able to develop fermentative metabolism pathways. The current drops are inversely proportional to the attraction of the anode that is itself correlated to its potential: when the P-MFC is in short-circuit condition, the potential of the anode is close to the potential at the cathode thus the anode is strongly attractive. Bacteria will mostly use the anode as an electron acceptor. Other comparatively strong alternative electron acceptors such as diffused oxygen will divert electrons. On the contrary, when the P-MFC is in open-circuit, the anode does not attract any electrons, and bacteria are more likely to select alternative electron acceptors, in the order of diffused oxygen, non-organic acceptors, and eventually also fermentation.

2.3 Environmental parameters

Afterwards the detailed description of a P-MFC, test conditions must be analyzed. Environmental conditions are very important because they dramatically influence the P-MFC performance so their measurement is fundamental. If they are not fully documented, the comparison between performance of different P-MFCs would be meaningless. The most important environmental parameters are the temperature,

humidity and solar radiation intensity. All these parameters can be useful in post-processing analysis to make some consideration to better understand how they affect the performance.

2.3.1 Temperature

Temperature largely influences electrical characteristics of a P-MFC [30]. An increasing of temperature improves performance due to higher kinetic and conduction processes. More precisely, in a P-MFC the discharge of rhizodeposition is directed by the temperature causing voltage and current fluctuation. The low temperature, as during the winter, leads to a decrease in electricity production or also no production during frost periods. The most trivial reason could be that some plants are not able to survive winter due to freezing of the roots. Another reason is that, during frost period, the water in the soil is frozen and ions can no longer be transported [31] [32]. Freezing symptoms involve also membrane disruption. Freezing air-temperatures are less damaging to the plant because it produces chlorophyll inhibition but generally leads to survival of the roots and rhizomes and will lead to regrowth when the temperature rises. The anode potential of the P-MFC is most influenced by temperature, leading to a decrease in electricity production during low temperature periods [11]. Cold insulation of the anode as well as selection of cold-resilient species are possibilities for increasing plant survival over winter. The concept is: the higher the temperature, the lower the anode potential so higher cell potential. Temperature can affect also the biofilm formation and the conductivity.

2.3.2 Humidity

Humidity plays an important role in the growth of the plant. High humidity causes the prevalence of various phytopathogens in plants [33]. Different studies reported a very slight effect of humidity in voltage generation at an initial stage with almost no difference once the plants start blooming. Moreover, humidity also affects the microbial metabolism. In addition to the effect of humidity on plant and microbes, its effect on electrode materials and conducting wire should also be interesting to study. Humidity effect would be more pronounced in the cathode aerobic region which absorbs atmospheric oxygen easily. The [34] suggest that the control of humidity in the cathode region promotes the long-term operation of a P-MFC. The presence of water in the soil allows to sufficiently help the current supply. Increasing flow usually improves performance.

2.3.3 Light intensity

The plant in the P-MFC uses the solar radiation from the sun to live i.e. photosynthesis. The variation during the day can affect the performance of the fuel cell. With an higher solar radiation, the photosynthesis process is stronger and it can lead to more exudation thus an increasing in energy production [11]. The potential at the cathode can have fluctuation with an indirect relationship with respect to the light intensity: plant produces oxygen during day and consume oxygen during night [35], thus inducing oxygen fluctuations available at the cathode for its reduction.

2.4 Analysis of a P-MFC

Now that the internal mechanisms of P-MFCs are presented, this section describes a P-MFC as a black box that converts the chemical energy from the reactants (i.e. organic matter and oxygen) into electrical as depicted in Figure 2.8. This conversion is studied in terms of static and dynamic electrical characteristics.

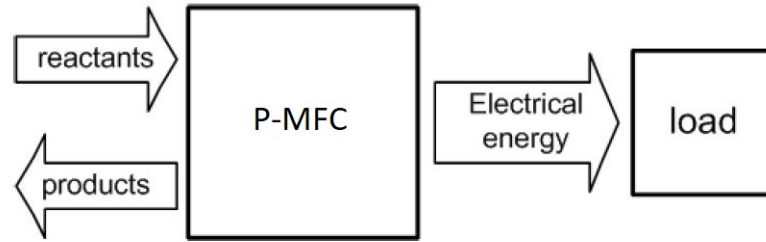


Figure 2.8: P-MFC seen as a black box

2.4.1 Static analysis

The static electrical characteristic of a P-MFC represents the voltage/current relationship in steady state. The blue curve of Figure 2.9 shows the typical static shape of a P-MFC. This curve is either called static electrical characteristic curve (or V-I curve) by physicists or polarization curve by bio-electrochemists.

Three different techniques can be used to obtain this curve:

- potentiostat method: imposing a fixed voltage across the unit and measuring the corresponding output current
- galvanostat method; imposing a fixed output current and measuring the corresponding voltage across the plant

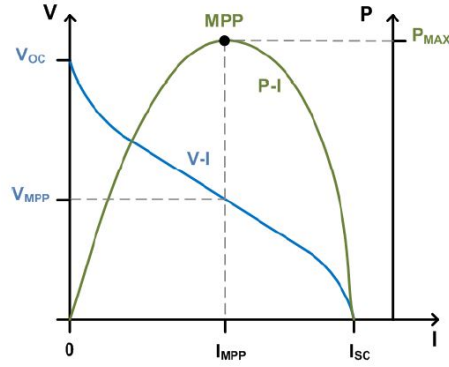


Figure 2.9: Typical polarization curve of P-MFC [16]

- resistorstat method: applying a variable resistance at the output port and monitoring either the voltage or the current

Depending on the method used and the parameters, the results can be different thus the choice of the acquisition method is still debated in the scientific community of P-MFCs at present. V_{OC} denotes the open circuit voltage while I_{SC} the short-circuit current. Approximating the polarization curve as straight line, the system can be analyzed using an equivalent electric model: a constant voltage source V_{OC} and a series resistance R_{INT} as depicted in Figure 2.10. The value of the voltage

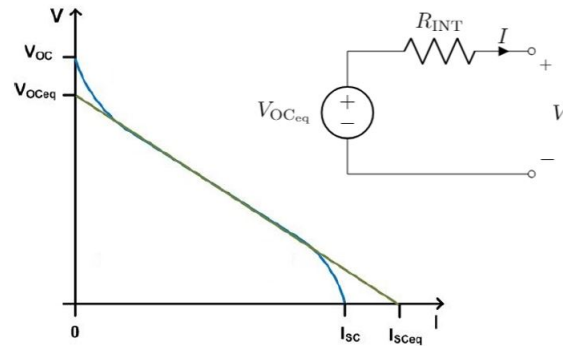


Figure 2.10: Polarization curve approximation of P-MFC and equivalent electronic circuit

source is the open-circuit one, i.e. the intersection of the approximated straight line with the voltage axis. From the slope, the internal resistance can be estimated:

$$R_{INT} = \frac{V_{OCeq}}{I_{SC}} \quad (2.7)$$

The red curve of the same graph shows the power delivered as a function of its

output current. The power delivered is null at the extreme points because in open-circuit condition the output current is null while in short-circuit condition the voltage across the plant is null. Between these points, the curve has a maximum called maximum power point (MPP). The voltage and current at MPP are respectively V_{MPP} and I_{MPP} . The derivation of the MPP allows to set the operating point to maximize the power extraction. In order to perform this analysis, steady-state conditions must be ensured. Steady-state means the voltage and current readings do not change with the time. When a step in condition is applied, the cell changes its state and it can takes minutes or even hours up to reach steady-state conditions. Derivation of V-I curve can be a time-consuming process. Frequently, time constraints only permits few points along the curve to be acquired. In practice, the fuel cell is subjected to a given state condition and the response is monitored until it no longer changes significantly in time thus the transient is extinguished. Then, the system is changed to a new state condition and the procedure is repeated. During the whole analysis several state conditions are gradually scanned in time. The system is continuously monitored to create at the end the polarization curve. The algorithm implemented to perform the static analysis is shown Figure 2.11.

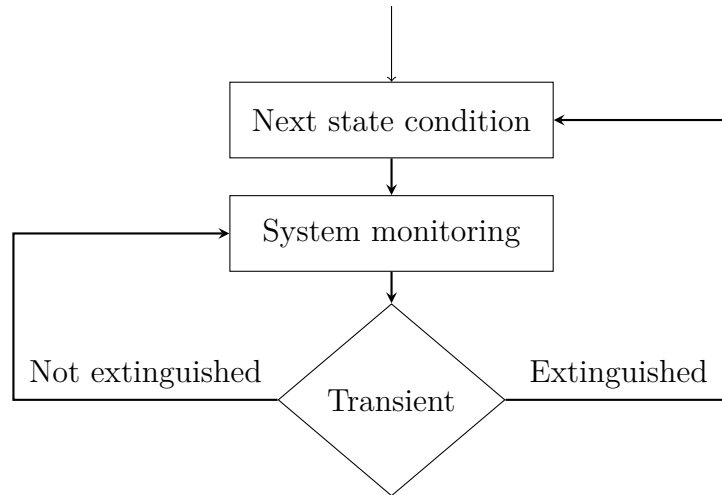


Figure 2.11: Static analysis flow chart

2.4.2 Dynamic analysis

The static electrical characteristic curves does not convey information on the dynamic properties of the fuel cell. P-MFC has slow dynamic behavior which can be outlined by recording its response to a step of the load resistance (Figure 2.12). The first thing can note is the presence of various time-constants. Initially it senses

an instantaneous voltage drop and then the voltage keeps falling down similar to a first order differential equation but it contains different time constants due to the internal mechanisms related to bacteria and to mass transfer phenomena [36]. The

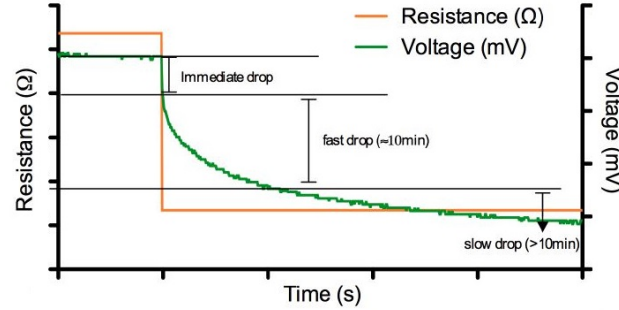


Figure 2.12: Time response to a load-resistance step for P-MFC [16]

fast initial dynamic could be explained assuming the bacteria are able to store electrons and release them later [37]. The bacteria can adapt quickly to small changes but they will take several hours to adapt to a completely different operating point. Different methods can be applied to understand how the P-MFC works during the transient but Electrochemical Impedance Spectroscopy [38] is the most widely used technique.

Electrochemical Impedance Spectroscopy

Electrochemical Impedance Spectroscopy (EIS) is the most sophisticated technique to characterize BES [39] [40] [41]. The information content of EIS is higher than the static value. It may be able to distinguish between two or more electrochemical reactions taking place and it provides information on the reactive behavior of the system. EIS is usually performed by applying a small perturbation to the cell and then measuring the response. Assuming to apply a small sinusoidal current excitation, the response is an AC voltage signal (Figure 2.13). Electrochemical cells

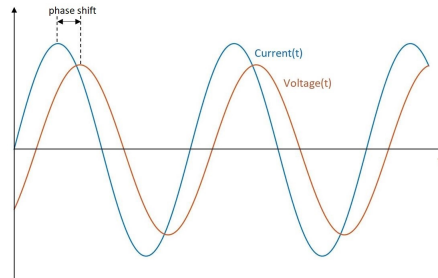


Figure 2.13: Voltage response to a sinusoidal current in a linear system

are not linear systems. However, they can be considered pseudo-linear because by looking at a small enough portion of the curve it appears to be linear as depicted in Figure 2.14.

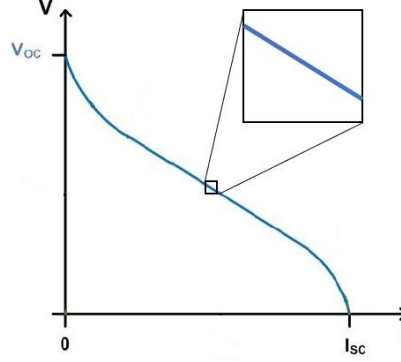


Figure 2.14: Zoom in V-I curve of P-MFC

The excitation signal has the form:

$$I(t) = I_0 \sin(\omega t)$$

where $I(t)$ is the current at the time t , I_0 is the amplitude of the signal and ω is the radial frequency expressed in rad/s . In a linear system, the response signal $E(t)$ has a phase shift ϕ and amplitude E_0 :

$$E(t) = E_0 \sin(\omega t + \phi)$$

An expression analogous to Ohm's law allows to calculate the impedance of the system as:

$$Z(t) = \frac{E(t)}{I(t)} = \frac{E_0 \sin(\omega t + \phi)}{I_0 \sin(\omega t)} = Z_0 \frac{\sin(\omega t + \phi)}{\sin(\omega t)}$$

where Z_0 is the impedance magnitude. For simplicity, the impedance can be represented as a complex function.

$$\begin{cases} E_t = E_0 e^{j\omega t + j\phi} \\ I_t = I_0 e^{j\omega t} \end{cases} \rightarrow Z(\omega) = \frac{E_t}{I_t} = \frac{E_0 e^{j\omega t + j\phi}}{I_0 e^{j\omega t}} = Z_0 e^{j\phi} = Z_0 (\cos(\phi) + j \sin(\phi)) \quad (2.8)$$

The expression of $Z(\omega)$ is composed of a real and an imaginary part. This impedance can be represented either in the Bode plot (Figure 2.15a) or in the Nyquist (Figure 2.15b).

In both, charge transfer processes can be identified but usually the Bode plot is used because the frequency is explicit and also small impedance in presence of large

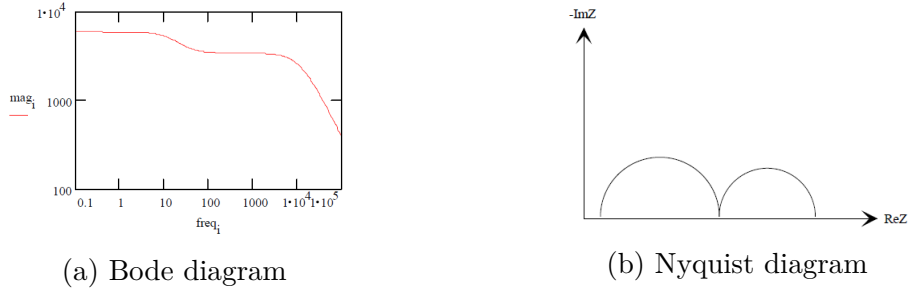


Figure 2.15: Electrochemical Impedance Spectroscopy

one can be easily distinguished. In EIS, the data can be represented in time and in frequency domain. An equivalent electronic circuit composed by resistors, capacitors and inductors can be used to model the behavior of the P-MFC impedance. The topology and the value of the components of this electrical model can be derived from the shape of the impedance obtained from EIS analysis. It is possible to switch between the two domains by Fourier transform (\mathcal{F}) and its inverse (\mathcal{F}^{-1}). Its computerized implementation is so called Fast Fourier Transform (FFT).

Electrochemical Impedance Spectroscopy with white noise

The EIS method usually relies on narrow-band signals and uses sinusoidal signal with a small amplitude and fixed frequency to estimate the impedance at this particular frequency. With this approach, EIS spectrum takes a lot of time thus in order to reduce the time needed to perform the whole analysis it's convenient to use a wide-band signal i.e. white noise (Figure 2.16) to estimate the impedance on a wider frequency band [42]. The input signal is a pseudo random binary sequence with a flat power spectral density on a chosen frequency band. The white noise is superimposed on a bias value.

This signal is applied to the system under test i.e. P-MFC and its response is measured. The system behavior depends on several internal and external conditions but they are assumed to be constant during the measurement process such that it can be considered as time-invariant system. The white noise amplitude is assumed small enough to have a linear response from the P-MFC. Under these assumption, it can be considered as a linear time-invariant (LTI) system during each measurement. The electrical impedance $Z(f)$ can be defined by the ratio between the cross power spectral density $S_{vi}(f)$ between voltage and current and the power spectral density $S_{ii}(f)$ of the current [43]:

$$Z(f) = \frac{S_{vi}(f)}{S_{ii}(f)} \quad (2.9)$$

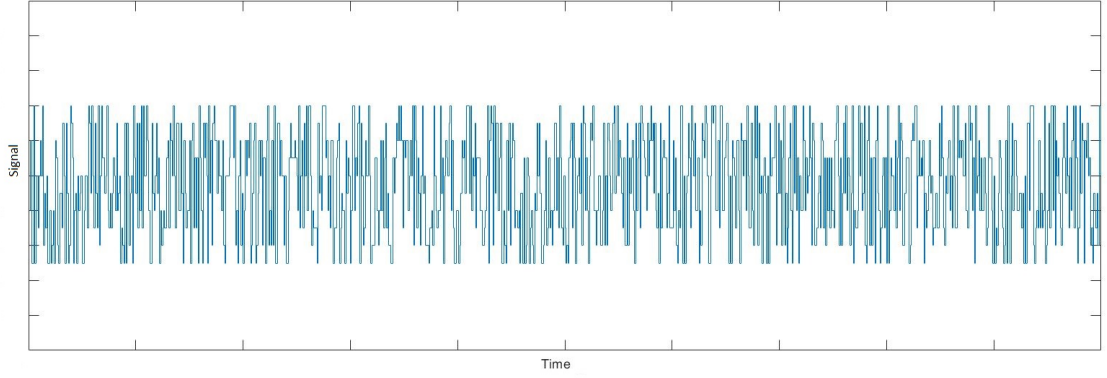


Figure 2.16: Wide-band signal i.e. white noise

In order to estimate $Z(f)$, a non recursive wide-band frequency estimation with Welch modified method is applied [42]. A possible flow chart shows the measure technique is depicted in Figure 2.17.

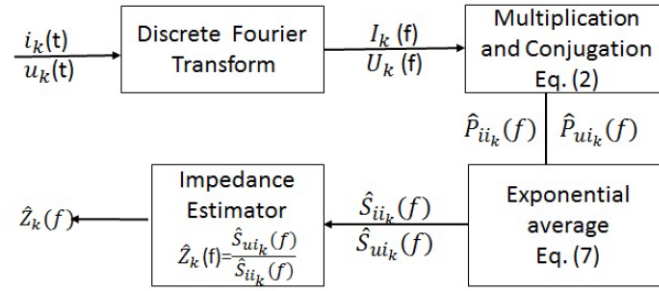


Figure 2.17: Recursive wide-band frequency estimation algorithm [42, p.4]

Chapter 3

Ad-hoc automatized sensing system: hardware

In this chapter, different solutions suitable to perform static and dynamic analysis needed to characterize the P-MFC are described in detail. The goal is to design an electronic circuit capable to fix the test conditions and at the same time to measure the parameters of interest. The method procedure presented in [5] is considered here as a starting point in which measurements are made by a Raspberry Pi and High-precision AD/DA boards so the designed solutions (hardware and software) are adapted to these ones. The use of these boards allows to keep the cost of the whole sensing system low. The generic scheme of the ad-hoc automatized sensing system is shown in Figure 3.1.

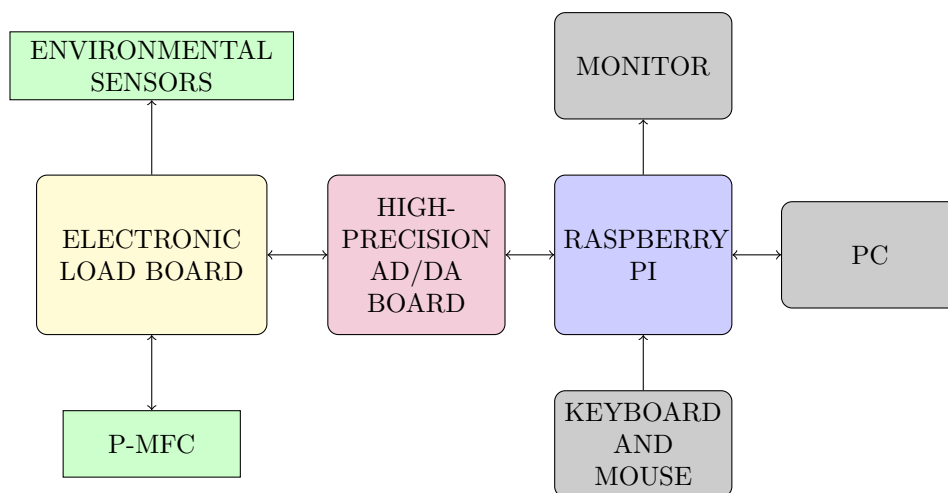


Figure 3.1: Basic scheme of the system

The electronic load board is able to measure the current and voltage of the P-MFC and to monitor the environmental parameters. This board is mounted on the High-precision AD/DA boards which has an analog-to-digital and a digital-to-analog converter. The high-precision AD/DA board is an expansion module mounted on the Raspberry Pi (RPi) and they communicate between them over an SPI-compatible serial interface. The RPi is a single-board computer to which a monitor, a keyboard and a mouse are connected to use it as a desktop computer and it is feed by its 5.1 V–2.5 A power supply. The RPi board can be connected to a PC to exchange data. This chapter is focused on the hardware part (Figure 3.2) and its design.

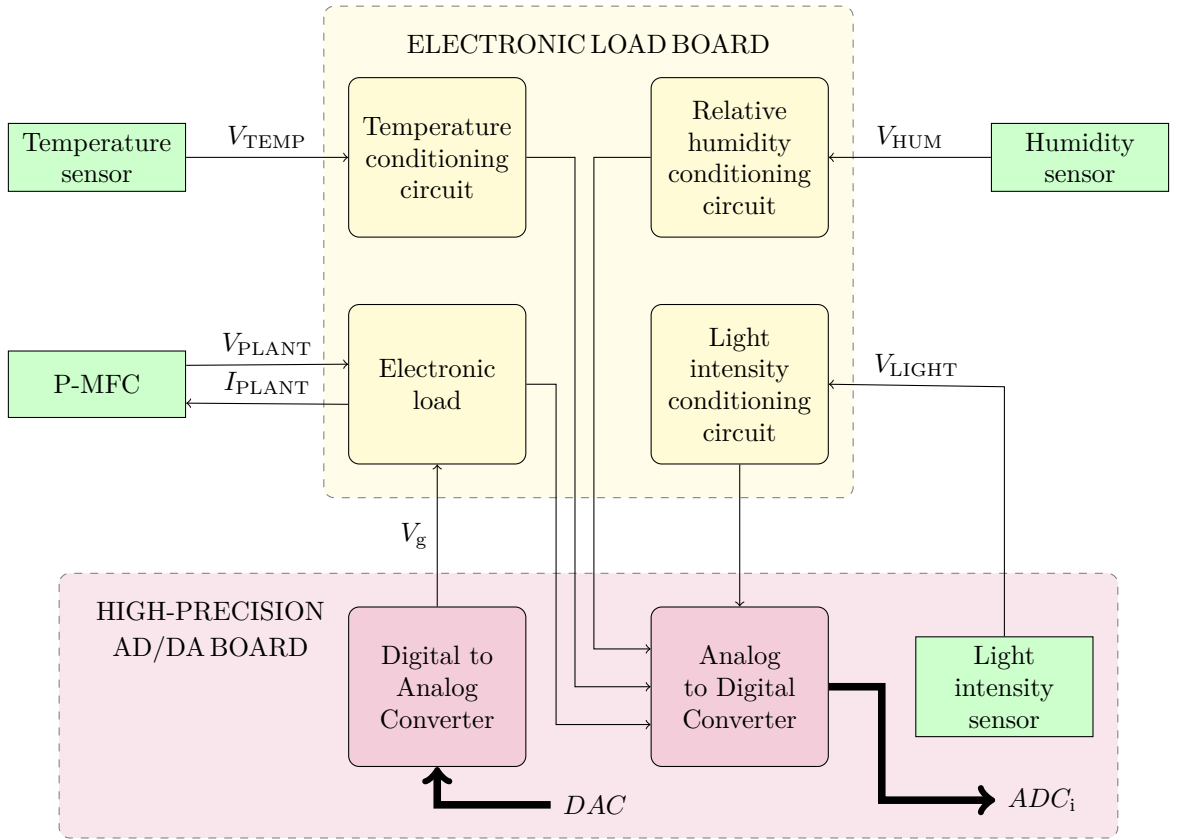


Figure 3.2: More detailed hardware block diagram of the system

Different environmental parameters must be taken into account in order to properly describe the ambient conditions in which the P-MFC system be: the air temperature is measured by the temperature sensor placed close to the plant, the relative humidity by a moisture sensor inserted in the ground and the light intensity through a light sensor (pre-mounted on the high-precision AD/DA board).

The signals provided by the sensors must be adapted for the input swing of the ADC so the electronic load board also contains the conditioning circuitry of these sensors. Their outputs are connected at the inputs of the ADC. The connections between sensors, the P-MFC and the electronic load board are made by a twisted-wire cable in order to improve rejection of external electromagnetic interference. The RPi implements the measurement algorithm. In this thesis, it is used the Raspberry Pi 3 Model B Vi.2 which also has a 40-pin extended general purpose input/output (GPIO). The main hardware characteristics of the RPi board are shown in table 3.1.

PARAMETER	CONDITIONS	MIN	TYP	MAX	UNIT
DC characteristics					
Voltage Output Low V_{OL}	$VDD = 3.3\text{ V}, I_{OL} = -2\text{ mA}$			0.14	V
Voltage Output High V_{OH}	$VDD = 3.3\text{ V}, I_{OL} = 2\text{ mA}$	3			V
Current Output Low I_{OL}	$VDD = 3.3\text{ V}, V_O = 0.4\text{ V}$	18			mA
Current Output High I_{OH}	$VDD = 3.3\text{ V}, V_O = 2.3\text{ V}$	17			mA

Table 3.1: Raspberry Pi 3 model B Vi.2 specifications [44, p.14]

The High-precision AD/DA board is equipped with an ADC (ADS1256) and a DAC (DAC8532) so it is able to acquire/generate analog signal from/to external world. The ADS1256 is a low-noise, 24-bit analog-to-digital converter where the main features are listed in the table 3.3.

PARAMETER	CONDITION	MIN	TYP	MAX	UNIT
Analog Inputs					
Full-scale input voltage V_{ADCIN}			$\pm 2 \cdot V_{REF}/PGA$		V
Programmable Gain Amplifier (PGA)		1		64	
System performance					
Resolution N_{ADC}		24			bit
Data Rate (f_{DATA})	$f_{CLKIN} = 7.68\text{ MHz}$	2.5		30000	SPS
Voltage Reference Inputs					
Reference input voltage V_{REF}		0.5	2.5	2.6	V
Negative reference input V_{REFN}	Buffer off	$AGND - 0.1$		$V_{REFP} - 0.5$	V
	Buffer on	$AGND$		$V_{REFP} - 0.5$	V
Positive reference input V_{REFP}	Buffer off	$V_{REFN} + 0.5$		$AVDD + 0.1$	V
	Buffer on	$V_{REFN} + 0.5$		$AVDD - 2$	V

Figure 3.3: ADS1256 specifications [45, pp. 3-4]

The DAC8532 is a dual-channel, 16-bit digital-to-analog converter. The main features of this converter are summarized in the table 3.2.

The following sections describe in details the hardware part: not only the electronic load connected to the P-MFC but also the temperature, relative humidity and light intensity sensors with the design of their conditioning circuitry.

All specifications at -40°C to 105°C , $V_{\text{DD}} = 2.7\text{ V}$ to 5.5 V unless otherwise noted

PARAMETER	CONDITIONS	MIN	TYP	MAX	UNIT
Output characteristics					
Output Voltage Range		0		V_{REF}	V
Static performance					
Resolution N_{DAC}		16			bit

Table 3.2: DAC specifications [46, pp. 2-3]

3.1 Electronic load and design

The electronic load is connected to the P-MFC and it implements the galvanistat method so a current I_{PMFC} is forced from the device under test (i.e. the plant) and the output voltage V_{PMFC} across it is measured (Figure 3.4).

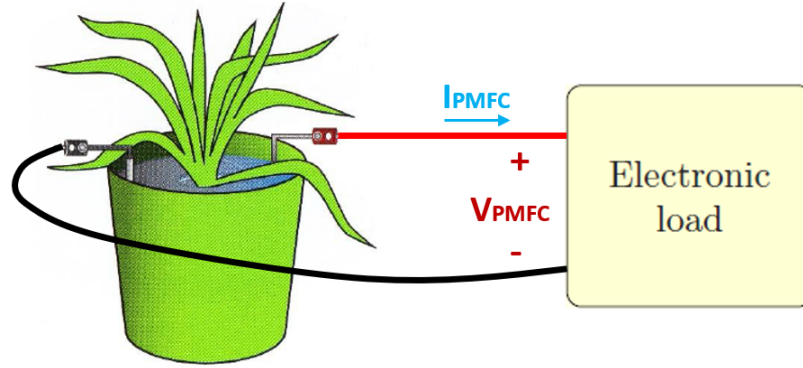


Figure 3.4: Connection of P-MFC to the electronic load

In what follows, different circuits which can implement this method are analyzed in details highlighting their pro and cons. For the final proposed circuitual solution also the design procedure will be explained.

3.1.1 Constant current source with operational amplifier

The galvanistat method can be implemented by using a constant current source circuit as depicted in Figure 3.5. The voltage V_i can be provided by the output of the DA converter and it defines the current that can flow in the resistor R . Considering negligible the current absorbed by the operational amplifier I_f , the current that flows in the resistor is the same of the P-MFC named I . The feedback loop composed by the operational amplifier and the transistor holds the current constant: if the current varies (for example, it increases), the negative input of the op amp experiences a voltage variation (positive) so its output changes (decreases) and also the gate voltage of the transistor; the variation of the gate-source voltage

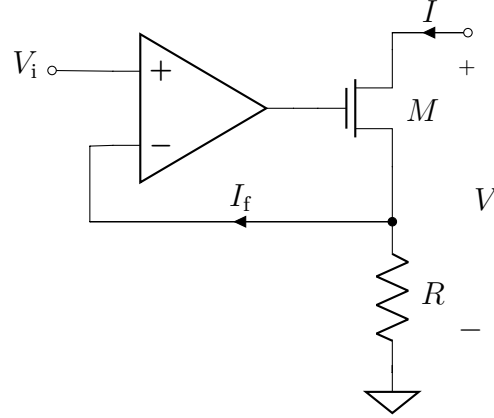


Figure 3.5: Constant current source with op amp and MOS

(lowering) leads to an adjustment of the current (reduction). Thanks to this negative feedback loop, the circuit is able to provide a constant amount of current independently of the voltage across the load V . The value of the current that flows through the P-MFC can be derived with Ohm's law by measuring the voltage across R . The voltage across the P-MFC can be measured between the drain of the transistor and the ground. The operational amplifier increases the cost of the system and introduces some errors such as offset and gain error.

3.1.2 Constant current source without operational amplifier

The negative feedback loop can be implemented software by removing the operational amplifier and inserting the RPi board as shown in Figure 3.6: the voltage across the resistance R is measured through an input of the ADC, the current is derived and the voltage V_g is modified by an output of the DAC. The proposed solution has some voltage and current limits. The transistor M sets the amount of current but to work properly it must be in saturation so a voltage limit is imposed by the minimum drain-source voltage $V_{DS_{sat}}$. Supposing the load (i.e. P-MFC) as a independent voltage source V_{OC} in series to its resistance R_{PMFC} , when the transistor is fully ON, ideally M is a short-circuit so R goes directly in series to R_{PMFC} limiting the maximum current $I_{PMFC_{MAX}}$:

$$I_{PMFC_{MAX}} = \frac{V_{OC}}{R_{PMFC} + R}$$

Further limits are given by the features of the AD and DA converters. The current resolution ΔI_{ADC} imposed by the ADC can be derived from its input voltage swing $V_{ADC_{IN}}$ and its number of bits N_{ADC} :

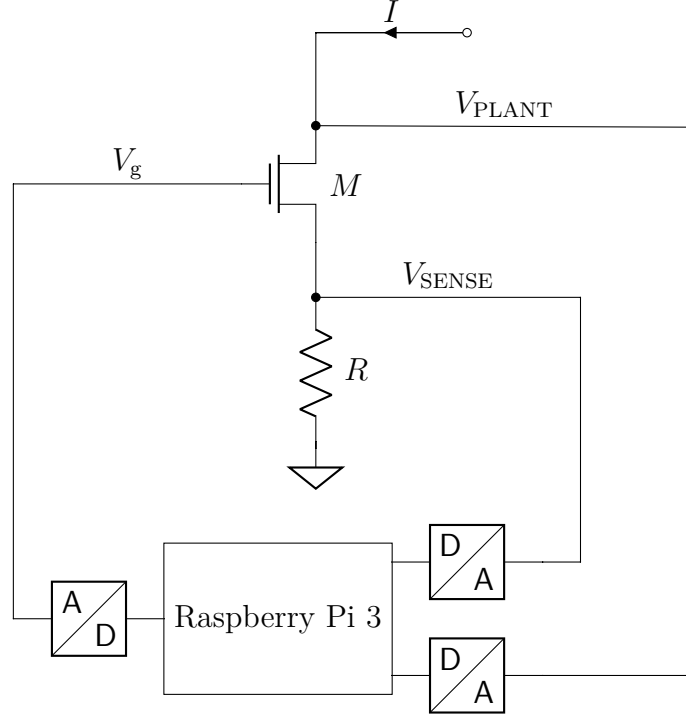


Figure 3.6: Constant current source with Raspberry Pi and MOS

$$\Delta V_{\text{ADC}} = \frac{V_{\text{ADC}_{\text{IN}}}}{2^{N_{\text{ADC}}}} \rightarrow \Delta I_{\text{ADC}} = \frac{\Delta V_{\text{ADC}}}{R} = \frac{V_{\text{ADC}_{\text{IN}}}}{R \cdot 2^{N_{\text{ADC}}}}$$

The current resolution ΔI_{DAC} imposed by the DAC can be derived from its output voltage swing $V_{\text{DAC}_{\text{OUT}}}$ and its number of bits N_{DAC} :

$$\Delta V_{\text{DAC}} = \frac{V_{\text{DAC}_{\text{OUT}}}}{2^{N_{\text{DAC}}}} \rightarrow \Delta I_{\text{DAC}} = \frac{\Delta V_{\text{DAC}}}{R} = \frac{V_{\text{DAC}_{\text{OUT}}}}{R \cdot 2^{N_{\text{DAC}}}}$$

The value of the resistor R will be a trade off between the resolution and the maximum current: small R makes possible to measure higher currents with low resolution while higher values reduce the maximum limit but increase the resolution. The current resolution ΔI of the circuit is given by:

$$\Delta I = \max(\Delta I_{\text{ADC}}, \Delta I_{\text{DAC}})$$

A numerical example shows that the resistance R has on the performance of the circuit. To meet the requirements, one can act either on the converters or on the circuit. Usually, it is possible to choose the proper converters but for this thesis the board (High precision AD/DA board) is already chosen so different circuital solutions must be explored. The idea is to split the current range in more

sub-intervals each with different characteristics. From the circuit point of view, the range division can be implemented modifying dynamically the value of the resistance R seen by the source of the MOS M . One can start from the highest resistance value with the possibility of decreasing it by adding in parallel smaller resistances (parallel resistances solution) or viceversa start from the lowest value and then adding resistances in series (series resistances solution).

Numerical example.

The system has an ADC with an input voltage swing of 0.5 V and 24 bit and a DAC with an output voltage swing of 5 V and 16 bit. The system under test is modeled by an independent voltage source of 0.3 V and a series impedance of 1 k Ω . The maximum current I_{MAX} that the system can provide is:

$$I_{\text{MAX}} = \frac{V_{\text{OC}}}{R_{\text{PMFC}}} = \frac{0.3 \text{ V}}{1 \text{ k}\Omega} = 300 \mu\text{A}$$

When the resistance R is placed in series to the P-MFC impedance creates a limit in the maximum current can be measured. Two different numerical examples are shown to see how much it is important this effect:

- $R = 50 \Omega \rightarrow I_{\text{MAX}} = \frac{V_{\text{OC}}}{R_{\text{PMFC}} + R} = \frac{0.3 \text{ V}}{1 \text{ k}\Omega + 50 \Omega} = 285.71 \mu\text{A}$

$$\begin{cases} \Delta I_{\text{ADC}} = \frac{V_{\text{ADCIN}}}{R \cdot 2^{N_{\text{ADC}}}} = \frac{0.5 \text{ V}}{50 \Omega \cdot 2^{24}} = 596 \text{ pA} \\ \Delta I_{\text{DAC}} = \frac{V_{\text{DACOUT}}}{R \cdot 2^{N_{\text{DAC}}}} = \frac{5 \text{ V}}{50 \Omega \cdot 2^{16}} = 1.5 \mu\text{A} \end{cases} \rightarrow \Delta I = \max(\Delta I_{\text{AD}}, \Delta I_{\text{DAC}}) = 1.5 \mu\text{A}$$
- $R = 500 \Omega \rightarrow I_{\text{MAX}} = \frac{V_{\text{OC}}}{R_{\text{PMFC}} + R} = \frac{0.3 \text{ V}}{1 \text{ k}\Omega + 500 \Omega} = 200 \mu\text{A}$

$$\begin{cases} \Delta I_{\text{ADC}} = \frac{V_{\text{ADCIN}}}{R \cdot 2^{N_{\text{ADC}}}} = \frac{0.5 \text{ V}}{500 \Omega \cdot 2^{24}} = 59.6 \text{ pA} \\ \Delta I_{\text{DAC}} = \frac{V_{\text{DACOUT}}}{R \cdot 2^{N_{\text{DAC}}}} = \frac{5 \text{ V}}{500 \Omega \cdot 2^{16}} = 152.6 \text{ nA} \end{cases} \rightarrow \Delta I = 152.6 \text{ nA}$$

With a small resistance R the maximum current measured is close to the maximum but with a measurement resolution of 1.5 μA while increasing the value of the resistance R it is possible to reach an higher measurement resolution of about 150 nA but the maximum value of current can be measured is 2/3 of the maximum one.

3.1.3 Constant current source with parallel resistances

This solution uses different branches composed by the series of a MOS M_i and a resistance R_i . Only one branch is composed by a single resistor R_{SENSE} while all others are connected in parallel to decrease the value of resistance R seen by the source of the MOS M_1 . The circuit shown in Figure 3.7 has three branches so it is possible to split the current range in three different intervals. Transistors M_i of branches can be driven by an output of the DAC but this is not a good idea due to the usual limited number of output of the converters. A better way is to use

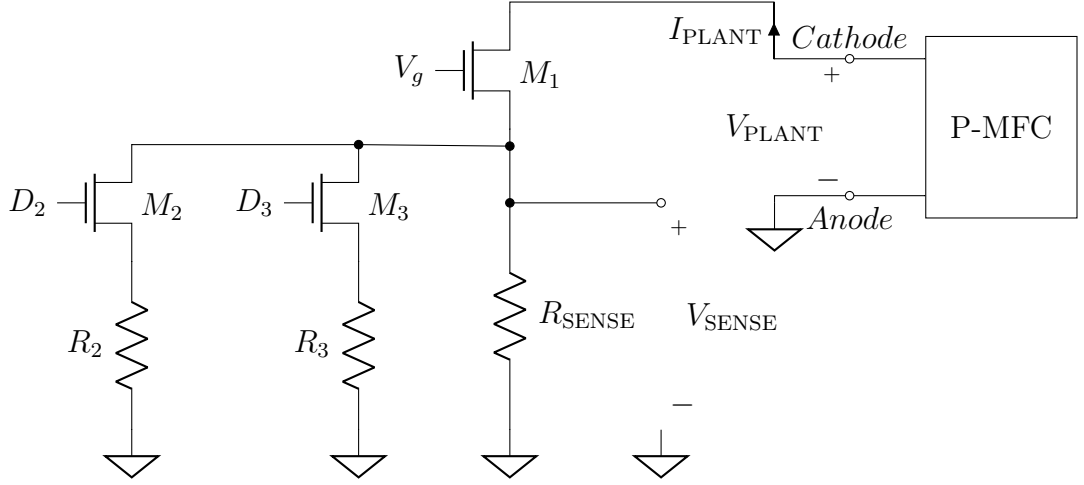


Figure 3.7: Constant current source with parallel resistances

the digital output of the Raspberry Pi board to drive them. The resistor R_{SENSE} sets the maximum resolution available.

$$\Delta I \propto \frac{1}{R} \quad I_{\text{PMFC}_{\text{MAX}}} \propto \frac{1}{R_{\text{PMFC}} + R}$$

The MOSFETs M_i have the task to place in parallel to R_{SENSE} other smaller resistors; in this way the overall resistance R at the source of the MOS M_1 is reduced. This reduction allows to reach higher value of current but decreases the current resolution. The current I_{PLANT} flowing into the P-MFC can be derived measuring the voltage across the resistance R_{SENSE} while the voltage between the drain of M_1 and ground represents the voltage V_{PLANT} of the plant. The advantages of this solution are:

- a lot of branches can be added depending on the number of available digital output of the RPi board thus splitting the current range in a lot of sub intervals
- only one output of the DAC is needed to drive the MOS M_1 of the feedback loop
- to read the current and the voltage of the P-MFC only the usual three nodes can be used without adding measuring nodes which would means increasing the number of input of the ADC required.

The main drawbacks of this solution are:

- difficult to reach very low current because is not possible to switch completely off the parallel MOSFETs M_i . This is due to the voltage output low V_{OL} of the output GPIO of the RPi board: to switch the MOS completely off, one has to fix the voltage at the gate either at ground or even lower (negative). If the MOS are not completely off, a small amount of current pass through them like an offset that fixes the lower limit.
- the MOS are not ideal switches but they act as a variable resistors: when it is completely on, it looks like a small resistor varying the overall resistance seen by the branch.
- in order to evaluate the current that flows in the P-MFC, the voltage across the resistor R_{SENSE} is measured. The leakage current that flows into the other branches modify the plant current but not the current reading.

These problems direct to an alternative solution.

3.1.4 Constant current source with series resistances

The idea to modify the resistance seen by the source of M_1 is a good one. A different solution is to use resistors in series. The number of resistors defines in how many current intervals is divided the whole range. The Figure 3.8 shows the circuit with the current range splitted in three different intervals where R_1 is a fixed resistor while R_{UP} and R_{DOWN} are variable ones. Depending on the value of the resistors, each interval has different resolution and current limit. The variable resistors R_{UP} and R_{DOWN} can be implemented by using a fixed resistor R_i to define the parameters with a parallel MOS M_i (Figure 3.9a) which acts as a switch to bypass it: when M_i is OFF, the resistance seen is R_i (Figure 3.9b) while when M_i is completely ON, the resistor R_i is short-circuited (Figure 3.9c). In this case, it is assumed to have an ideal switch ($r_{DS_{on}} = 0\Omega$) but in practice, the MOS has not a negligible on resistance ($r_{DS_{on}} \neq 0\Omega$). The resistance seen by the source of M_1 , named R_L , is defined as the overall resistance:

$$R_L = R_1 + R_{UP} + R_{DOWN} \quad (3.1)$$

The maximum current value and the current resolution of each interval are determined by the combination of the status of each MOS. The current I_{PLANT} flowing through the P-MFC can be derived measuring the voltage across R_1 with one input of the ADC:

$$I_{PLANT} = \frac{V_{SENSE}}{R_1}$$

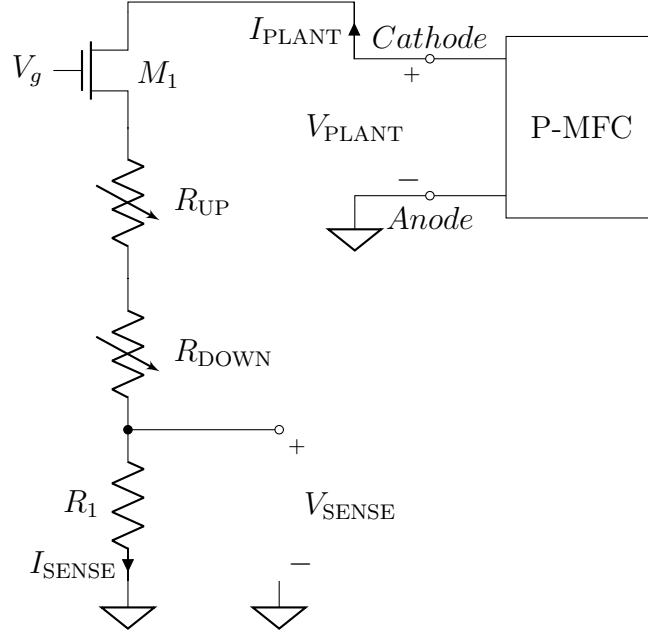


Figure 3.8: Constant current source with series resistances

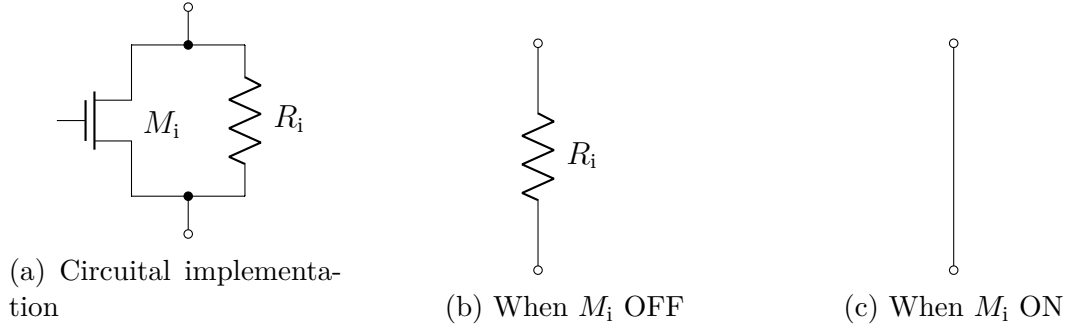


Figure 3.9: Variable resistance implementation and possible states

Once the value of R_1 is fixed, the measurement accuracy is kept constant for all the intervals so the resolution $\Delta I_{\text{READING}}$ of the current readings is:

$$\Delta I_{\text{READING}} = \Delta I_{\text{ADC}} = \frac{V_{\text{ADCIN}}}{R_1 \cdot 2^{N_{\text{ADC}}}} \quad (3.2)$$

The reading takes into account all the leakage currents that in the parallel solution are neglected so it is closer to the current through the P-MFC. The voltage V_{PLANT} can be obtained measuring the voltage between the drain of M_1 and ground with an input of the ADC. The resolution ΔV of the voltage readings is:

$$\Delta V = \Delta V_{\text{ADC}} = \frac{V_{\text{ADCIN}}}{2^{N_{\text{ADC}}}} \quad (3.3)$$

The ability to keep the current constant depends both on the features of the ADC and the value of the resistor R_1 and on the features of the DAC and the resistance R_L seen by the source of the MOS M_1 . The gate of the MOS M_1 is connected to one output of the DA converter while the other MOS $M_i \forall i > 1$ are driven by digital outputs D_i of the RPi board.

Design procedure

Before to start the design, it is important to know all the requirements. The voltage and current specifications of the sensing system are derived from previous measurements in [5, pg. 83]. The P-MFC is a very slow system and can take very long time (like several minutes or hours) to change from a steady state to another one, so it is useless to sample the parameters too frequently meaning that a good choice could be take measurements at least every 1 s. The requirements used for the design is summarized in the table 3.3. The RPi 3 board manages all

Parameter	Value/Range
P-MFC current range	100 nA \rightarrow 500 μ A
Maximum P-MFC voltage	$V_{MAX} = 0.6$ V
Minimum sample time from consecutive measurements	$t_{SAMPLE_{min}} = 1$ s

Table 3.3: Design requirements

the sensing system during the measurements. It has the possibility to accommodate on it different expansion boards. For the purpose of this thesis, it is used the High Precision AD/DA board [47] which has an analog-to-digital converter ADC (ADS1256 [45]) and a digital-to-analog converter (DAC8532 [46]). The converters can be connected to the electronic load circuit: the ADC can acquire voltage measurements whereas the DAC is able to drive the MOS. Study the internal structure of the converters helps to design properly the electronic load circuit. The design procedure is divided into parts, each of which focuses on a particular section: the set up of the AD and DA converters, the analysis of the model used for the load (i.e. P-MFC) and at the end the design of the components of the electronic load circuit.

- Design related the AD converter

The Figure 3.10 shows the block diagram of the ADS1256. It supports differential inputs but, in this work, it is set to have eight single-ended ones. The input multiplexer selects which input pin is connected to the AD converter. The input buffer is enabled because it greatly reduces the circuitry loading by providing up to 80 M Ω of input impedance. The low-noise PGA provides different gains from 1 up to 64. The converter is comprised of a 4th order delta-sigma modulator followed by

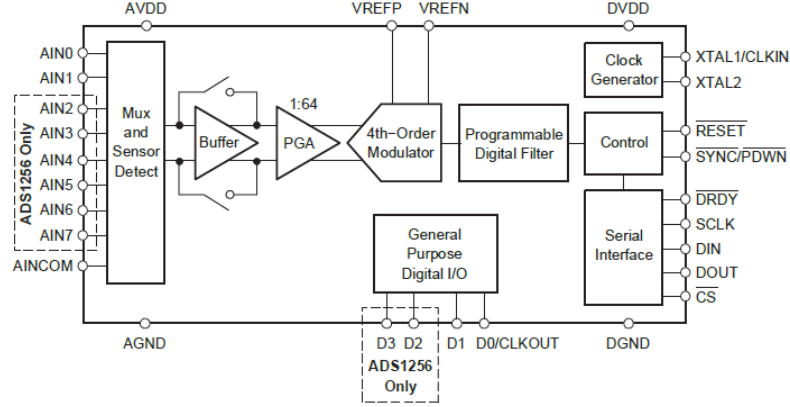


Figure 3.10: Block diagram of ADS1256 [45, p.11]

a programmable digital filter. The modulator measures the amplified differential signal $V_{\text{IN}} = (A_{\text{IN}_P} - A_{\text{IN}_N})$ against the differential reference V_{REF} . The reference input voltage V_{REF} is set to be 2.5 V by the voltage reference LM285D-2.5 [48] mounted on the board. The differential reference is scaled internally by a factor of two so the full-scale input range is $\pm 2 \cdot V_{\text{REF}}$ for $PGA = 1$. The value of PGA must be chosen to have input swing of the ADC $V_{\text{ADC}_{\text{IN}}}$ higher but as close as possible to the maximum voltage measurable V_{MAX} in order to optimize the reading resolution. The optimum value of PGA can be chosen from the table of [45, p.16]:

$$PGA = 8 \rightarrow V_{\text{ADC}_{\text{IN}}} = \frac{2 \cdot V_{\text{REF}}}{PGA} = \frac{2 \cdot 2.5 \text{ V}}{8} = 0.625 \text{ V} \quad (3.4)$$

so the full-scale input voltage $V_{\text{ADC}_{\text{FS}}}$ is twice this value because it considers also the negative range

$$V_{\text{ADC}_{\text{FS}}} = \pm \frac{2 \cdot V_{\text{REF}}}{\text{PGA}} = \pm 0.625 \text{ V}$$

The digital filter receives the modulator signal and provides a low-noise digital output. The data rate of the filter is programmable from 2.5 SPS to 30 kSPS. The choice of the data rate is a trade-off between resolution and speed: filter more for higher resolution, filter less for higher data rate. The ADC works at the maximum rate $f_S = 30$ kSPS and then the filter averages N_{AVE} samples before to produce an output value. Further considerations must be done about the presence of the input multiplexer. Multiplexing reduces the rate at which data can be acquired from an individual channel because of the time-sharing strategy. Supposing to use all of available them of the ADC $N_{\text{CH}} = 8$, each channel has a sample rate f_{SCH} :

$$f_{S_{CH}} = \frac{f_s}{N_{CH}} = \frac{30 \text{ kSPS}}{8} = 3.75 \text{ kSPS}$$

The P-MFC is a very slow system so it is important to have a better resolution with respect the speed. The number of average for programmable filter N_{AVE} can be picked from the table [45, p.18] and it is choose $N_{\text{AVE}} = 1200$ so the acquisition time required t_{ACQ} to obtain the measurements for all the channels:

$$t_{\text{ACQ}} = \frac{1}{f_{\text{SCH}}} N_{\text{AVE}} = \frac{1}{3.75 \text{ kSPS}} \cdot 1200 = 320 \text{ ms}$$

After this choice, one must take into account that $t_{\text{SAMPLE}_{\text{min}}}$ must be higher than the acquisition time of all the parameters t_{ACQ} and also of the time required for the algorithm calculations. In this case, the time for the algorithm is about 680 ms and it can be considered enough to perform it in time. The resolution of the ADC given by the datasheet is $N_{\text{ADC}} = 24 \text{ bit}$ but what is important is the effective number of bits (ENOB) because all real ADC circuits introduce noise and distortion. The ADS1256 allows to optimize the noise performance by adjusting the data rate or PGA setting. As the averaging is increased by reducing the data rate, the noise drops correspondingly. From the table of ENOB with buffer on in [45, p.12], it is possible to see with $\text{PGA} = 8$ and data rate of 25 SPS (it corresponds to $N_{\text{AVE}} = 1200$) that $\text{ENOB} = 23 \text{ bit}$ so the resolution is reducing. The requirements give the possibility to change the data rate but not the PGA. Decreasing the data rate, the ENOB increases but reduces the amount of time for the algorithm so the loss of ADC resolution is not so critical because the DAC mainly affects the system resolution. From this point on, the number of bit of the ADC N_{ADC} is set equals to ENOB so $N_{\text{ADC}} = \text{ENOB} = 23 \text{ bit}$. The resolution in voltage reading is fixed by this limit:

$$V_{\text{ADC}_{\text{RIS}}} = \frac{V_{\text{ADC}_{\text{IN}}}}{2^{N_{\text{ADC}}}} = \frac{0.625 \text{ V}}{2^{23}} = 74.5 \text{ nV}$$

- Design related the DA converter

The Figure 3.11 shows the block diagram of the DAC8532. It is a dual channel, 16-bit digital-to-analog converter. Each on-chip precision output amplifier allows rail-to-rail output swing to be achieved over the supply range of 2.7 V to 5.5 V. The DAC8532 requires an external reference voltage to set the output range of each DAC channel and it can be chosen through a jumper on the board between 3.3 V and 5 V. In this case, the jumper is set at 5 V. Also incorporated into the device is a power-on reset which ensures that the DAC outputs power up at zero-scale and remain there until a valid write take place. It is a low-power converter since it consumes 2.5 mW at 5 V and 1 μW in power-down mode. The architecture of each channel consists of a resistor string DAC followed by an output buffer amplifier as shown in the simplified block diagram of Figure 3.12. Its output voltage swing $V_{\text{DAC}_{\text{OUT}}}$ is equal to the reference voltage $V_{\text{DAC}_{\text{OUT}}} = 5 \text{ V}$ and the resolution of

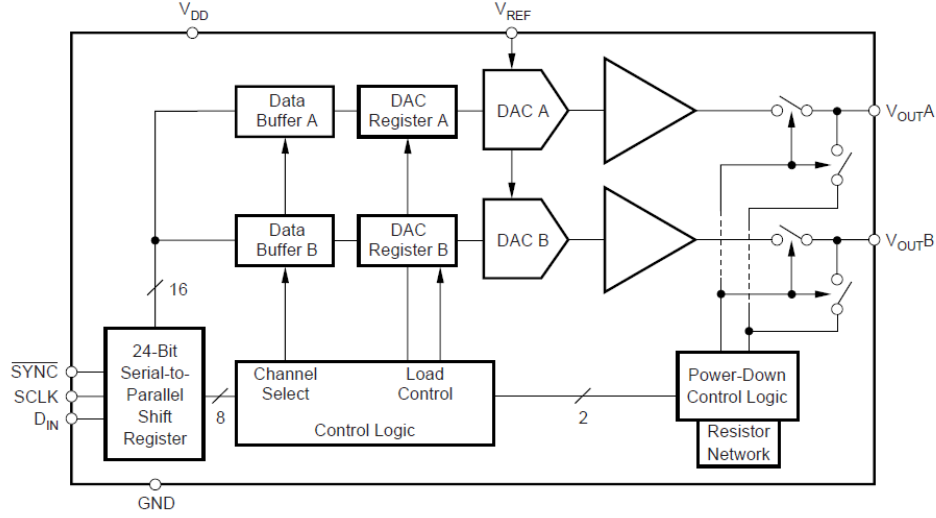


Figure 3.11: Block diagram of DAC8532 [46, p.1]

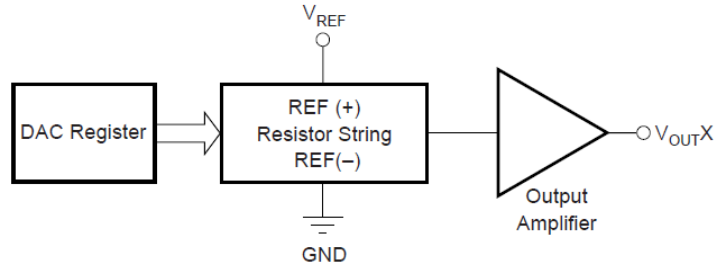


Figure 3.12: Simplified block diagram of DAC8532 [46, p.10]

the DAC $N_{DAC} = 16$ bits. For each device, the input coding is unipolar straight binary and setting the decimal equivalent of the binary code D loaded into the DAC register, the ideal output voltage is given by:

$$V_{OUTX} = \frac{V_{REF} \cdot D}{2^{N_{DAC}}}$$

This DAC exhibits temperature stability of 5 ppm/°C typical output voltage drift over the specified temperature range of the device. This enables the output voltage of each channel to stay within a $\pm 25 \mu V$ window for a $\pm 1^\circ C$ ambient temperature change.

- Model used for the P-MFC

Before to start the design of the components of the electronic load circuit, it is

important to show the system that will be connected. The P-MFC has to be characterized so it is the load connected to the electronic load circuit. First, the P-MFC is model by an independent voltage source V_{OC} in series to a resistor R_{INT} (as depicted in Figure 3.13) which chosen values are $V_{OC} = 0.5 \text{ V}$ and the maximum current $I_{MAX} = 500 \mu\text{A}$ so the series resistance of the P-MFC is:

$$R_{INT} = \frac{V_{OC}}{I_{MAX}} = \frac{0.5 \text{ V}}{500 \mu\text{A}} = 1 \text{ k}\Omega \quad (3.5)$$

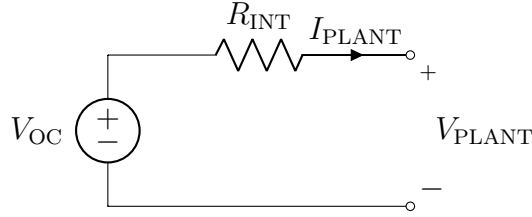


Figure 3.13: Equivalent electronic circuit to model the P-MFC

- Proposed circuit solution

The proposed circuit (Figure 3.14) is a constant current source with series resistances. It considers the current range splitted in three intervals so three series resistors are used. The resistors R_2 and R_3 can be bypassed depending on the state of the respective transistor M_2 and M_3 . As previously explained, the feedback loop that sense the current I_{SENSE} to modify the voltage V_g is implemented by the RPi. At this point, the components of this circuit have to be designed.

- Transistors design

At this point, one has the necessary knowledge to design the transistors. The choice of the MOS has to take into account the worst case conditions: the maximum voltage across the drain-source port $V_{DS_{MAX}}$, the maximum drain-source current $I_{DS_{MAX}}$, the drain-source on resistance $r_{DS(on)}$ and the maximum power consumption $P_{d_{MAX}}$. The maximum voltage across the drain-source port is the maximum P-MFC voltage $V_{MAX} = 0.6 \text{ V}$. Since all the transistors could be in series, the maximum drain current that can flow through them is the maximum P-MFC one $I_{PLANT_{MAX}} = 500 \mu\text{A}$. The power consumption of the MOS can be computed by the product of the maximum drain-source voltage and the maximum drain current:

$$P_{d_{MOS}} = V_{MAX} \cdot I_{MAX} = 0.6 \text{ V} \cdot 500 \mu\text{A} = 300 \mu\text{W} \quad (3.6)$$

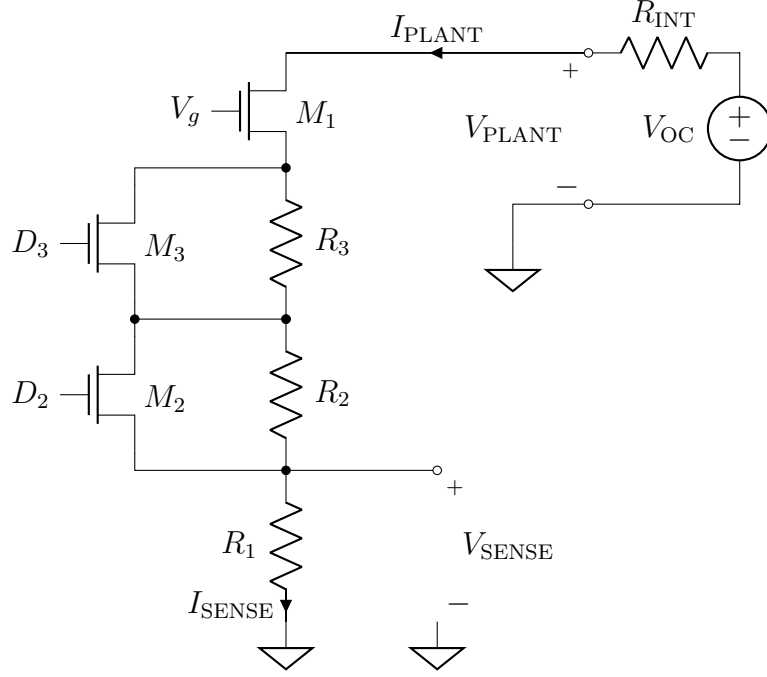


Figure 3.14: Proposed circuit solution

Parameter	Value	Unit
Maximum drain source voltage $V_{DS_{MAX}}$	60	V
Maximum drain current $I_{D_{MAX}}$	500	mA
Total device dissipation $P_{d_{MAX}}$	350	mW
Maximum drain-source resistance $r_{DS(on)}$	5	Ω

Table 3.4: BS170 specifications

The MOS chosen is the BS170 [49] and the specifications are summarized in the table 3.4. Maximum voltage and current values of the BS170 are far higher with respect to the design requirements and also the power consumption is lower with respect to the maximum power device dissipation $P_{d_{MAX}} = 350 \text{ mW}$. The MOSFETs M_2 and M_3 must be driven from two output pins of the GPIO port of the RPi board. These pins are directly connected to the gate of the transistors. The GPIO drives the gate pin with a low level (V_{OL}) when the transistor M_i has to be off while drive a high level (V_{OH}) when the transistor M_i has to short-circuit the relative resistance R_i . Since their change are not so frequently, the driving capability of the GPIO does not create problem to switch on and off them inside the t_{SAMPLE} time.

- Detailed analysis of the constant current source circuit

In what follows, the constant current source with series resistances circuit will be analyzed in details in each combination. When M_2 and M_3 are ON (Figure 3.15a), the resistors R_2 and R_3 are short-circuited so the whole resistance is $R'_L = R_1 + R_{DS(on)} + R_{DS(on)} = R_1 + 2 \cdot R_{DS(on)}$. The maximum current can flow is:

$$I'_{PLANT_{MAX}} = \frac{V_{OC}}{R_{INT} + R'_L} = \frac{V_{OC}}{R_{INT} + R_1 + 2 \cdot R_{DS(on)}} \quad (3.7)$$

while the resolution of the current is given by the DAC:

$$\Delta I'_{DAC} = \frac{V_{DAC_{OUT}}}{R'_L \cdot 2^{N_{DAC}}} = \frac{V_{DAC_{OUT}}}{(R_1 + 2 \cdot R_{DS(on)}) \cdot 2^{N_{DAC}}} \quad (3.8)$$

When M_2 is OFF and M_3 is ON (Figure 3.15b), the resistor R_3 is short-circuited so the whole resistance is $R''_L = R_1 + R_2 + R_{DS(on)}$. The maximum current can flow is:

$$I''_{PLANT_{MAX}} = \frac{V_{OC}}{R_{INT} + R''_L} = \frac{V_{OC}}{R_{INT} + R_1 + R_2 + R_{DS(on)}} \quad (3.9)$$

while the resolution of the current is given by the DAC:

$$\Delta I''_{DAC} = \frac{V_{DAC_{OUT}}}{R''_L \cdot 2^{N_{DAC}}} = \frac{V_{DAC_{OUT}}}{(R_1 + R_2 + R_{DS(on)}) \cdot 2^{N_{DAC}}} \quad (3.10)$$

When both M_2 and M_3 are OFF (Figure 3.15c), the whole resistance is $R'''_L = R_1 + R_2 + R_3$. The maximum current can flow is:

$$I'''_{PLANT_{MAX}} = \frac{V_{OC}}{R_{INT} + R'''_L} = \frac{V_{OC}}{R_{INT} + R_1 + R_2 + R_3} \quad (3.11)$$

while the resolution of the current is given by the DAC:

$$\Delta I'''_{DAC} = \frac{V_{DAC_{OUT}}}{R'''_L \cdot 2^{N_{DAC}}} = \frac{V_{DAC_{OUT}}}{(R_1 + R_2 + R_3) \cdot 2^{N_{DAC}}} \quad (3.12)$$

- Resistors design

The final step is the design of the resistors. The current range is splitted in three different regions and each of them with different specifications. For the first region, the value of the resistor seen by the source of the MOS is chosen $R'_L = 100 \Omega$. The value of R_1 can be so derived:

$$R'_L = R_1 + 2 \cdot R_{DS(on)} \rightarrow R_1 = R'_L - 2 \cdot R_{DS(on)} = 100 \Omega - 2 \cdot 5 \Omega = 90 \Omega \rightarrow R_1 = 100 \Omega^1 \quad (3.13)$$

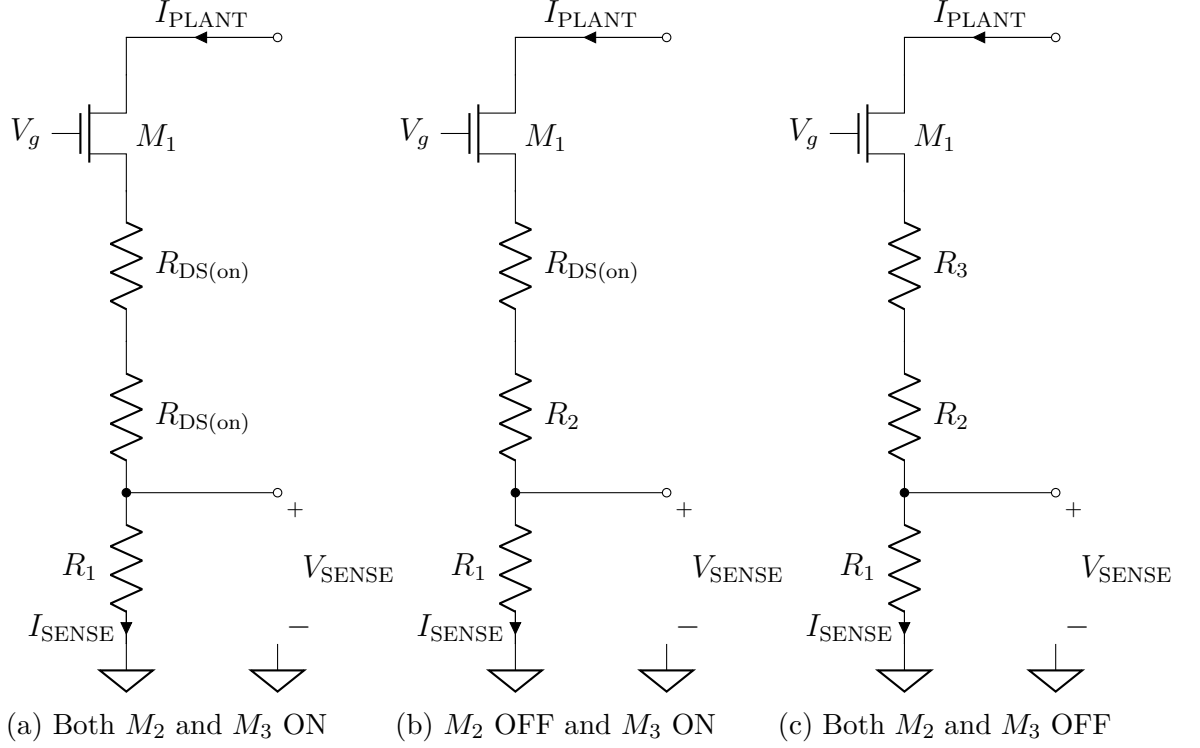


Figure 3.15: Different combination of series circuit

Replacing the value in the equations 3.7 and 3.8 allows to compute the maximum current and the resolution of the current in the first region:

$$\begin{cases} I'_{\text{PLANT}_{\text{MAX}}} = \frac{V_{\text{OC}}}{R_{\text{INT}} + R_1 + 2 \cdot R_{\text{DS(on)}}} = \frac{0.5 \text{ V}}{1 \text{ k}\Omega + 100 \Omega + 2 \cdot 5 \Omega} = 450.45 \mu\text{A} \\ \Delta I'_{\text{DAC}} = \frac{V_{\text{DAC}_{\text{OUT}}}}{(R_1 + 2 \cdot R_{\text{DS(on)}}) \cdot 2^{N_{\text{DAC}}}} = \frac{5 \text{ V}}{(100 \Omega + 2 \cdot 5 \Omega) \cdot 2^{16}} = 693.58 \text{ nA} \end{cases} \quad (3.14)$$

This is the larger range but the resolution is higher with respect the specifications. To reduce the resolution, the value of the resistance R_L must be increased so for the second region, the value of the resistor becomes $R'_L = 1 \text{ k}\Omega$ and the value of R_2 can be computed:

$$R'_L = R_1 + R_2 + R_{\text{DS(on)}} \rightarrow R_2 = R'_L - R_1 - R_{\text{DS(on)}} = 1 \text{ k}\Omega - 100 \Omega - 5 \Omega = 895 \Omega \rightarrow R_2 = 1 \text{ k}\Omega^1 \quad (3.15)$$

¹The round up operation is made considering the E12 series of resistor.

Replacing the value in the equations 3.9 and 3.10 allows to compute the maximum current and the resolution of the current in the second region:

$$\begin{cases} I''_{\text{PLANT}_{\text{MAX}}} = \frac{V_{\text{OC}}}{R_{\text{INT}} + R_1 + R_2 + R_{\text{DS(on)}}} = \frac{0.5 \text{ V}}{1 \text{ k}\Omega + 100 \Omega + 1 \text{ k}\Omega + 5 \Omega} = 237.52 \mu\text{A} \\ \Delta I''_{\text{DAC}} = \frac{V_{\text{DAC}_{\text{OUT}}}}{(R_1 + R_2 + R_{\text{DS(on)}}) \cdot 2^{N_{\text{DAC}}}} = \frac{5 \text{ V}}{(100 \Omega + 1 \text{ k}\Omega + 5 \Omega) \cdot 2^{16}} = 69.04 \text{ nA} \end{cases} \quad (3.16)$$

The lower limit of the current range is 100 nA and the current resolution should be lower than $\frac{1}{10}$ of this so less than 10 nA. The resolution computed is still larger than the desired one. The third region has to have the higher value of resistance R_L so $R_L''' = 10 \text{ k}\Omega$. The design of the value of R_3 :

$$R_L''' = R_1 + R_2 + R_3 \rightarrow R_3 = R_L''' - R_1 - R_2 = 10 \text{ k}\Omega - 100 \Omega - 1 \text{ k}\Omega = 8.9 \text{ k}\Omega \rightarrow R_3 = 10 \text{ k}\Omega^1 \quad (3.17)$$

Replacing the value in the equations 3.11 and 3.12 allows to compute the maximum current and the resolution of the current in the third region:

$$\begin{cases} I'''_{\text{PLANT}_{\text{MAX}}} = \frac{V_{\text{OC}}}{R_{\text{INT}} + R_1 + R_2 + R_3} = \frac{0.5 \text{ V}}{1 \text{ k}\Omega + 100 \Omega + 1 \text{ k}\Omega + 10 \text{ k}\Omega} = 45.05 \mu\text{A} \\ \Delta I'''_{\text{DAC}} = \frac{V_{\text{DAC}_{\text{OUT}}}}{(R_1 + R_2 + R_3) \cdot 2^{N_{\text{DAC}}}} = \frac{5 \text{ V}}{(100 \Omega + 1 \text{ k}\Omega + 10 \text{ k}\Omega) \cdot 2^{16}} = 6.87 \text{ nA} \end{cases} \quad (3.18)$$

The resolution meets the specifications but the maximum current is lower with respect to the maximum current that can achieve.

- Design considerations

The current division is useful to get higher resolution at lower current but lower resolution for higher current. For all the regions, the resolution in the reading is fixed by the parameters of the ADC (equation 3.2) and the value of the resistor R_1 :

$$\Delta I_{\text{READING}} = \frac{V_{\text{ADC}_{\text{IN}}}}{R_1 \cdot 2^{N_{\text{ADC}}}} = \frac{0.625 \text{ V}}{100 \Omega \cdot 2^{23}} = 745.06 \text{ pA} \quad (3.19)$$

On the firmware, the plant voltage V_{PLANT} is directly the measurement from the respective input of the ADC ADC_{PLANT} while the plant current I_{PLANT} is derived from the Ohm's law reading the voltage across the resistance R_1 so the input of the ADC ADC_{SENSE} :

$$\begin{cases} V_{\text{PLANT}} = ADC_{\text{PLANT}} \\ I_{\text{PLANT}} = \frac{ADC_{\text{SENSE}}}{R_1} \end{cases} \quad (3.20)$$

The electronic load circuit designed is shown in Figure 3.16.

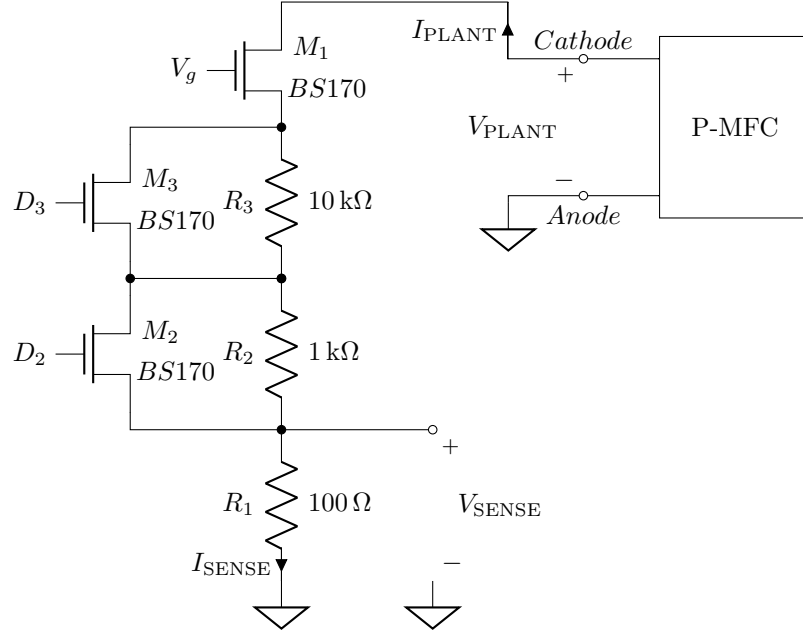


Figure 3.16: Electronic load circuit designed

3.2 Temperature sensing and design

Once the electronic load circuit is defined, one can start to analyze the environmental sensors. First the ambient temperature sensor is described. For this thesis, it is assumed to use a plant able to live in an office environment so with temperature range $10^{\circ}\text{C} \rightarrow 40^{\circ}\text{C}$ with an accuracy of $\pm 1^{\circ}\text{C}$.

3.2.1 DHT22 - Air temperature and humidity sensors

On the market, different kind of temperature sensors are available. A lot of solutions implement in the same package both air temperature and air humidity sensor. An example is the DHT22 [50] (Figure 3.17). It is a low-cost component with capacitive humidity sensor and a thermistor to measure surrounding air and send a digital signal on the output pin. The temperature ($-40^{\circ}\text{C} \rightarrow 80^{\circ}\text{C}$, $\pm 0.5^{\circ}\text{C}$) and humidity ($0\% \rightarrow 100\%$, $\pm 5\%$) ranges meet the specifications of the thesis and the accuracy as well. The only limitation is given by the maximum sampling rate of 0.5 Hz so it is not possible to sample the sensor before than every 2s. This component could be a good candidate but the humidity must be measured mainly in the soil because the humidity in the air less affects the conditions of the P-MFC. Since the humidity sensor in the package is useless, a different solution with only air temperature sensor is explored.

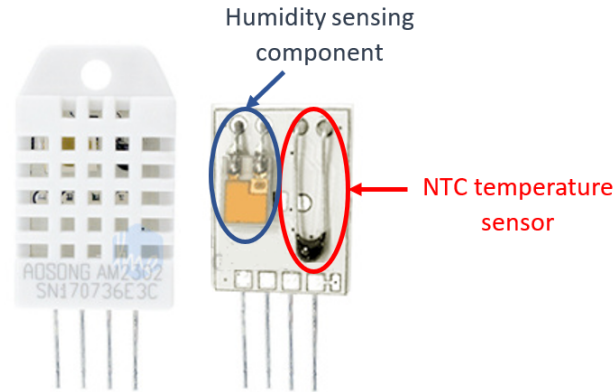


Figure 3.17: Internal view of DHT22

3.2.2 LM335 - Temperature sensors

A different solution is to use the LM335 [51] that is an integrated temperature sensor. The temperature range ($-40^{\circ}\text{C} \rightarrow 100^{\circ}\text{C}$) but the accuracy (typical after calibration: $\pm 2^{\circ}\text{C}$) is higher than the thesis specification. Another drawback is the essential use of a resistor to bias the sensor (zener) and a potentiometer for the calibration (Figure 3.18).

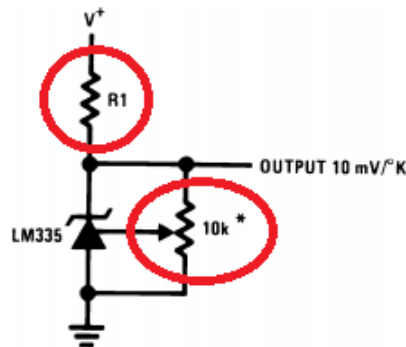


Figure 3.18: Circuit with calibration and bias resistors for LM335 [51]

3.2.3 LM35 - Temperature sensors

A better choice can be LM35DZ [52]. It is an integrated temperature sensor with an output voltage linearly-proportional to the temperature. This characteristic simplifies the design since it does not require preconditioning for Kelvin to Centigrade conversion. This device does not require neither external calibration or trimming



Figure 3.19: LM35DZ

nor resistor for bias the sensor. It meets the temperature range requirement of the thesis because the bound are $-55^{\circ}\text{C} \rightarrow 150^{\circ}\text{C}$ with an ensured accuracy of $\pm 0.5^{\circ}\text{C}$ at 25°C .

Design procedure

The output voltage V_{OUT} of the sensor with respect the temperature T is linked by its sensitivity S and the offset voltage V_{OFFSET} :

$$V_{\text{OUT}} = S \cdot T + V_{\text{OFFSET}} \quad (3.21)$$

The output voltage is an analog signal so a dedicated input of the ADC is used to acquire this voltage and, in the firmware, convert it into a temperature value. The maximum voltage that the ADC is able to measure is $V_{\text{ADC}_{\text{MAX}}} = 625 \text{ mV}$ (derived in Electronic load design equation 3.4) so there is an upper limit in the temperature measurable T_{MAX} . The equation 3.21 must be estimated in the maximum voltage range $V_{\text{OUT}_{\text{MAX}}}$:

$$V_{\text{OUT}_{\text{MAX}}} = S \cdot T_{\text{MAX}} + V_{\text{OFFSET}} \rightarrow T_{\text{MAX}} = \frac{V_{\text{OUT}_{\text{MAX}}} - V_{\text{OFFSET}}}{S}$$

From the datasheet of the component [52], the sensitivity $S = 10 \frac{\text{mV}}{\text{mC}}$ and $V_{\text{OFFSET}} = 0 \text{ mV}$ are obtained and due to the direct connection (without partition) between the output pin sensor and the input of the ADC the $V_{\text{OUT}_{\text{MAX}}} = V_{\text{ADC}_{\text{MAX}}}$:

$$T_{\text{MAX}} = \frac{V_{\text{OUT}_{\text{MAX}}} - V_{\text{OFFSET}}}{S} = \frac{V_{\text{ADC}_{\text{MAX}}} - V_{\text{OFFSET}}}{S} = \frac{625 \text{ mV} - 0 \text{ mV}}{10 \frac{\text{mV}}{^{\circ}\text{C}}} = 62.5 ^{\circ}\text{C}$$

Since T_{MAX} is higher than the thesis specification, no voltage division is needed. From the datasheet [52, p.1], the minimum temperature T_{MIN} is 2°C so also the lower bound allows to measure the desired temperature. Supposing to feed the sensor with the power supply of the RPi board (5V), that is high enough since the allowed range for the sensor is $4\text{V} \rightarrow 30\text{V}$, the power consumption is about $300\text{ }\mu\text{W}$ since it sinks a $60\text{ }\mu\text{A}$ to work properly. The pin of output signal V_{OUT}

is directly connected to the input of the ADC ADC_{TEMP} . In the firmware, the relationship to estimate the temperature T from the voltage reading ADC_{TEMP} :

$$T(^{\circ}\text{C}) = \frac{ADC_{\text{TEMP}}(\text{mV}) - 0 \text{ mV}}{10 \frac{\text{mV}}{^{\circ}\text{C}}} \quad (3.22)$$

The whole temperature sensor circuit as block scheme is shown in Figure 3.20.

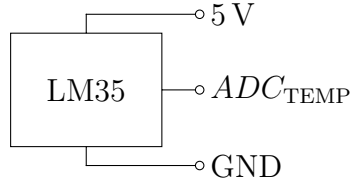


Figure 3.20: Temperature sensor block

3.3 Humidity sensing and design

Another important environmental parameter to measure is the relative humidity of the soil. A possible solution is the moisture sensor. As depicted in Figure 3.21, the sensor has two large and exposed pads as probes which act as a variable resistor R_{PROBE} . The sensor has the capability to measure the relative humidity of the soil up to a depth of 38 mm.

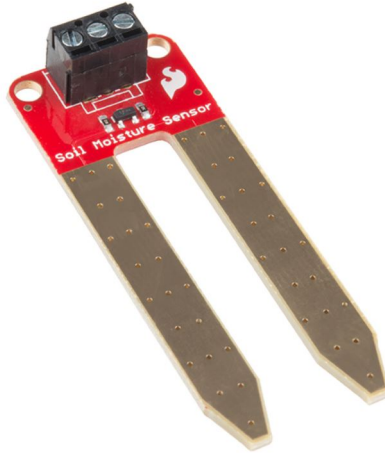


Figure 3.21: Moisture sensor

The higher is the humidity in the soil the better conductivity between the pads will be, resulting in a lower resistance and a higher output voltage.

Design procedure

Figure 3.22 shows the circuit mounted on the sensor board. This sensor module

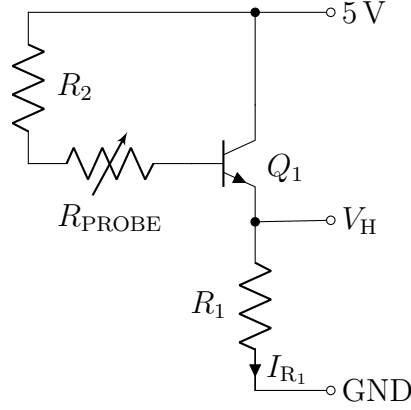


Figure 3.22: Internal circuit of moisture sensor

is an application of current amplifier that through a BJT Q_1 and the variable resistance $R_2 + R_{\text{PROBE}}$ set the current flowing in the load resistor R_1 . The variable resistance that sets the base current of Q_1 starts from an higher value ($R_{\text{PROBE}} \rightarrow$ tens of $M\Omega$) when the soil is dry while decreases up to the value of R_2 when it is completely wet ($R_{\text{PROBE}} \rightarrow$ few Ω). The voltage across this resistor becomes the output signal V_H proportional to the relative humidity of the soil. It is an analog output and it can be read from an input of the ADC. The power supply can go $2\text{ V} \rightarrow 5\text{ V}$ so it can be feed by the RPi board. Since the output signal can goes up to the power supply (5 V), it needs a voltage divider to adapt it to the input swing of the ADC. The voltage division can be implemented by only two series resistors R_6 and R_7 . The circuit with the internal and the external voltage divider component is shown in figure 3.23. The current flows in these two resistors I_{VD} must be "lower enough" with respect to the current I_{R_1} of the sensor. In order to obtain a relative accuracy of 0.5% in the humidity measure, one has to know the current flows in this condition and can be computed by the proportion $5\text{ V} : 100\% = V_H|_{0.5\%} : 0.5\%$ so the output signal V_H is:

$$V_H|_{0.5\%} = \frac{5 \cdot 0.5\%}{100\%} = 25\text{ mV}$$

and the current of the sensor I_{R_1} is:

$$I_{R_1}|_{0.5\%} = \frac{V_H|_{0.5\%}}{R_1} = \frac{25\text{ mV}}{100\ \Omega^2} = 250\ \mu\text{A} \quad (3.23)$$

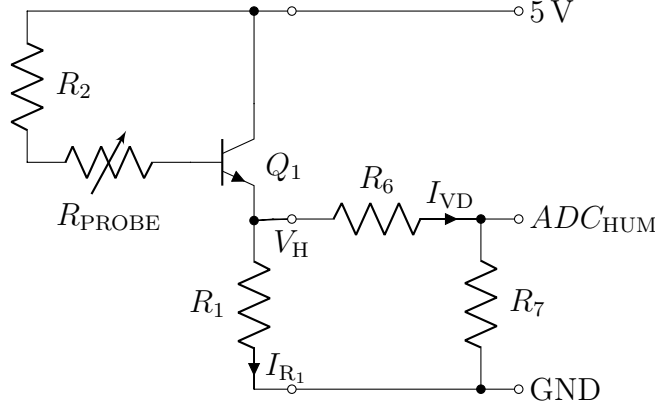


Figure 3.23: Internal circuit of moisture sensor with the external voltage divider

The current sinking by the voltage divider I_{VD} must be negligible with respect to this value to not affect the measurement voltage. In engineering field, it is usual to consider *lower enough* or *negligible* a value $\frac{1}{10}$ lower:

$$I_{VD}|_{0.5\%} = \frac{V_H|_{0.5\%}}{R_6 + R_7} < \frac{1}{10} I_{R_1}|_{0.5\%} \rightarrow R_6 + R_7 > 10 \frac{V_H|_{0.5\%}}{I_{R_1}|_{0.5\%}} = 10 \frac{25 \text{ mV}}{250 \text{ } \mu\text{A}} = 1 \text{ k}\Omega \quad (3.24)$$

The ratio between the output ADC_{HUM} and the input voltage V_H is defined as K . From a voltage divider:

$$ADC_{HUM} = V_H \cdot \frac{R_7}{R_6 + R_7} \rightarrow \frac{ADC_{HUM}}{V_H} = K = \frac{R_7}{R_6 + R_7} \quad (3.25)$$

From the equation 3.25, it is possible to derive the ratio between the two resistors in function of the parameter K :

$$R_6 = R_7 \frac{1 - K}{K} \quad (3.26)$$

The value of K is derived considering the maximum voltage situation so with the dynamic of the ADC $ADC_{HUM_{MAX}} = 0.625 \text{ V}$ and the signal $V_{T_{MAX}} = 5 \text{ V}$:

$$K = \frac{ADC_{HUM_{MAX}}}{V_{T_{MAX}}} = \frac{0.625 \text{ V}}{5 \text{ V}} = \frac{1}{8}$$

²On the datasheet $R_1 = 10 \text{ k}\Omega$ but for the thesis it is replaced on the PCB with a resistor of 100Ω

and replacing the value of K in the equation 3.26:

$$R_6 = R_7 \frac{1 - K}{K} = R_7 \frac{1 - \frac{1}{8}}{\frac{1}{8}} = 7 \cdot R_7 \quad (3.27)$$

With the result of 3.27 in 3.24 it is possible to derive and choose the proper value of the voltage divider resistors:

$$\begin{cases} R_6 + R_7 > 1 \text{ k}\Omega \rightarrow 8 \cdot R_7 > 1 \text{ k}\Omega \rightarrow \\ R_7 = 6.8 \text{ k}\Omega \\ R_6 = 7 \cdot R_7 = 7 \cdot 6.8 \text{ k}\Omega = 47.6 \text{ k}\Omega \rightarrow R_6 = 47 \text{ k}\Omega \end{cases}$$

In the firmware, the relationship to estimate the relative humidity of the soil RH from the voltage reading ADC_{HUM} :

$$RH(\%) = \frac{ADC_{\text{HUM}}(\text{V}) \cdot 100\%}{5 \text{ V}} \left(1 + \frac{R_6}{R_7} \right) \quad (3.28)$$

The whole humidity sensor circuit as block scheme is shown in Figure 3.24.

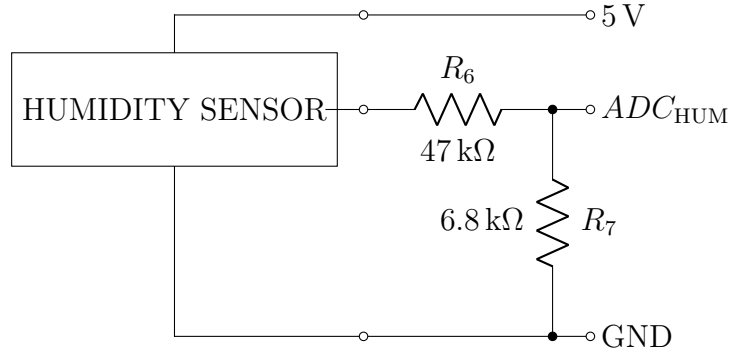


Figure 3.24: Internal circuit of light sensor with the external voltage divider

A good improvement could be to increase the value of the resistor R_1 to get lower power consumption while still getting a good ADC reading.

3.4 Light intensity sensing and design

Photosynthesis is the process in which light energy is converted into chemical energy. The light in the P-MFC system is an important component because is the fuel of the plant, so measuring the light intensity allows to understand how

it affects the energy production as well. The thesis focuses on understanding the possible energy variation due to the moments of the day for example in broad daylight rather than midnight. For this purpose, the High-precision AD/DA board is provided with a light sensor already mounted (Figure 3.25). The sensor is a light-



Figure 3.25: LDR on High precision AD/DA board

controlled variable resistor and is named photoresistor (LDR). The bias circuit is composed by a bias resistor in series to the LDR as shown in Figure 3.26. The

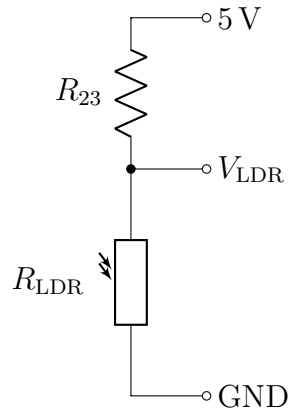


Figure 3.26: Bias circuit of the light sensor

resistance of a photoresistor decreases with increasing incident light intensity. In the dark, a photoresistor can have higher resistance ($R_{LDR} \rightarrow \text{several } M\Omega$) so the current flow in the branch is very low producing an high output voltage while in the light, the LDR can have a lower resistance ($R_{LDR} \rightarrow \text{few hundred } \Omega$) so there is an increasing in the current flow and lowering the output voltage. From the manual or the schematic, it is not possible to derive the relationship between light intensity and resistance because no info are provided but it can be used to understand the light variation or to understand the moment of the day. If the light intensity is kept constant, the resistance may still vary significantly due to temperature changes so they are unsuitable for precise light intensity measurements.

Design procedure

The Figure 3.26 shown the circuit on the board with the light sensor. The resistor R_{23} fixes the bias current and by placing in series the variable resistor R_{LDR} allows to read a voltage across the sensor proportional to the light intensity. The relationship between the incident light intensity falling on the device and the corresponding resistance of the sensor is the sensitivity S . Like the human eye, the sensitivity is dependent on the wavelength of the incident light. Since the sensitivity of the sensor is not given, only a theoretical estimation can be done. The relationship computed in the numerical example can be used just for an approximate estimation. Another assumption is that the relationship is linear but usually this kind of sensors have strongly non linearity behavior. In the thesis, one supposes the voltage V_{LDR} range is from 0 V up to the power supply voltage 5 V and this voltage V_{LDR} represents the percentage with respect to the supply voltage. Since an increasing of light means a decreasing of the output voltage, the voltage V_{LDR} is proportional to the dark intensity DI :

$$V_{\text{LDR}} = \frac{DI \cdot 5 \text{ V}}{100 \%} \quad (3.29)$$

The voltage V_{LDR} is out of the range of the input ADC ($V_{\text{ADCIN}} = 0.625 \text{ V}$) so a voltage divider composed by two series resistor R_4 and R_5 is needed (Figure 3.27). The complete circuit is depicted in Figure 3.27. As for the relative humidity sensor,

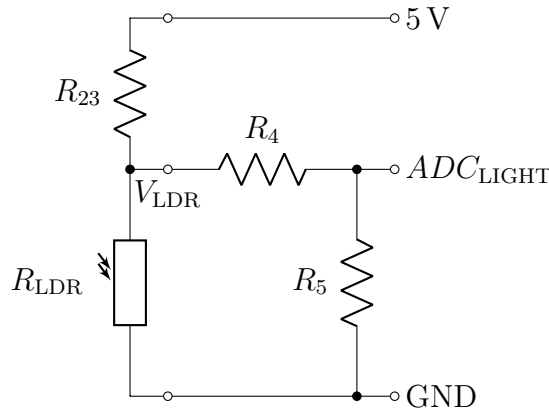


Figure 3.27: Internal circuit of the light sensor with the external voltage divider

the multiplicative factor K is equal to $\frac{1}{8}$. Since it is a voltage divider:

$$K = \frac{R_5}{R_4 + R_5} \rightarrow R_4 = R_5 \frac{1 - K}{K} \quad (3.30)$$

Estimation of the sensitivity and numerical example.

Assuming a linear behavior of the light intensity sensor, the sensitivity can be computed from two known points of the graph. Averaging different commercial datasheets, it is assumed that the two points are given as in the table:

Parameter	Conditions	Typical value	Unit
Cell resistance R_{CELL}	1000 lux	400	Ω
	10 lux	9000	Ω

The illuminance E_V represents the luminous flux incident per unit area and it is measured in lux. The characteristic from resistance R_{CELL} and illuminance E_V is approximated as a straight line

$$R_{\text{CELL}} = S \cdot E_V + R_{\text{OFFSET}}$$

so this curve has a slope (sensitivity S):

$$S = \frac{9000 \Omega - 400 \Omega}{10 \text{ lux} - 1000 \text{ lux}} \approx -8.68 \Omega/\text{lux}$$

but also an offset (resistance R_{OFFSET}) and can be computed in one of the two point:

$$R_{\text{OFFSET}} = R_{\text{CELL}} - S \cdot E_V = 9000 \Omega - -8.68 \Omega/\text{lux} \cdot 10 \text{ lux} \approx 9000 \Omega$$

So the relationship can be written as:

$$R_{\text{CELL}} = -8.68 \Omega/\text{lux} \cdot E_V + 9000 \Omega$$

With this function, it is possible to estimate the cell resistance in a dark day (500 lux) and in deep twilight condition (1 lux):

$$\text{Dark day} \rightarrow R_{\text{CELL}} = -8.68 \Omega/\text{lux} \cdot 500 \text{ lux} + 9000 \Omega = 4.66 \text{ k}\Omega$$

$$\text{Deep twilight} \rightarrow R_{\text{CELL}} = -8.68 \Omega/\text{lux} \cdot 1 \text{ lux} + 9000 \Omega \approx 9 \text{ k}\Omega$$

Since it is just important to understand in which period of the day the measurements are made, the value of the resistors are taken in usual range:

$$\begin{cases} R_5 = 1.5 \text{ k}\Omega \\ R_4 = R_5 \frac{1-K}{K} = 1.5 \text{ k}\Omega \frac{1-\frac{1}{8}}{\frac{1}{8}} = [10.5 \text{ k}\Omega]^3 \rightarrow R_4 = 12 \text{ k}\Omega \end{cases}$$

At this point, the function between the dark intensity DI and the voltage at the input of the ADC ADC_{LIGHT} is:

$$ADC_{\text{LIGHT}} = V_{\text{LDR}} \cdot K = \frac{DI \cdot 5 \text{ V}}{100 \% } \frac{R_5}{R_4 + R_5} \quad (3.31)$$

From the equation 3.31, it is possible to estimate the dark intensity from the voltage reading at the input of the ADC:

$$DI = \frac{ADC_{\text{LIGHT}} \cdot 100 \% }{5 \text{ V}} \frac{R_4 + R_5}{R_5} \quad (3.32)$$

but our goal is to estimate the light intensity $LI = 100 \% - DI$ so:

$$LI = 100 \% - \frac{ADC_{\text{LIGHT}} \cdot 100 \% }{5 \text{ V}} \frac{R_4 + R_5}{R_5} \quad (3.33)$$

In the firmware, the relationship to estimate the light intensity LI from the voltage reading ADC_{LIGHT} :

$$LI(\%) = 100 \% \left[1 - \frac{ADC_{\text{LIGHT}}(V)}{5 \text{ V}} \left(1 + \frac{R_4}{R_5} \right) \right] \quad (3.34)$$

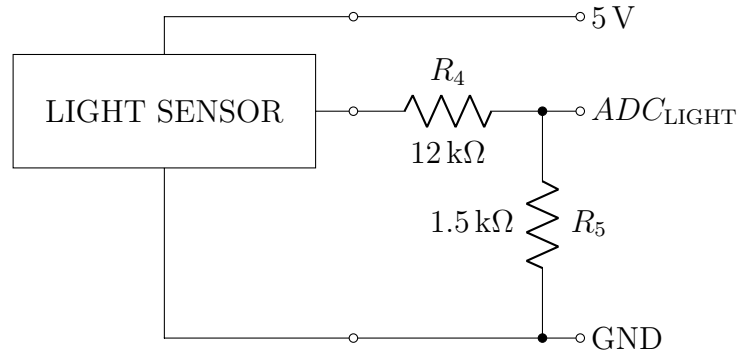


Figure 3.28: Internal circuit of light sensor with the external voltage divider

³The round up operation is made considering the E12 series of resistor.

Chapter 4

Ad-hoc automatized sensing system: software and test

After the description and the design of the electronic load board with also the conditioning circuitry for the sensors, the attention must be focused on how manage the system in an automatized way. This chapter is focused on the software part (Figure 4.1). The RPi is the core of the system and it must be able to communicate with both the high precision AD/DA board and the PC.

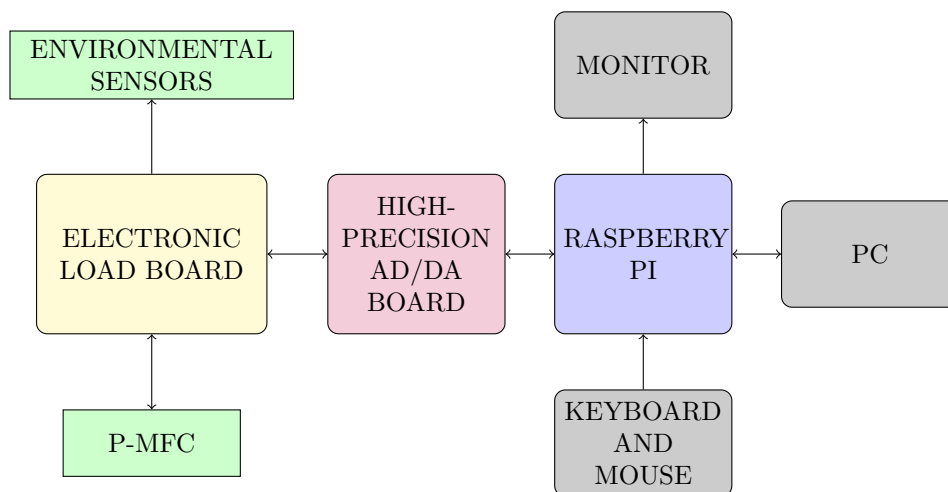


Figure 4.1: Basic scheme of the system

From the high precision AD/DA board side, it must be able to manage the sensing system during the analysis while once the measurements are obtained, they must be sent to the PC for post-processing analysis. The RPi is a single-board computer developed in United Kingdom by the Raspberry Pi Foundation in 2012. In this

thesis, it is used the version 3 model B and the main characteristics are summarized in the table 4.1. It contains the Raspbian OS (booted from a microSD card).

SoC	Broadcom2837
CPU	1.2 GHz quad-core ARM Cortex A53
Memory (SDRAM)	1 G LPDDR2 shared with GPU
USB Port 2.0	4
Memory	microSD
Network connections	Ethernet 10/100 Mbit/s
I/O connections	GPIO 40 pin

Table 4.1: Raspberry Pi 3 model B Vi.2 specifications [44, p. 14]

In order to use it as a desktop computer, some external devices are connected like a monitor through an HDMI cable, a keyboard and a mouse with USB cables. Once the microUSB power supply is connected, it is possible to use it like a PC. It can be programmed in order to perform the algorithm to manage the automatized sensing system. The code should be written as independent as possible with respect to the kind of measurements it will perform. Since the galvanostat method is used, the main task of the algorithm is to keep the desired current profile and measure both the quantities under measurement (e.g. voltage and current) and the environmental parameters (Figure 4.2). All the measurements will be stored in a dedicated file.

The RPi board is also connected to a PC through Ethernet cable. On it, an user interface is installed in order to allow the easiest and most intuitive management possible of the whole sensing system i.e. automatized system by an user. The user is able through this interface to choose the parameters and the type of the analysis (calibration, static or dynamic) that the system has to perform. After the analysis, the measurements will be acquired and then post-processed. The Figure 4.3 shows graphically a summary of the analysis flow using the user interface. This chapter will describe in detail the implemented algorithm on the RPi and the user interface application with their circuitual configuration. At the end of the chapter, the whole system will be tested to check its behavior by replacing the P-MFC with a known load connected e.g. 1-time constant electronic circuit.

4.1 Raspberry Pi interface

The firmware implemented on the RPi manages the sensing system. The interface between the RPi and the sensing system is the High precision AD/DA board (Figure 4.4).

The AD and DA converters present on high precision AD/DA board have a SPI-compatible serial interface. The System-on-a-chip (SoC) BCM2837 [53] of the RPi

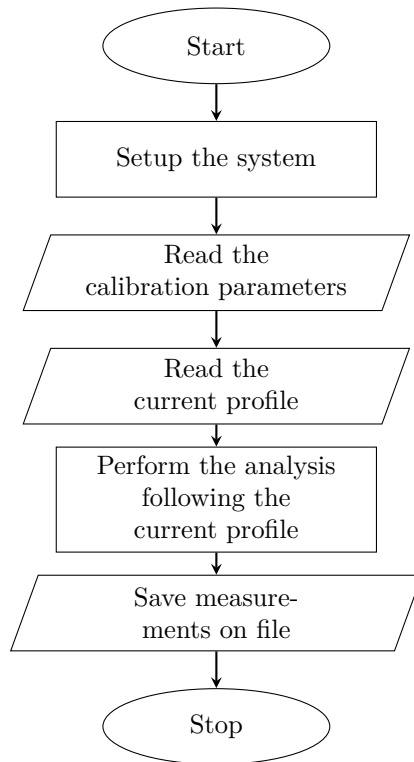


Figure 4.2: Short flow chart of the algorithm on the Raspberry Pi

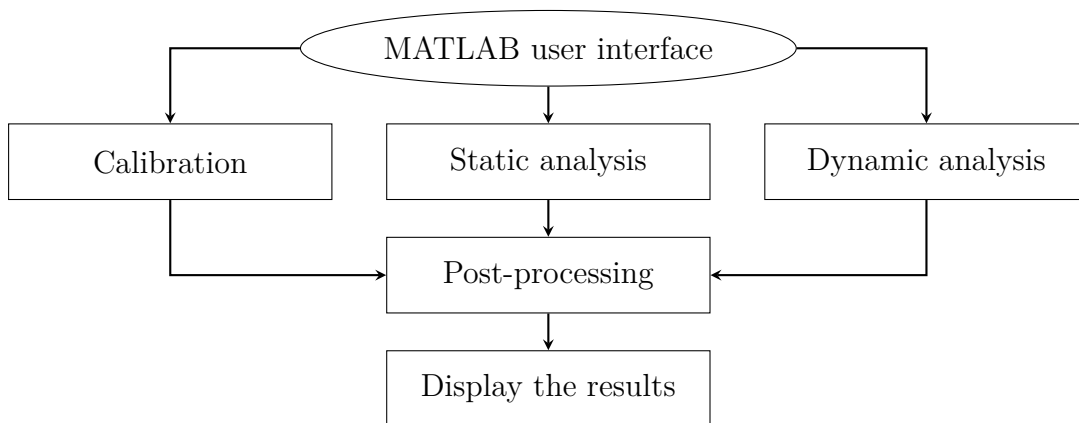


Figure 4.3: Analysis flow using the user interface

integrates the CPU and different peripherals as well on the same chip. One of the peripherals on this SoC is the SPI block.

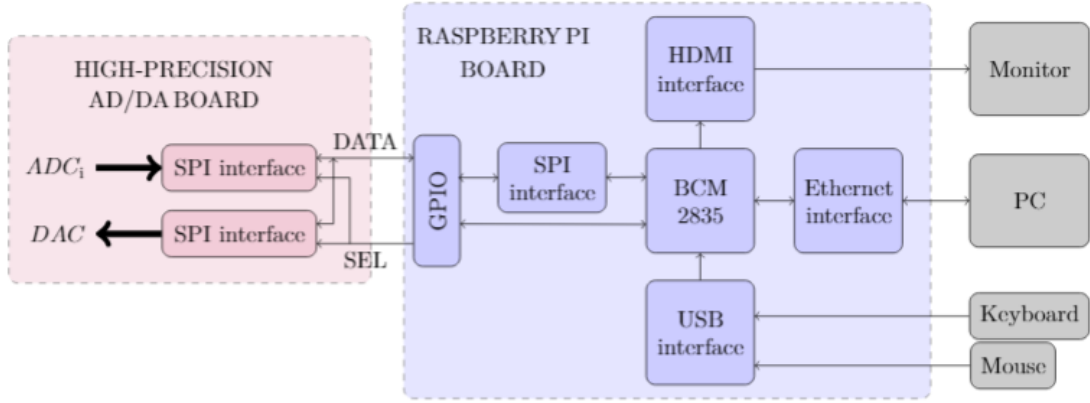


Figure 4.4: Basic scheme of the system

Communication protocol with High precision AD/DA board

Since both the RPi and high precision AD/DA board have the SPI block component, the SPI is the communication protocol used to communicate between them.

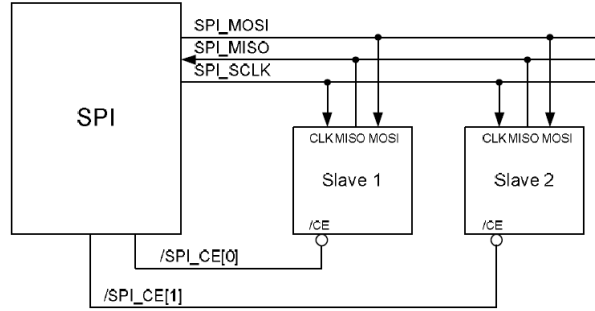


Figure 4.5: SPI Master of BCM2835 [53, p.148]

The SPI implements 2-wire serial protocol in standard mode so using the MISO and MOSI bus. The protocol specifies four logic signals: the serial clock (SCLK) output from the master, a bus for data output from the master (Master Out Slave In: MOSI), a bus for the data output from the slave (Master In Slave Out: MISO) and a signal output from the master to select the slave (Slave Select: SS) (Figure 4.5). The RPi is the master while the ADC and DAC are the slaves. These pins are directly connected and available on the GPIO port of the RPi board (Figure 4.6). The clock signal is provided by the master (i.e. RPi) and also the SS signals. There are two signal SS in this case because one needs for the ADC and other one for the DAC.

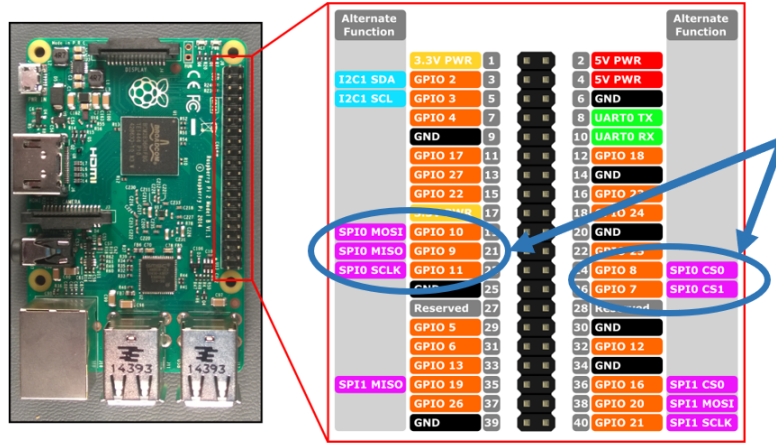


Figure 4.6: SPI pins on the GPIO of the Raspberry Pi

4.2 Firmware on the Raspberry Pi

In what follows, the measurement algorithm is described in detail. The firmware to perform this algorithm is written in C language and the most important part are listed in Appendix B. As previously explained, the code written on Raspberry Pi must be as independent as possible with respect the type of analysis has to be done.

System set up

Before to start with the measuring algorithm description, the system must be set up correctly. The first thing is to define the libraries that will be used during the algorithm development like `bcm2837` and `wiringPi` which enable the use of the general-purpose input-output (GPIO). The system has to impose a current flows into the load and measure the voltage across it. The value of the current has to be defined in each time instant i.e. current profile. These values are picked up from a file with a structure similar to Figure 4.7. In the next section, the calibration will be described in detail and this operation provides some corrective parameters i.e. calibration parameters, used to adjust the sensing system in order to provide more accurate readings. These parameters are defined for each current interval and are picked up from a dedicated file. The last thing to do before the analysis is to set up the ADC and the DAC converters with the parameters defined in hardware design part: the programmable gain amplifier $PGA = 8$, the voltage reference $V_{REF} = 2.5\text{ V}$, the sample rate $f_s = 25\text{ SPS}$, the number of channel $N_{CH} = 8$ for the ADC and the initial value of the output of the DAC V_{DAC} . The value V_{DAC} is set initially just larger than the threshold voltage of the MOS M_1

```

SIMULATION PARAMETERS
t_sample[s]= 1
t_sim[s]= 54000
*****
CURRENT PROFILE
t[s]      I[uA]
0         0.0
20        2.0
40        1.0
60        6.0
5400      2.4
10800     3.6
16200     4.8
21600     6.0

```

Figure 4.7: Example of current profile saved on file

(Figure 3.14) in order to have the system immediately reactive. Since the ADC read a digital value, it is useful to define also the maximum value ADC_{MAX} than can be read:

$$ADC_{MAX} = 2^{N_{ADC}-1} = 2^{24-1} = 8\,388\,607 \text{ LSB}$$

In this case it is considered $N_{ADC} = 24$ bit because is the parallelism with which the acquired data are provided. On the high-precision AD/DA board, there are two LEDs which can be connected through a jumper to the outputs of the DAC. Since one of the two output of the DAC is always free, it is connected to one LED (Figure 4.8) as a flag to warn when the analysis is over so initially it is switched off.



Figure 4.8: LED used as flag to warn when the analysis is over

4.2.1 Measurement algorithm

At this point, the algorithm that performs the analysis can be described.

Parameters estimation

First the measured values are acquired from all the channels of the ADC. From the measurements it is possible to estimate all the quantities under measurement using the formula derived in the previous chapter (equations 3.20, 3.22, 3.28, 3.34). The estimate of the current is subjected to a correction derived from the calibration operation. The calibration parameters file provides the correction gain FC and offset adjustment I_{OFF} :

$$I_{\text{SENSE_ADJUSTED}} = I_{\text{SENSE_MEASURED}} \cdot FC + I_{\text{OFF}} \quad (4.1)$$

The correction factors are provided to adjust the current readings for all the regions so the algorithm is able to choose, depending on the region, the proper parameters. The Figure 4.9 shows a practical example for a single region to understand how are the measurement before (Figure 4.9a) and after (Figure 4.9b) the adjustment compared to a reference value.

Keep the current constant

After the measurements, there is a critical phase: the voltage V_g has to be processed in order to keep the current constant. This voltage is modified at each sample time by adding or removing a step voltage V_{STEP} . It is computed depending how different are the sampled current I_{SENSE} and the nominal one I_{NOM} : higher difference leads to a large V_{STEP} while similar currents produce small voltage step. Due to the non-linear relationship between the gate voltage and the drain current (trans-characteristic in Figure 4.10) of a MOSFET, the amplitude of the voltage step does not have to depend only on the current difference. To have a step current, a smaller voltage step is needed at higher current value while at lower current value an higher voltage step is required. The simplest method could be to use the relative difference of current instead of using the absolute one. The relationship between the voltage step V_{STEP} and the measured current I_{SENSE} is linear:

$$V_{\text{STEP}} = m \frac{I_{\text{SENSE}} - I_{\text{NOM}}}{I_{\text{NOM}}} \quad (4.2)$$

where the coefficient m relates the amplitude of the voltage step with respect the relative current variation and it is expressed in $\frac{\text{V}}{\mu\text{A}}$. This parameter is produced during the calibration for all the current regions. The Figure 4.11 shows graphically the amplitude of the voltage step V_{STEP} with respect the measured current I_{SENSE} when varying the nominal current value I_{NOM} . The adjustment of the gate voltage V_g of the MOS M_1 is important because it sets the time needed to reach current step but also if the variation is too high, the risk is to have too large oscillation across the steady state (ringing). An improvement to reduce the current ringing

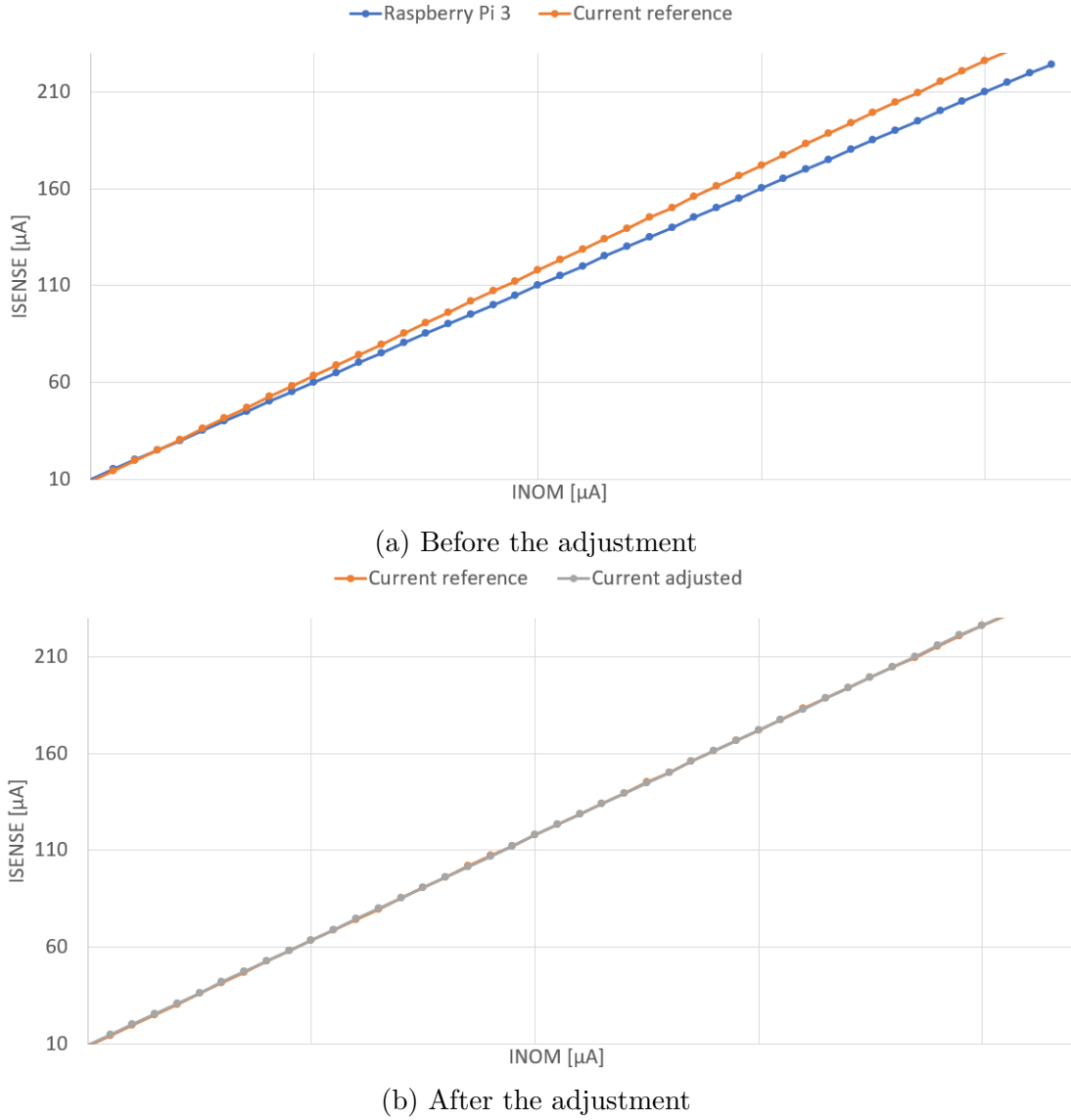


Figure 4.9: Adjustment process after calibration operation

is provided by setting a margin. This margin is defined for each current region and it represents the maximum difference current at which no voltage variation occurs. This margin is named I_{ERROR_MAX} and it is provided with the calibration parameters. The I_{ERROR_MAX} must be at least higher than the current resolution of the range. The Figure 4.12 shows a graphical example of this improvement. The orange line represents the desired current while the two dashed lines are the interval: when the acquired data are inside this interval, the voltage V_g is not changed while the acquired data are outside the voltage will be modified.

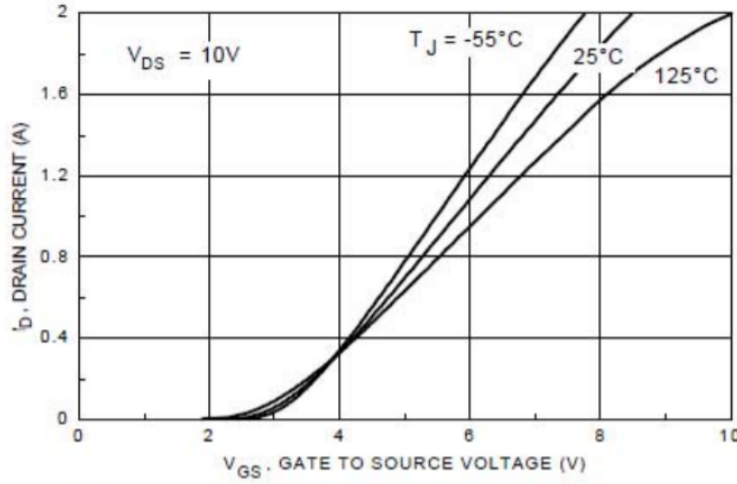
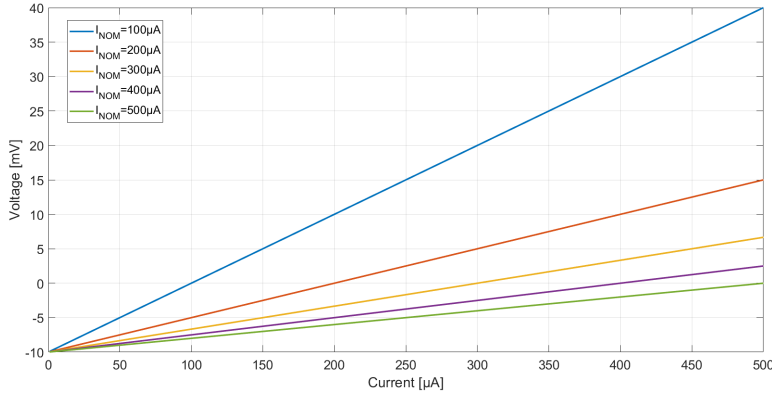


Figure 4.10: Transfer characteristic of BS170

Figure 4.11: V_{STEP} with respect I_{SENSE} with different I_{NOM}

Region transitions

Another consideration must be done about the change from a region to another one. During this transition two operation must be performed: switching on or off of the MOSFETs depending on the region but also the arrangement of the V_{DAC} . This process is done because, for example, in the jump from region 2 to region 3, the upper bound of the region 2 with a defined load resistance means a certain gate voltage value V_{g2} while passing at region 3, the load resistance has a large variation but the gate voltage has a slower transient meaning a large step in current (orange curve of Figure 4.13a). This phenomena has to be reduced and can be made by modifying properly also the voltage V_g when there is a transition from a region to another one (orange curve of Figure 4.13b).

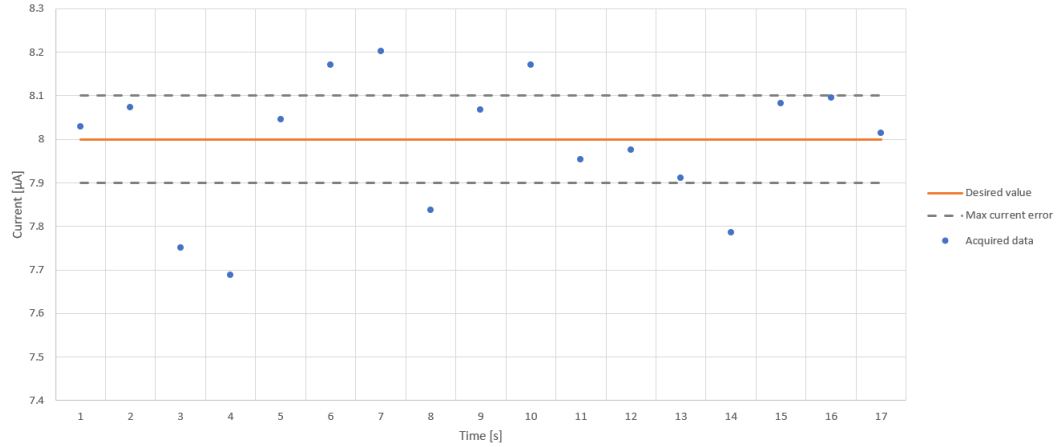
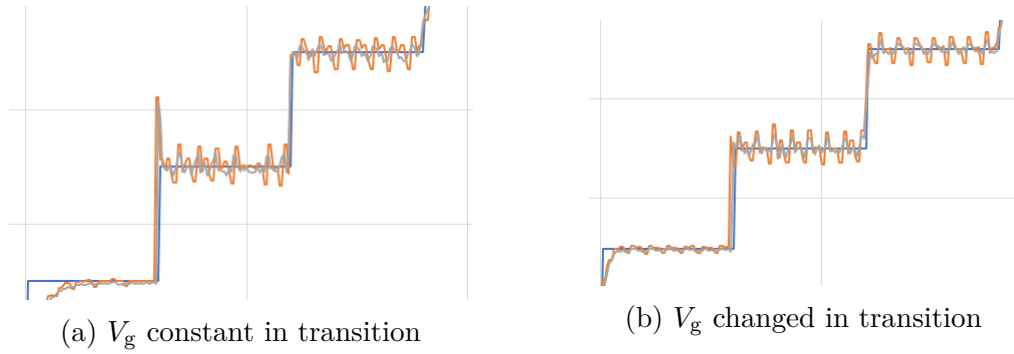
Figure 4.12: Graphical example of the $I_{\text{ERROR}_{\text{MAX}}}$ interval

Figure 4.13: Compensation of current step problem in region transition

Not only how set up the parameters during the transition is important but also when. Initially the system chose the region depending on the desired current at a determined time instant. This approach could be the first idea because it works properly if we use a load close to that used during the design. Since the system is used to characterize a generic load, the circuit under test could be very different and it can creates some problems. A different solution exploit uses a dynamic behavior: the system should understand when reaching the bounds of the region without achieve the desired current and be able to change region automatically. Instead to use complex timing control mechanisms on the current, it is a better idea to control the output voltage of the DAC. The output voltage of the DAC V_{DAC} has not to be read because it is a variable already inside the firmware so the control must be performed without modifying the hardware (software control). The Figure 4.14 shows a practical example: the blue line represents the measured current while the orange dashed line the desired one.

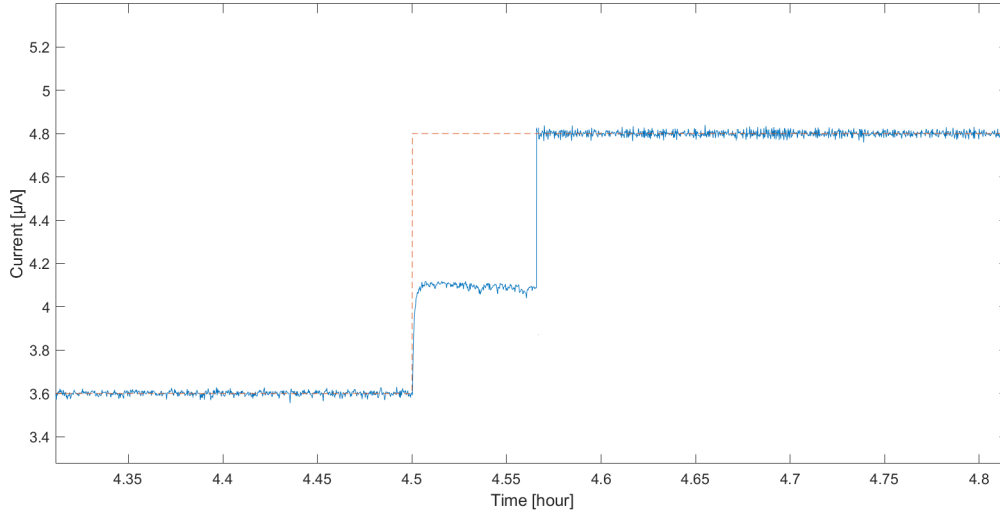


Figure 4.14: Graphical example of the $I_{\text{ERROR_MAX}}$ interval

Up to 4.5 h the desired current is set to 3.6 μA while at this point the next current value is 4.8 μA but it is possible to observe that it reaches a current limit lower with respect the desired one although the value is designed to be inside the range. With the optimized approach, since the current does not reach the desired value, the system keeps to increase voltage at the gate of the transistor; once this value reaches its maximum, it understand automatically that it needs to change region and then it can achieve the desired current value. This mechanism takes time but since the system is very slow, this does not create problems.

Data backup

All these operations just described mean the core of the sensing algorithm. After that, it waits up to the end of samples time t_{SAMPLE} and then prints the estimates on screen. This loop is repeated till the end of the analysis. At the end, it saves the results on file and closes the open libraries. The flow chart of the main program is shown in Figure 4.15.

Code considerations

The main interesting part of the code written on the Raspberry Pi can be found at the Appendix B. The structure of the code is hierarchic: a main file contains the set up and the sensing algorithm while separate files (libraries) contain the used functions at a lower level. Each library is composed by the header *.h* and by the file contains the functions *.c*. One library is dedicated to the functions related the

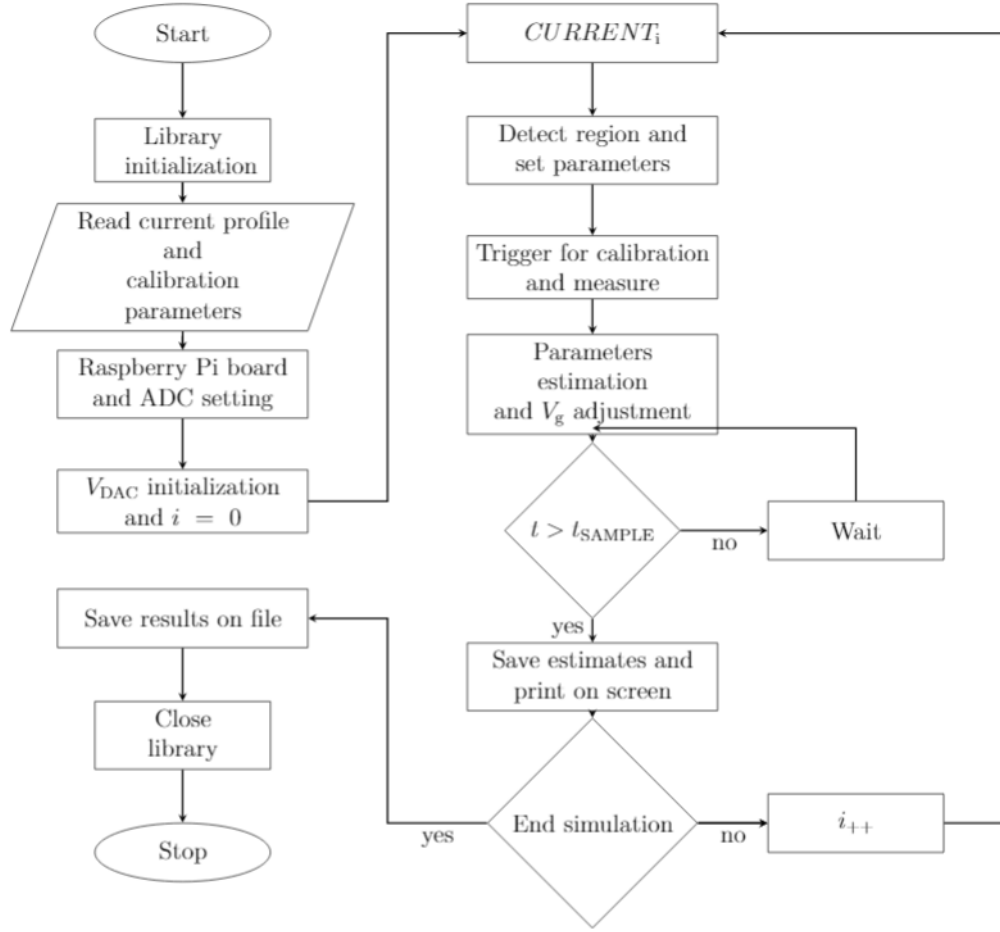


Figure 4.15: Flow chart of the main program

settings, communications and commands for the ADC and DAC while the second one the functions related to the reading/writing from/to the files.

4.3 User interface application

Up to this point, the firmware present on the RPi board has been analyzed. In what follows, a graphical interface will be described in detail that is useful to make the use of the sensing system easier i.e. user interface application (UIA). The aim of this UIA is to exchange info with the RPi: it gives the parameters to the RPi to perform an analysis, get back its measurements for post-processing operation and shows on a screen the results. The MATLAB environment is used to create the application by the App Designer tool.

4.3.1 Use of the application

The PC is connected to the Raspberry Pi board through an Ethernet cable. The RPi board has be connected to the sensing system.

Access to Raspberry Pi board and project folder definition

First, a connection between PC and RPi board must be created. The access to the RPi board can be done through IP address (Figure 4.16).

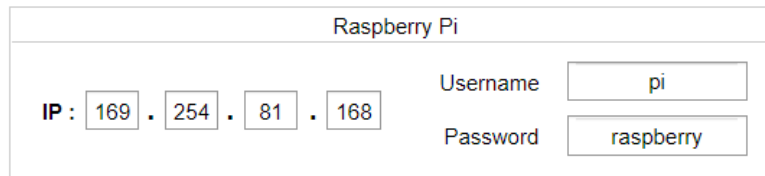
A screenshot of a web-based interface titled "Raspberry Pi". It contains two rows of input fields. The first row is for IP address, labeled "IP :", followed by four input boxes containing the numbers "169", "254", "81", and "168" separated by dots. The second row has two fields: "Username" with an input box containing "pi", and "Password" with an input box containing "raspberrry".

Figure 4.16: Raspberry Pi interface window

On the PC, the project folder must be selected for MATLAB environment, where it saves the several files produced and where the file downloaded from RPi has to be saved (Figure 4.17).

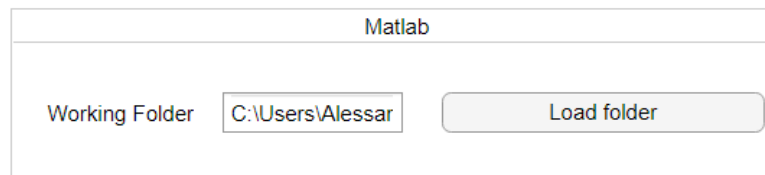
A screenshot of a web-based interface titled "Matlab". It features a label "Working Folder" followed by an input box containing the path "C:\Users\Alessar". To the right of this input box is a button labeled "Load folder".

Figure 4.17: Matlab folder window

Static analysis

The static analysis allows to obtain the polarization curve of the load connected to the sensing system. For this thesis, measurements are made galvanostatically. In practice, the P-MFC is subjected to a given current and the voltage response is monitored until it no longer changes significantly in time so the transient is extinguished. Its voltage and current are recorded. Then, the current is increased to a new predetermined value and the procedure is repeated. In a scan galvanostatic measurement, the current demanded from the P-MFC is gradually scanned in time from zero to some predetermined limit. The equivalent model circuit for the P-MFC derived from the the usual shape of the polarization curve is shown in

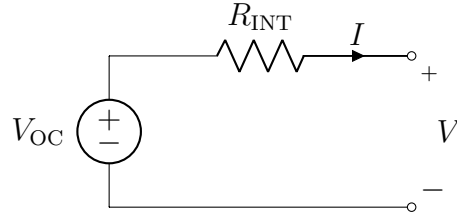


Figure 4.18: Static model for the P-MFC

Figure 4.18. A window is dedicated to perform the static analysis. Before to start, different parameters have to be defined: the time between two different current values t_{INTERVAL} , the current bounds I_{min} and I_{MAX} and the number of point N inside the range. Each point of the V-I graph is computed averaging the samples acquired after the transient. The parameter t_{AVERAGE} indicates the last second of each interval to be averaged. It is possible to insert the electrode area in m^2 in order to show the V-I curve and the power of the P-MFC with respect the current density (Figure 4.19 item 1). Different buttons can perform the generation of current profile and uploading on the Raspberry Pi board, the downloading from the board after the measurements and the analysis of the results (Figure 4.19 item 2). There is the possibility to estimate the static parameters (V_{OC} and R_{INT}) of the equivalent static model of the P-MFC from the measurements acquired. Results from the acquired data and a curve generated from the estimated values can be compared in a graphical way (Figure 4.19 item 3).

Figure 4.19: Static analysis interface window

Dynamic analysis

The dynamic analysis allows to obtain the characteristics related to model the transient between two operating point. For this purpose, the EIS with white noise is the used technique. It is convenient to use a wide-band signal i.e. white noise to largely reduce the time needed for the analysis. The input current is a pseudo random binary sequence with a flat power spectral density on a chosen frequency band. The white noise is superimposed on current bias current. This current signal is applied to the system under test (e.g. P-MFC) and the voltage across it is measured. The system depends on several internal and external conditions but they are assumed to be constant during the measurement process such that the system can be considered as time-invariant system. The white noise amplitude is imposed small enough to have a linear response. The estimation of the electrical impedance $Z(f)$ is defined:

$$Z(f) = \frac{S_{vi}(f)}{S_{ii}(f)}$$

In order to estimate $Z(f)$, a non recursive wide-band frequency estimation with Welch modified method is applied. First $S_{vi}(f)$ and $S_{ii}(f)$ are estimated by Welch modified periodogram. Then the data are divided into L blocks of the same length by using a time window and their FFT is computed. The results obtained in each block are averaged. The choice of the window is very important because allows to distribute the spectral leakage in different ways, according to the needs of the particular application. The duration of the segments sets the frequency resolution of the FFT. Another important aspect is the overlapping window that helps to mitigate the loss at the edges of the window. This operation can be done by the Matlab code `[pxx,f] = pwelch(x>window,noverlap,f,fs)`. Starting from the static model, the resistance R_{INT} is replaced by an impedance Z that is able to consider also the dynamic behavior of the system.

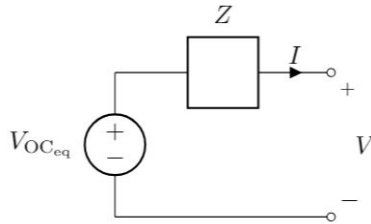


Figure 4.20: General equivalent circuit of P-MFC with impedance

The behavior of P-MFC can be approximated with a circuit with two time constants [?] so the impedance can be replaced by an equivalent circuit (Figure 4.21)

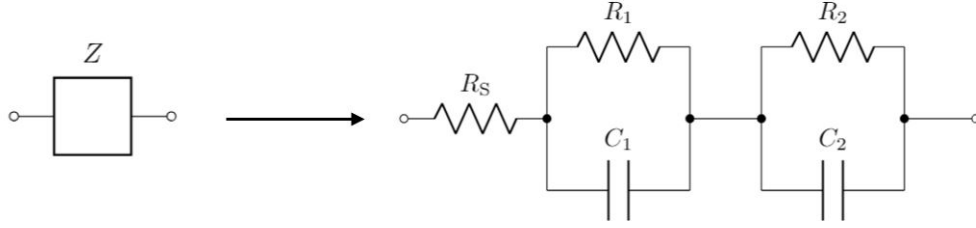


Figure 4.21: Equivalent complex impedance with two time constants

where each component represents some phenomena or is due to some element present inside the configuration. The transfer function of this impedance is:

$$Z(s) = (R_S + R_{P1} + R_{P2}) \frac{1 + s \frac{R_S(R_{P1}C_1 + R_{P2}C_2) + R_{P1}R_{P2}C_1C_2}{R_S + R_{P1} + R_{P2}} + s^2 \frac{R_S R_{P1} R_{P2} C_1 C_2}{R_S + R_{P1} + R_{P2}}}{1 + s(R_{P1}C_1 + R_{P2}C_2) + s^2 R_{P1} R_{P2} C_1 C_2} \quad (4.3)$$

From the denominator of equation 4.3, one can obtain the equation of the zeros and poles. Important for our purpose are the pole frequencies:

$$f_{P1} = \frac{1}{2\pi R_{P1} C_1} \quad (4.4)$$

$$f_{P2} = \frac{1}{2\pi R_{P2} C_2} \quad (4.5)$$

A possible representation of the transfer function in equation 4.3 is shown in Figure 4.22

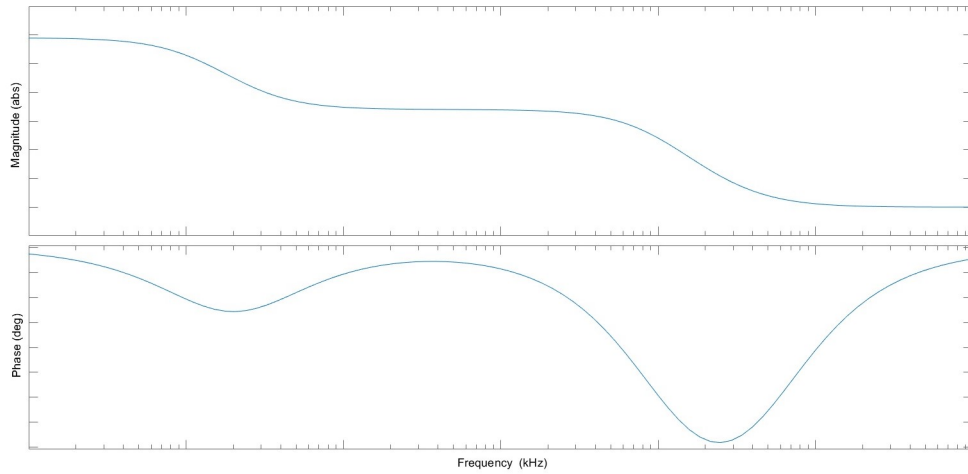


Figure 4.22: Bode diagram of equivalent two time constants circuit

A window is dedicated to perform the dynamic analysis (Figure 4.24). The useful parameters are the time between two different current values t_{INTERVAL} , the duration of the analysis t_{ANALYSIS} and also the characteristics of the white current noise so its amplitude $I_{\text{AMPLITUDE NOISE}}$ and bias $I_{\text{BIAS NOISE}}$ (Figure 4.24 item 1). Different buttons can perform the generation of current profile and uploading on the Raspberry Pi board, the downloading from the board after the measurements and the analysis of the results showing the graphs (Figure 4.24 item 2). As for the static window, there is the possibility to estimate the value of the components (R_s , R_1 , R_2 , C_1 and C_2) of the equivalent model of the P-MFC (Figure 4.24 item 3). Results from the acquired data and a curve generated from the estimated values can be compared in a graphical way (Figure 4.24 item 3).

DYNAMIC PARAMETERS

Method FFT

Transient 100 s

(a) FFT method

DYNAMIC PARAMETERS

Method Welch

Window Flat top

Window length 1000 s

Overlap 90 %

(b) Welch method

Figure 4.23: Dynamic analysis interface windows

Dynamic analysis

CURRENT PROFILE

1 Time interval 1 s

Simulation time 10000 s

Noise amplitude 1.0 μA

Noise bias 40.0 μA

Preparing the simulation

Generate Current Profile

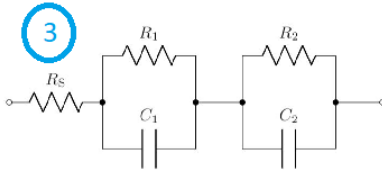
Upload on Raspberry Pi

2 Analysis post-measure

Download from Raspberry

Analysis of the results

3



R_s 1000 Ω

R_1 3400 Ω

C_1 0.001 F

R_2 0 Ω

C_2 0.001 F

Figure 4.24: Dynamic analysis interface window

As in the previous section is explained, the results of the dynamic analysis can be

obtained with different methods: FFT (Figure 4.23a) and Welch (Figure 4.23b). Once the method is chosen, the relative parameters have to be inserted to process properly the data.

4.3.2 Calibration

Calibration is defined as the set of operations that allows the calibration relation to be estimated, therefore it is mandatory before the instrument use. Usually it is performed applying at the input of the instrument a set of known values and recording the corresponding outputs. For this purpose, a different approach is exploited: it is applied an unknown value but the same quantity will be measured with the sensing system (to be characterized) and a more accurate instrument as depicted in Figure 4.25. The measurements acquired by the more accurate instrument will be used as a reference values.

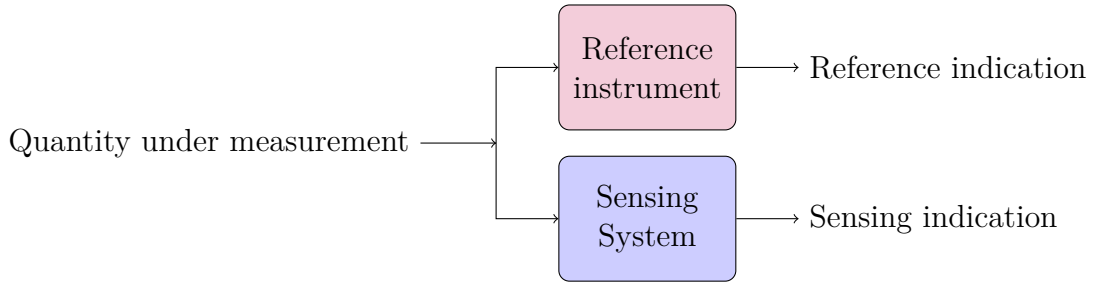


Figure 4.25: Calibration scheme

The second operation is the adjustment which allows the calibration relation to be corrected with respect the reference ones. The quantity under measurement is the current that flows through the load. The connection scheme is shown in Figure 4.26. The load is the equivalent static circuit (Figure 4.18) where the independent voltage source is replaced by a bench power supply Rigol DP832 [54] with a series resistance $R_{INT} = 1\text{ k}\Omega, \pm 5\%, \frac{1}{4}\text{ W}$. The reference instrument placed in series to the load measures the current flowing through it. The instrument used is the multimeter Agilent Technologies 34401A [55]. The voltage V_{OC} is set at 0.5 V. The multimeter is set to measure DC current with range of 10 mA with a maximum resolution of 10 nA. The sensing system is connected to the load to be able to measure the same current. In order to make the measurements at the same time between the sensing system and the multimeter, a trigger signal generated by the Raspberry Pi board is used to synchronize the two measurements (Figure 4.31). On the multimeter it is possible to select an external trigger with 0 s time delay. The multimeter takes one reading each time a trigger signal is received. In the external trigger mode, the multimeter accepts a hardware trigger applied to

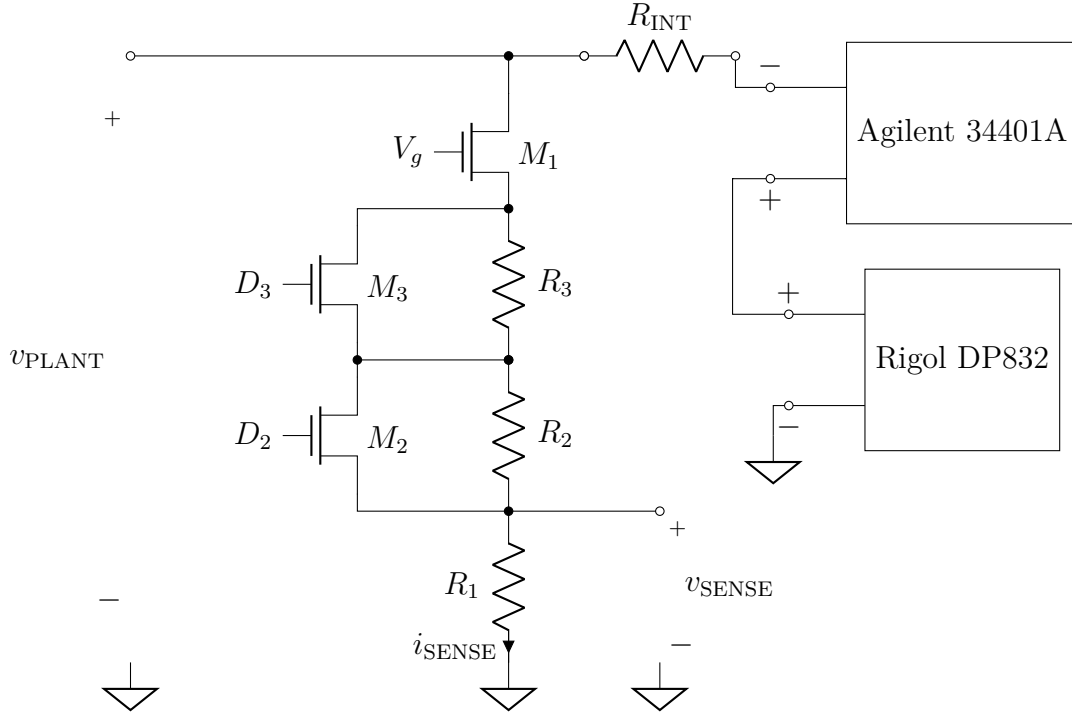


Figure 4.26: Calibration operation interface window

the rear-panel *Ext Trig* terminal (Figure 4.28).



Figure 4.27: Ext Trig terminal on Agilent 34401A

The triggering operation can be made by applying a low-true pulse larger at least $1\ \mu\text{s}$ [55, pg. 83] (Figure 4.28). The RPi board is able to provide an output signal with an amplitude of 3.3 V while the multimeter needs a signal TTL compatible so a common-source configuration is used as voltage-level translation (Figure 4.29). The duration of this pulse is set to be 20 ms. Both measurements of the reference instrument and the sensing system have to be sent to the UIA on the PC to perform

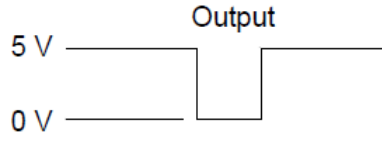


Figure 4.28: Trigger signal [55, p.83]

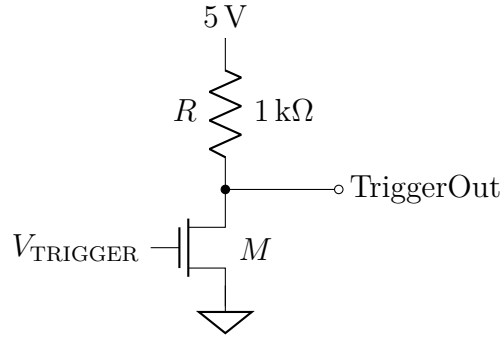


Figure 4.29: Circuit to translate the voltage level for trigger signal

the post-processing analysis. To create this connection, a remote interface must be set. The connection cable is a plug-and-play interface 82357 USB/GPIB [56]. This connection is made by the rear-panel of the multimeter (Figure 4.30) and a USB2.0 port of the PC.

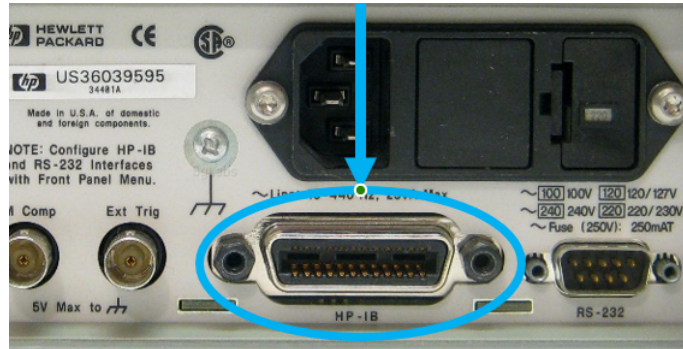


Figure 4.30: GPIB terminal on Agilent 34401A

A generic scheme of the connections is shown in Figure 4.31. The MATLAB environment is able to create a connection and communicate with the instrument with a commands. This device must have a unique address in the range $0 \rightarrow 31$ (23 in the thesis case).

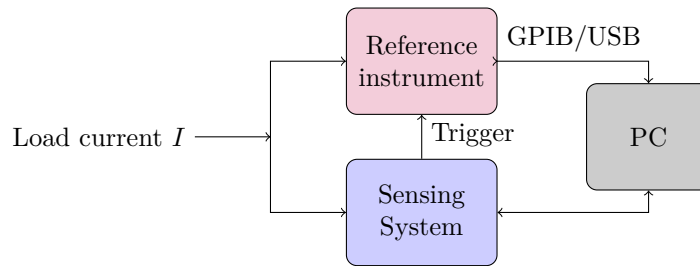


Figure 4.31: Basic scheme during calibration

User interface application: calibration window

On the PC side, first the drivers of the instrument and the Instrument Control tool have to be installed and then an instrument object of the 34401A has to be created.

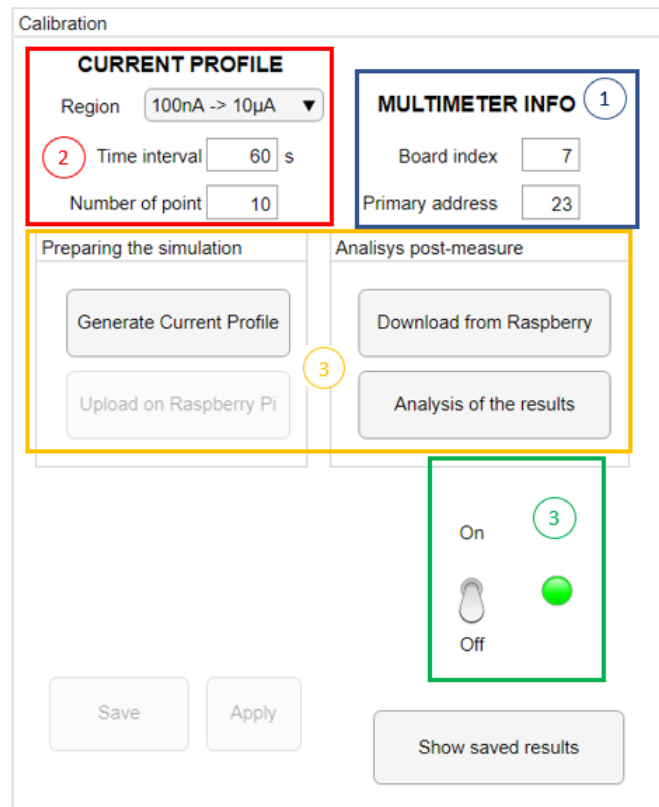


Figure 4.32: Calibration operation interface window

At this point, the system is ready to receive commands and work. A window is

dedicated to perform the calibration operation (Figure 4.32). For the instrument, the board index and the primary address must be inserted (Figure 4.32 item 1). Through the drop-down component, it is possible to choose the region of the calibration. Other parameters must be set are the time between two current value t_{INTERVAL} and how many points inside the current range N (Figure 4.32 item 2). Different buttons can perform the generation of current profile and uploading on the RPi board, the downloading from the board after the measurements and the analysis of the results showing on a graph (Figure 4.32 item 3). Before to run the program on the RPi board, the vertical switch (Figure 4.32 item 4) on the application has to be clicked: it starts to set in the proper way the multimeter for receiving the trigger signal.

Calibration parameters

At the end of the measurements, both MATLAB and RPi programs produce a file containing the respective readings. The results of this analysis are the computation of the gain and offset error and also the non linearity (INL and DNL) for both RPi and multimeter. The offset and gain error are derived by the Ordinary Least Squares (OLS) from the measurements:

$$\begin{cases} G = \frac{n \sum_{i=1}^n (I_{\text{DES}_i} \cdot I_{\text{MEAS}_i}) - \sum_{i=1}^n I_{\text{DES}_i} \cdot \sum_{i=1}^n I_{\text{MEAS}_i}}{n \sum_{i=1}^n I_{\text{DES}_i}^2 - \left(\sum_{i=1}^n I_{\text{DES}_i} \right)^2} \\ I_{\text{OFFSET}} = \overline{I_{\text{MEAS}}} - FC \cdot I_{\text{DES}} \end{cases} \rightarrow I_{\text{MEAS}} = I_{\text{OFFSET}} + G \cdot I_{\text{DES}} \quad (4.6)$$

where n is the number of couple of data for each region, I_{DES} is the desired current and I_{MEAS} is the measured current. The non-linearity error INL and DNL are derived from a theoretical formula:

$$\begin{cases} \text{INL} = \max(|I_{\text{DES}_i} - I_{\text{MEAS}_i}|) \\ \text{DNL} = \max(|A_{\text{D}_i} - A'_{\text{D}_i}|) \text{ with } \begin{cases} A_{\text{D}_i} = I_{\text{DES}_i} - I_{\text{DES}_{i-1}} \\ A'_{\text{D}_i} = I_{\text{MEAS}_i} - I_{\text{MEAS}_{i-1}} \end{cases} \end{cases} \quad (4.7)$$

The gain and the offset error of the measurement from RPi are compared with those from the multimeter to derive the calibration parameters (Figure 4.33) that will be used during the static and dynamic analysis to adjust the current readings (equation 4.1):

$$\begin{cases} G_{\text{ERROR}} = \frac{G_{\text{RPi}}}{G_{\text{REF}}} \\ I_{\text{ERROR}} = I_{\text{OFFSET}_{\text{REF}}} - I_{\text{OFFSET}_{\text{RPi}}} \end{cases}$$

```

Region1
0.10000
10
FC 0.9978
Ioff -0.74
Region2
0.100
10
FC 0.9971
0.8405
Region3
0.020000
1000
FC 0.9725
Ioff 10.3196

```

Figure 4.33: Example of calibration parameters saved on file

where the new parameters are computed adjusting the old ones already present on the file:

$$\begin{cases} FC = \frac{FC_{\text{PREV}}}{G_{\text{ERROR}}} \\ I_{\text{off}} = I_{\text{off}_{\text{PREV}}} + I_{\text{ERROR}} \end{cases}$$

This operation must be performed for each current range and to obtain an improvement of the performances, it can be repeated more times but at least two: the first one to compare the errors and the second one to check the effective corrections and evaluation if to repeat the process.

4.4 Test of the sensing system

The whole sensing system is tested in a practical case: the circuit under test is a circuit with 1-time constant and it is composed by an independent voltage source V_{OC} in series to a resistor R_{S} and the parallel between the resistor R_1 and the capacitor C_1 as shown in Figure 4.34. This circuit is useful both to test the static and dynamic analysis. From the static point of view, the measurements are taken after the transient while for the dynamic one the EIS with white noise is used.

4.4.1 Circuit design

The value of components are chosen in the same order of magnitude for usual P-MFC [5]. The independent voltage source V_{OC} is provided by the RPi 3 power supply of 3.3 V with a voltage divider composed by the resistors R_{A} and R_{B} properly designed. The value of two resistors R_{S} and R_1 fix the amount of current that

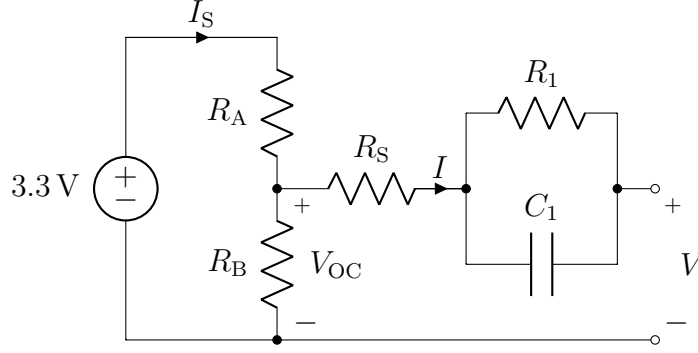


Figure 4.34: Circuit used for test the sensing system

the source is able to provide and it's fixed to about $I_{\text{MAX}} = 500 \mu\text{A}$. In order to keep V_{OC} constant for all the current range, the voltage divider is designed to flows the current I_S larger enough with respect to I .

$$I_S = \frac{3.3 \text{ V}}{R_A + R_B} \gg I_{\text{MAX}} \rightarrow R_A + R_B \ll \frac{3.3 \text{ V}}{I_{\text{MAX}}} \quad (4.8)$$

Larger enough means at least 10 times higher so $I_S > 10 \cdot I_{\text{MAX}}$:

$$R_A + R_B < \frac{3.3 \text{ V}}{10 \cdot I_{\text{MAX}}} = \frac{3.3 \text{ V}}{10 \cdot 500 \mu\text{A}} = 660 \Omega \quad (4.9)$$

The value of the resistors chosen are $R_A = 100 \Omega$ and $R_B = 10 \Omega$ which provides a voltage V_{OC} and a current consumption I_S :

$$\begin{cases} V_{\text{OC}} = 3.3 \text{ V} \frac{R_B}{R_A + R_B} = 3.3 \text{ V} \frac{10 \Omega}{100 \Omega + 10 \Omega} = 0.3 \text{ V} \\ I_S = \frac{3.3 \text{ V}}{R_A + R_B} = \frac{3.3 \text{ V}}{100 \Omega + 10 \Omega} = 30 \text{ mA} \end{cases} \quad (4.10)$$

To properly design the other components, the circuit must be analyzed in frequency: the presence of one capacitor means that the circuit will have just one pole. The transfer function of this impedance is:

$$Z(s) = R_S + R_1 \parallel \frac{1}{sC_1} = (R_S + R_1) \frac{1 + s(R_S \parallel R_1)C_1}{1 + sR_1C_1}$$

The frequency of the pole f_P is defined by the resistor R_1 and the capacitor C_1 :

$$f_P = \frac{1}{2\pi R_1 C_1} \quad (4.11)$$

Now to analyze the circuit, one can consider both at low frequency or at high frequency with respect f_P . At low frequency, the capacitor C_1 acts as an open circuit so the impedance Z can be considered as the series between R_S and R_1 (Figure 4.35a) while at high frequency, the capacitor C_1 behaves as a wire so the resistor R_1 is short-circuited and the impedance Z can be considered as only the resistor R_S (Figure 4.35b). At high frequency, the impedance is lower ($Z = R_S$) so

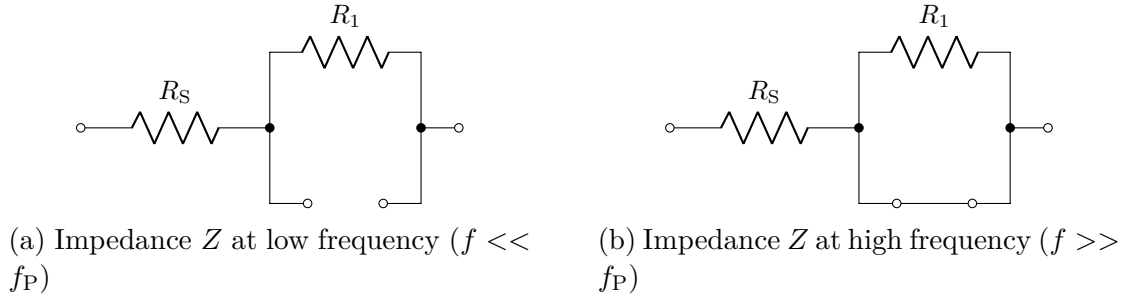


Figure 4.35: Different combination of series circuit

there is the maximum current and it should be lower than I_{MAX} and it is chosen $R_S = 1 \text{ k}\Omega$ so:

$$I_{MAX_HIGH_FREQUENCY} = \frac{V_{OC}}{R_S} = \frac{0.3 \text{ V}}{1 \text{ k}\Omega} = 300 \mu\text{A} \quad (4.12)$$

The P-MFCs are very slow system so as an example, the pole f_P is placed at 50 mHz and choosing a very large capacitor for example C_1 of 1 mF it is possible to compute the value of the resistor R_1 :

$$f_P = \frac{1}{2\pi R_1 C_1} \rightarrow R_1 = \frac{1}{2\pi f_P C_1} = \frac{1}{2\pi \cdot 50 \text{ mHz} \cdot 1 \text{ mF}} = [3.183 \text{ k}\Omega]^1 = 3.3 \text{ k}\Omega \quad (4.13)$$

Considering the maximum current deliverable by the system at low frequency is equal to the maximum current in the static condition:

$$I_{MAX_LOW_FREQUENCY} = \frac{V_{OC}}{R_S + R_1} = \frac{0.3 \text{ V}}{1 \text{ k}\Omega + 3.3 \text{ k}\Omega} = 69.76 \mu\text{A} \quad (4.14)$$

The complete schematic becomes depicted in Figure 4.36.

¹The round up operation is made considering the E12 series of resistor.

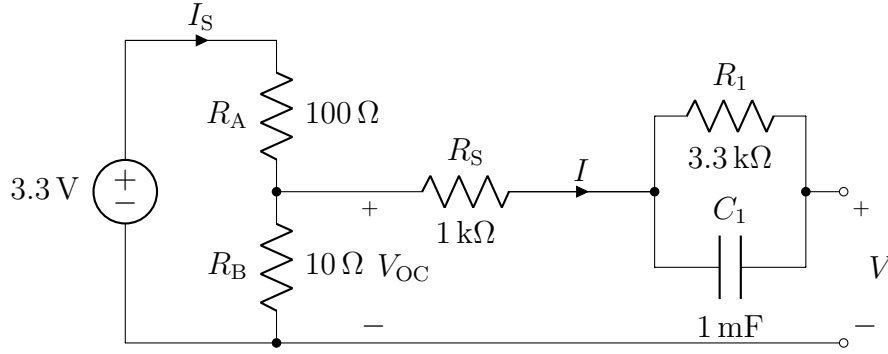


Figure 4.36: Circuit used for test the sensing system

4.4.2 Static analysis

First, the static parameters has to be estimated performing the static analysis. The set up is a time interval t_{INTERVAL} of 120 s, the current range $1\mu\text{A} \rightarrow 80\mu\text{A}$ divided in 50 number of points. For every time interval, the average to calculate the mean value is made on the last 20 s. After the current profile generation and update the file on RPi, the analysis is performed. The analysis is performed indoor. At the end, the file with the measurements is downloaded from RPi and the post-processing analysis is performed. In Figure 4.37 are shown the results of the static analysis.

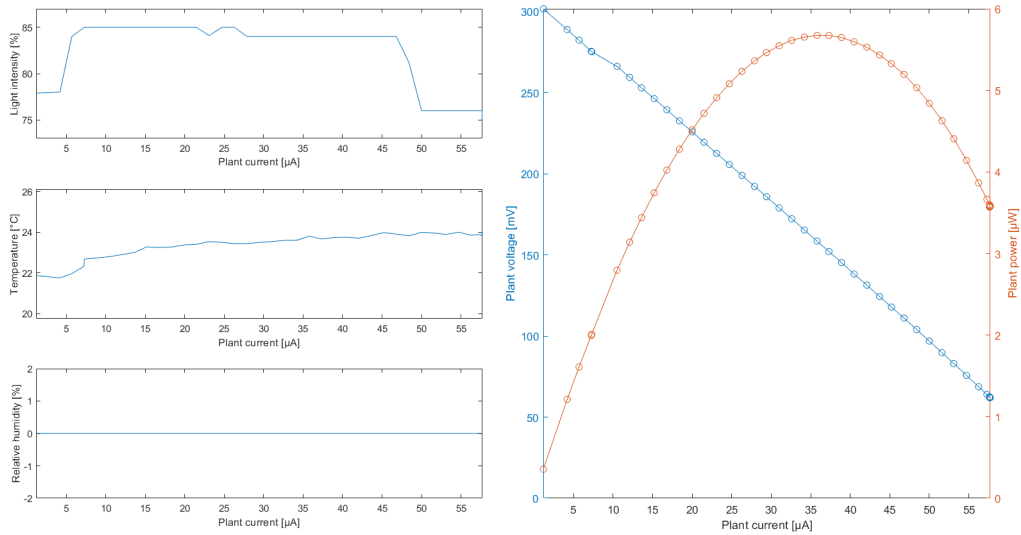


Figure 4.37: Static analysis results with the test circuit

On the left hand side, there are the measurements of the environmental parameters: the light intensity has a step due to the lights switching on and off during

the measurements and the temperature increases from about 22 °C up to approximately 24 °C due to heating up. The relative humidity graph keeps at 0 % because the sensor is not used. On the right hand side, it is shown the graph of polarization curve (or V-I curve) superimposed on that of power versus the current. From the last chart it is possible to find out the maximum power delivered by the system and which value of current it shows up.

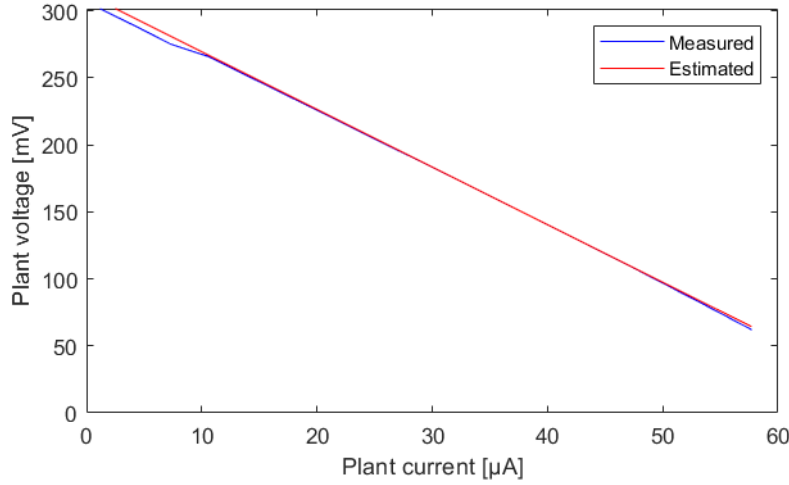


Figure 4.38: Static comparison between the measured and estimated measurements

From the compare operation (Figure 4.38) between the measurements and the results with the estimated circuit model, it comes out that the open circuit voltage $V_{OC_{eq}} = 0.31$ V and the internal resistance is $R_{INT} = 4.3$ k Ω . Since V_{OC} is designed to be 0.3 V and the resistances placed are $R_S = 1$ k Ω and $R_1 = 3.3$ k Ω , it demonstrates a good behavior with respect to the static analysis. In the Figure 4.39 is shown a small piece of analysis where on the left axis there is the current both measured and desired while on the right axis there is the voltage. It is possible to see the small oscillations of the measured current across the desired current and a small time to reach the desired value (about 2 s). Increasing the current, the voltage decreases due to the losses for the internal resistance.

4.4.3 Dynamic analysis

The dynamic analysis aims to obtain the value of the equivalent circuit which can be used as a model for the design of the energy harvester. The EIS method with the white noise is used. The parameters of the analysis has to be designed in order to meet the requirements. The pole f_P is set at 50 mHz so the choice of the sampling frequency f_S and the duration $t_{ANALYSIS}$ fixes the frequency range in which the impedance can be computed. The noise signal is generated by changing

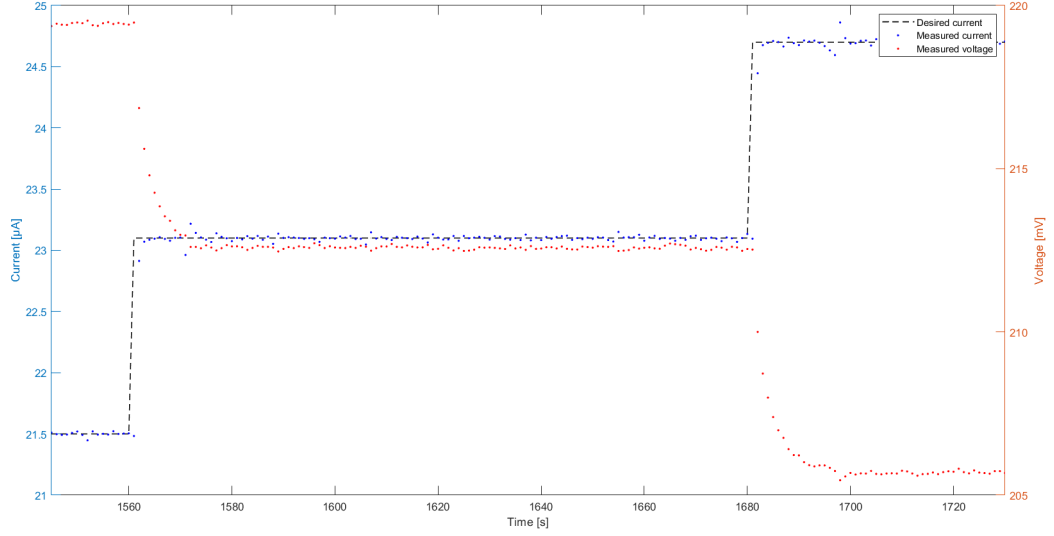


Figure 4.39: Current desired and measured and voltage measured in time of a small period of the analysis

value every 1 s so the current flowing through and the voltage across the P-MFC are measured every $t_{\text{INTERVAL}} = 1$ s:

$$f_s = \frac{1}{t_{\text{INTERVAL}}} = \frac{1}{1 \text{ s}} = 1 \text{ Hz} \quad (4.15)$$

Nyquist-Shannon sampling theorem states the sampling frequency f_s determines the maximum bandwidth f_{MAX} of a signal which can be reconstructed correctly:

$$f_{\text{MAX}} = \frac{f_s}{2} = \frac{1 \text{ Hz}}{2} = 500 \text{ mHz} \quad (4.16)$$

The number of spectral components N fixes the frequency resolution Δf in FFT operation and it can be derived from the duration of the analysis $t_{\text{ANALYSIS}} = 10\,000$ s:

$$N = t_{\text{ANALYSIS}} \cdot f_s = 10\,000 \text{ s} \cdot 1 \text{ Hz} = 10\,000 \rightarrow \Delta f = \frac{f_s}{N} = \frac{1 \text{ Hz}}{10\,000} = 100 \text{ } \mu\text{Hz} \quad (4.17)$$

The noise signal is placed around the maximum power point $I_{\text{BIAS}} = 40 \text{ } \mu\text{A}$ and in order to be in a small-signal condition, the amplitude of the noise signal should be small enough and it is chosen $I_{\text{AMPLI}} = 1 \text{ } \mu\text{A}$. The white noise cannot have an infinite resolution because the system has a minimum one (100 nA) so before to generate the current file, a round operation is performed. Then the current profile file is generated and uploaded on the RPi. After the complete simulation, the

measurements are downloaded on the PC and they are shown on the Figure 4.40: the blue curve is the current injected while the red one is the measured voltage.

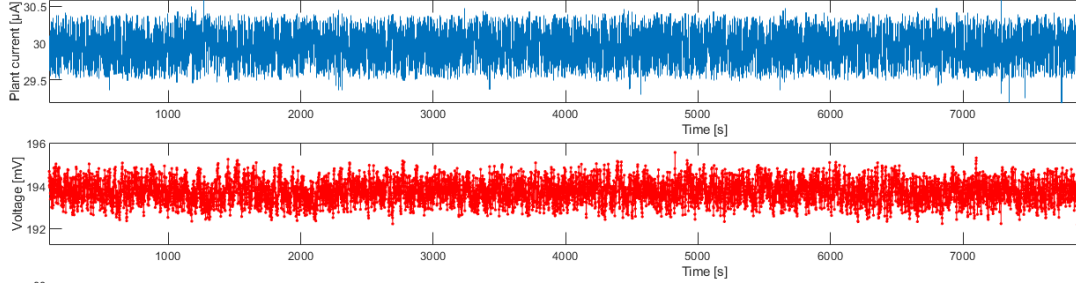


Figure 4.40: Current and voltage measured from equivalent circuit

At this point two different method are implemented as a comparison of the two method previously detailed. The FFT method allows to obtain the impedance in frequency of the P-MFC both for the amplitude and for the phase but at the upper bound, there are a lot of spikes that make the reading not accurate (Figure 4.41) while using the Welch method with the proper window function, the phase information is lost but the amplitude graph is cleaner and estimation of the parameter is easier (Figure 4.42).

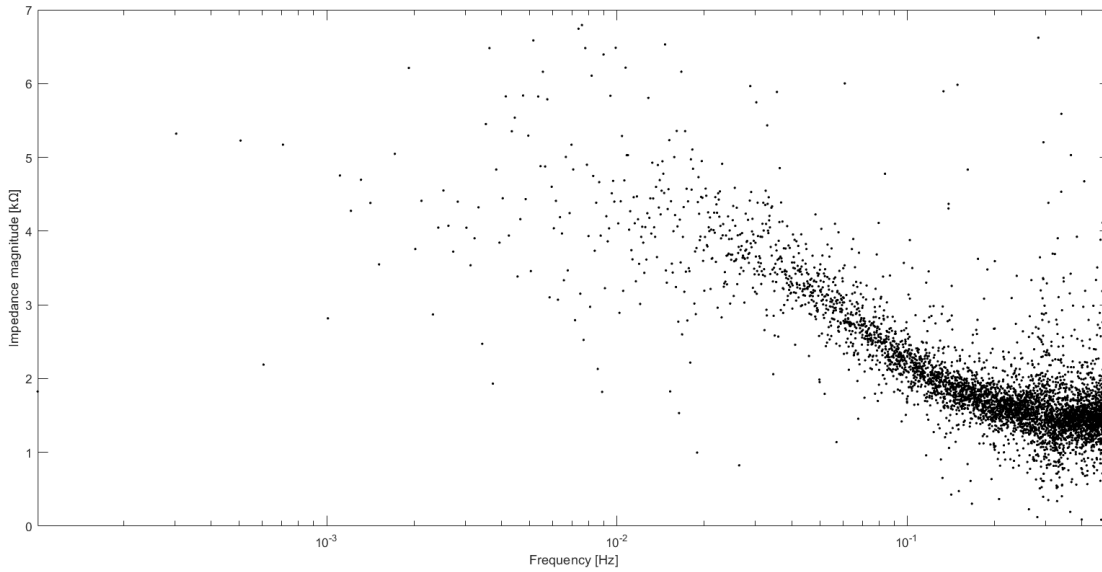


Figure 4.41: FFT method

For the Welch method, the amplitude of the window $L_{\text{WINDOW}} = 4000$ s fixes the

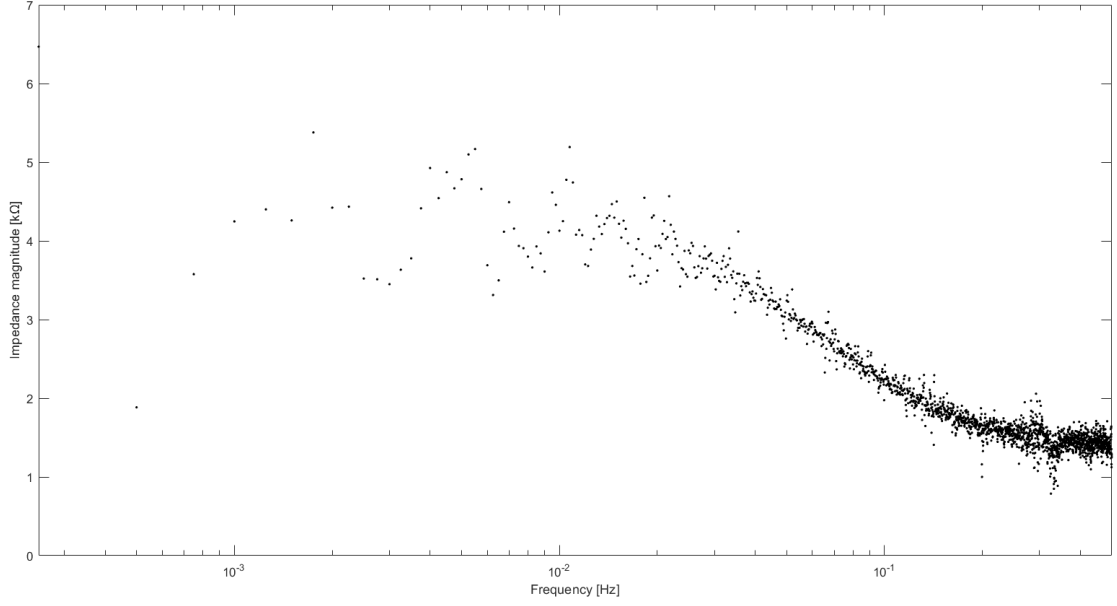


Figure 4.42: Welch algorithm with Flat top windows

frequency resolution Δf while the overlap allows to have a better graph:

$$N_{\text{WELCH}} = L_{\text{WINDOW}} \cdot f_S = 4000 \text{ s} \cdot 1 \text{ Hz} = 4000 \rightarrow \Delta f = \frac{f_S}{N_{\text{WELCH}}} = \frac{1 \text{ Hz}}{4000} = 250 \text{ } \mu\text{Hz} \quad (4.18)$$

The choice of the windowing function affects the quality of the final result. Different windowing functions are used and the results are compared: Hanning (Figure 4.43), Hamming (Figure 4.44), Flat top (Figure 4.45) and Blackman-Harris (Figure 4.46). The effective frequency resolution of the system does not depend only from the length but also the kind of the window: the curves have different behavior at the lowest limit in frequency depending on the width of the main lobe of each window function. From the comparison operation (Figure 4.47) between the measurements and the results from the estimated model, it comes out that the series resistances $R_s = 1 \text{ k}\Omega$, $R_1 = 3.3 \text{ k}\Omega$ and $R_2 = 0 \text{ k}\Omega$ while the capacitance $C_1 = 1 \text{ } \mu\text{F}$. The estimated value are close to the components placed in the test circuit, it is demonstrated the good behavior of the dynamic analysis.

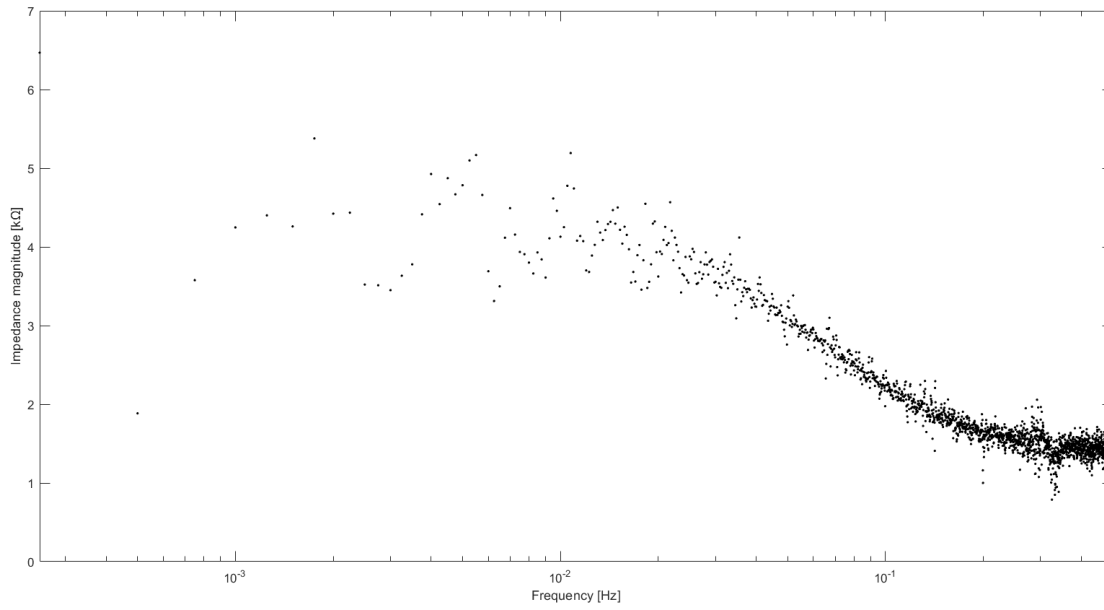


Figure 4.43: Impedance in frequency with Welch method and Hanning window

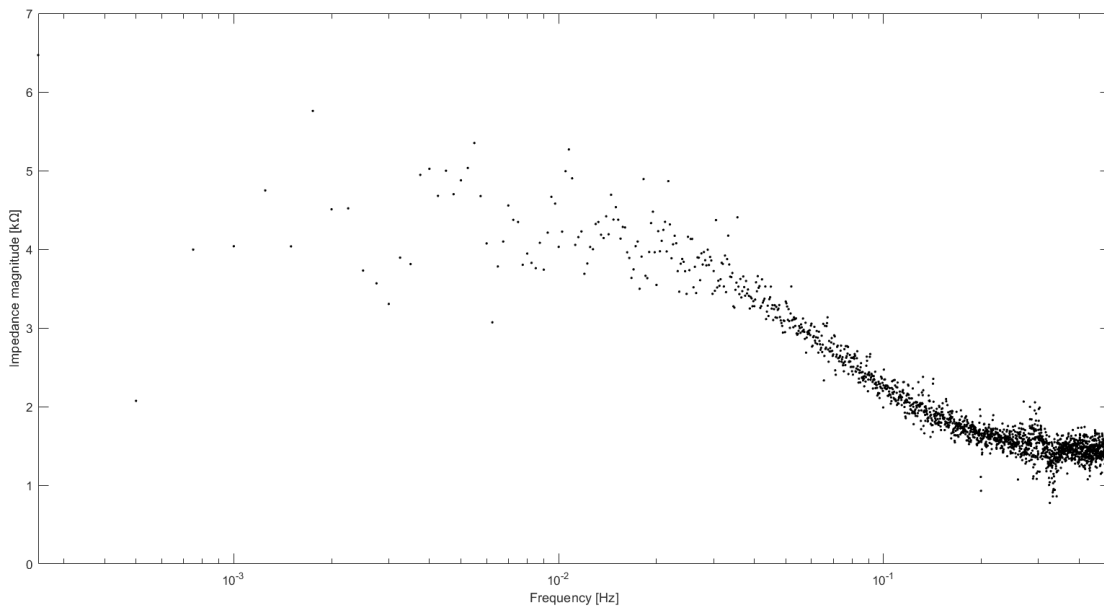


Figure 4.44: Impedance in frequency with Welch method and Hamming window

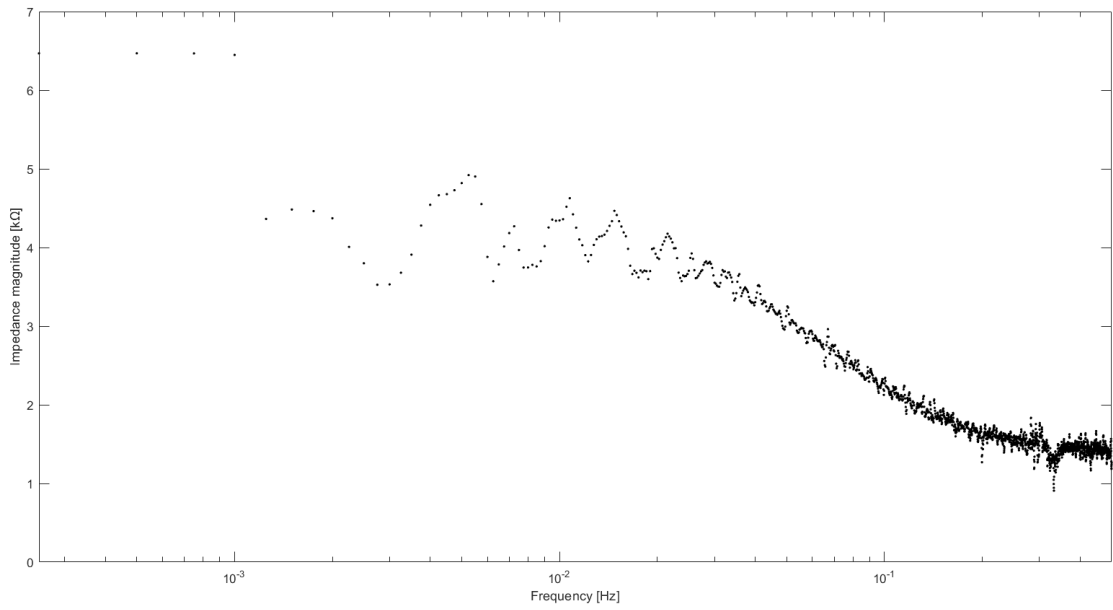


Figure 4.45: Impedance in frequency with Welch method and Flat top window

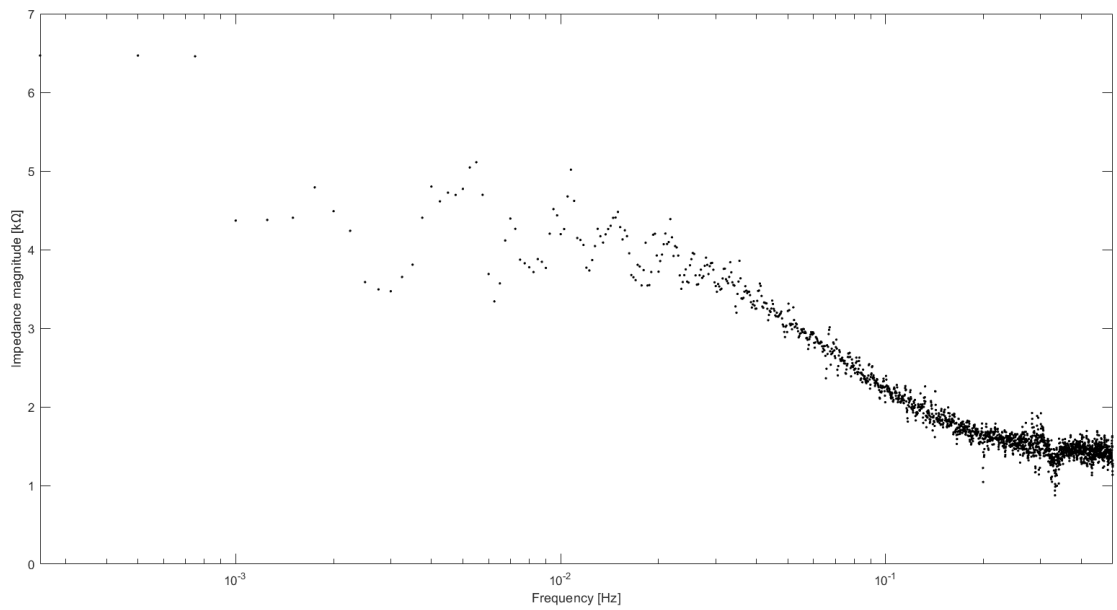


Figure 4.46: Impedance in frequency with Welch method and Blackman-Harris window

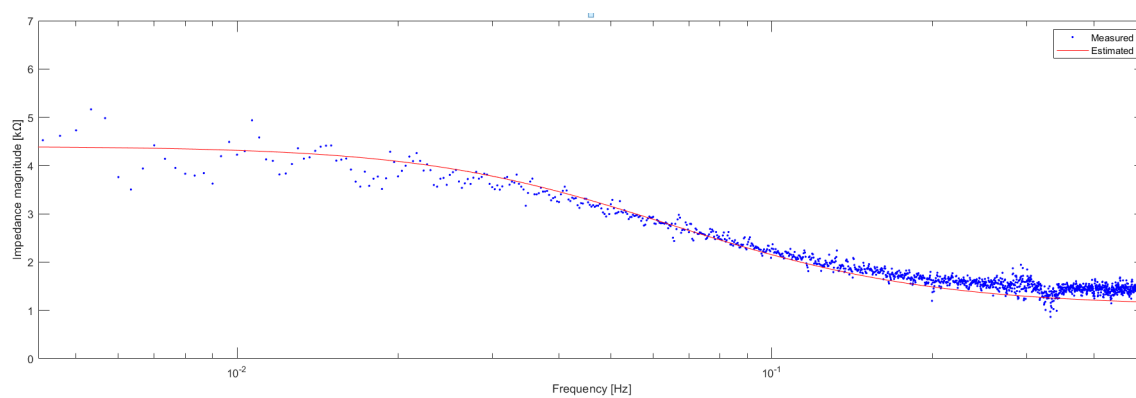


Figure 4.47: Dynamic comparison between the measured and estimated measurements

Chapter 5

P-MFC in practice

Once the electronic load board is tested and it gives good precision in measurement results, the P-MFC can be connected to it for its characterization. Initially, a detailed description on how the electronic load board is implemented in practice is described and then are shown the procedure and the results obtained from the measurements of a P-MFC. Different P-MFC systems were built in order to check the repeatability of measurements and to guarantee reliability of results. The constant between all of them is the kind of plant to do not introduce too much variables. This assumption allows to understand the variation in the generation power depending only on the environmental parameters and on plant health.

5.0.1 PCB of the electronic load board

Before to start, it is important to show how the sensing system is implemented in practice. Initially, the electronic load and the conditioning circuitry are mounted on a breadboard. This way gives the possibility to modify the components (resistors, transistors and capacitors) freely. On the contrary, the use of a breadboard introduces several parasitic elements e.g. relatively large parasitic capacitance (approximately 2pF between adjacent contact columns), high inductance of some connections and a relatively high and not very reproducible resistance due to the long connections and contacts. Once the testing results of the whole sensing system meet the design specifications, to reduce these effects, the through-hole technology (THT) is replaced with the surface mounted technology (SMT) thus the breadboard is replaced by the printed circuit board (PCB). The use of surface mounted components (SMD) also reduces the circuit area due to their small dimensions. The schematic, PCB layers (Figure A.1) and a 3D viewer of the designed PCB (Figure A.2) are shown in the Appendix A. The PCB is designed like an expansion board for the high precision AD/DA board to be accommodate on it thus the external

dimensions and sockets position are bounded. In practice, this board was realized with a L-shape (Figure 5.1). This particularity has a functional reason: the

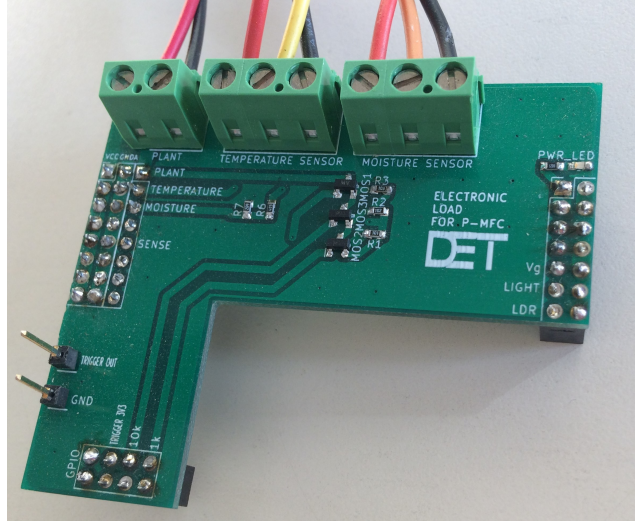


Figure 5.1: Picture of the realized PCB

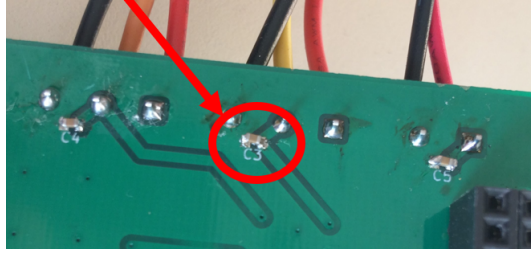
light intensity sensor is mounted on the underlying board so it allows the sensor to experience the solar light (Figure 5.2). The interface with the external world



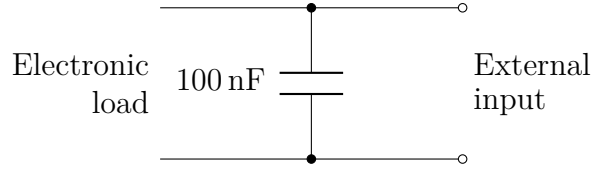
Figure 5.2: Light intensity sensor

(i.e. P-MFC and sensors) are terminals with the screw which allow to connect the twisted-wire cables. In certain environments and situations, these input signals can pose a threat to the electronics reading them. Good practical rule, with the addition of a capacitor, more protection can be added by turning the current limit circuit into a simple low-pass filter (Figure 5.3). The value of these capacitors is

chose to be 100 nF. On the electronic load board, a small LED indicates the power



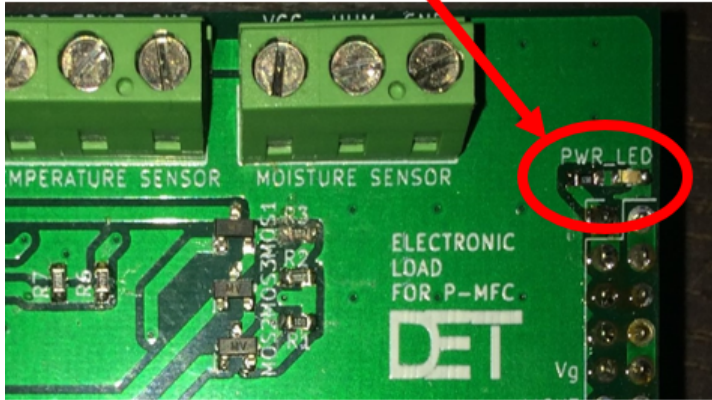
(a) Picture of on input capacitor (bottom board side)



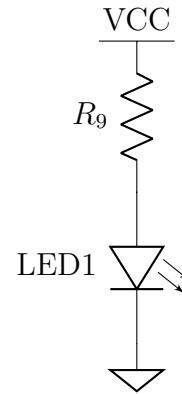
(b) Input capacitor circuit

Figure 5.3: Input filter

supply (Figure 5.4a). The circuit is a resistance $300\ \Omega$ in series to a LED (Figure 5.4b).



(a) Picture of power LED



(b) Power LED circuit

Figure 5.4: Power LED

5.0.2 System connections

The connections of the P-MFC and the sensors to the electronic load board are shown in the scheme in Figure 5.5. The connections are made by twisted-wire cable in order to reduce electromagnetic radiation from the pair, crosstalk between neighboring pairs and improves rejection of external electromagnetic interference. The cathode and anode of the P-MFC are connected to the positive (+) and ground (–) of the PLANT connector (Red circle of Figure 5.6), respectively. The temperature sensor must be placed close to the plant and connected to the TEMPERATURE SENSOR connector (Yellow circle of Figure 5.6). The soil humidity

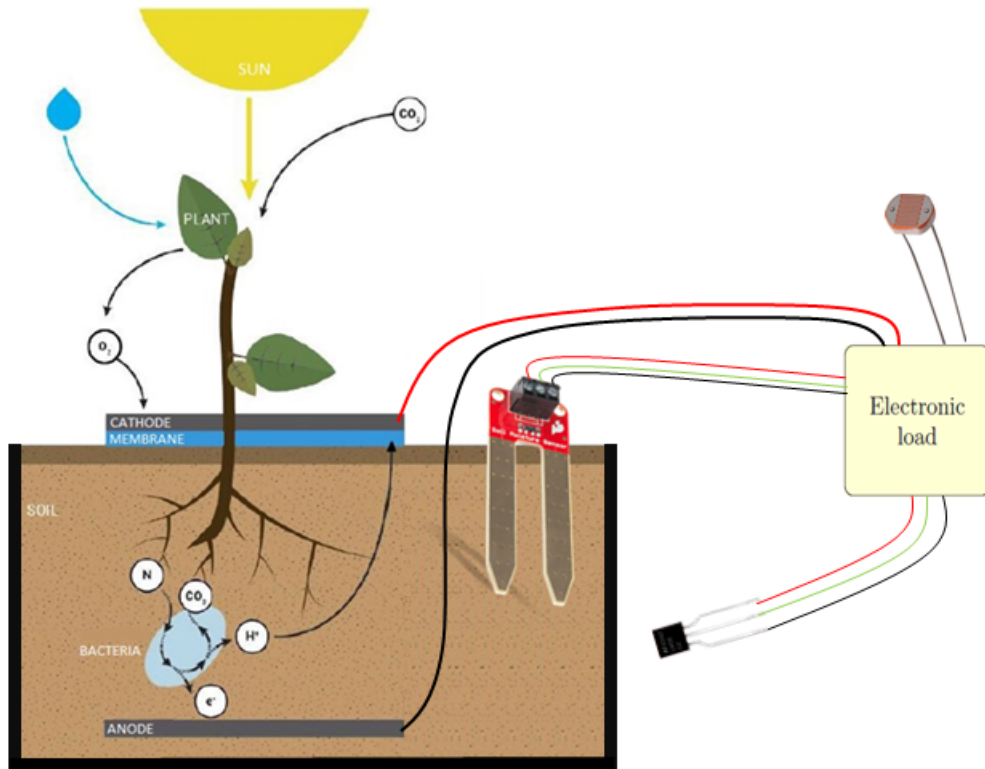


Figure 5.5: Sensing system connections with P-MFC and sensors

sensor must be inserted into the soil of the plant and connected to the MOISTURE SENSOR connector (Blue circle of Figure 5.6).

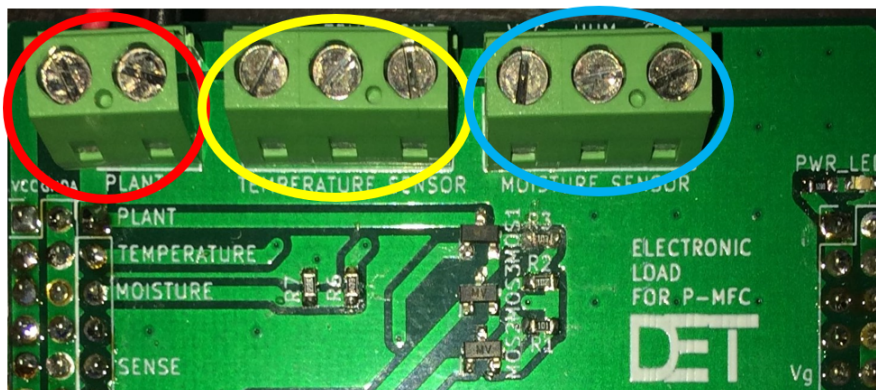


Figure 5.6: Plant connector on the electronic load board

The light sensor (Figure 5.2) is mounted on the High-precision AD/DA board so the sensing system must be placed as close as possible to sense the solar radiation

that the plant experiences. Once the system is set up, the user is able, from the user interface on the PC, to configure all the parameters to perform the desired analysis.

5.0.3 Moisture sensor problem

As described in detail in Section 3.3, the moisture sensor is composed by two large and exposed pads as probes which act as a variable resistor. Once the pads are inserted into the soil, the values of the acquired readings from input of the ADC related to the plant voltage gives a constant value $V_{\text{PLANT}} = 625 \text{ mV}$. This problem could be seen as a sort of saturation of the input of the ADC since it is fixed to the maximum of the input voltage swing V_{ADCIN} (equation 3.4). The cause of this saturation is given by the interaction between the moisture sensor and the soil. From the circuit of Figure 3.23, the voltage V_{PAD} of each pad is at least higher than the voltage V_{H} across the resistor R_1 plus the base-emitter voltage V_{be} of the bipolar transistor Q_1 . Supposing to have the relative humidity $\text{RH} = 50 \%$, the voltage V_{H} can be derived from the proportion $5 \text{ V} : 100 \% = V_{\text{H}} : \text{RH}\%$:

$$V_{\text{H}} = \frac{\text{RH}\%}{100 \%} \cdot 5 \text{ V} = \frac{50 \%}{100 \%} \cdot 5 \text{ V} = 2.5 \text{ V}$$

The lower potential at one pad is higher than 2.5 V. The problem is that these pads are inserted into the soil that is directly connected to the anode of the P-MFC; the pads fix the voltage of the anode higher than 2.5 V creating a saturated measure. The moisture sensor could be inserted in the soil of the plant but covered by a sort of sock made of a material that acts as an electrical insulator and also water permeable as represented in Figure 5.7. The electrical insulation allows to eliminate the interference of the sensor with the electrical measurements while the water permeability permits however to measure the humidity of the soil. This allows to not modify the circuit already designed and produced but only add one part in the P-MFC system. Hence, the following measurements and results are made without considering the humidity of the soil effects.

5.0.4 Plant description

Different plants (on the same family) and configurations are used trying to understand which one is the most efficient. The plant chosen is the **Carex**: commonly called true sedges, perennial herb belonging to the Cyperaceae family and to the large group of grasses, Carex presents a thick tuft of ribbon-like leaves, robust and shiny, elegantly curved. The Carex hachijoensis 'Evergold' variety, with its linear green foliage veined with yellow, is particularly suitable for growing in pots: compact, tall and wide at most 40 cm, it is excellent combined with other higher

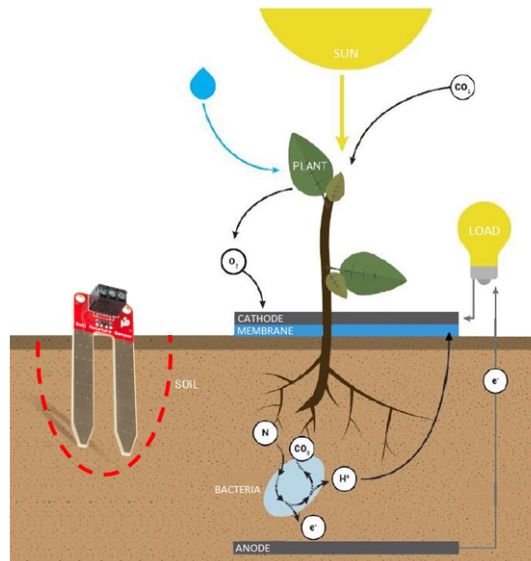


Figure 5.7: Moisture sensor in the soil with electrical insulator



Figure 5.8: Plant Carex in the family of Cyperaceae

grasses. They are recommended plants for gardens, balconies or terraces. They prefer a sunny but partially shaded exposure and support minimum temperature $-10^{\circ}\text{C} \rightarrow -5^{\circ}\text{C}$. Carex like a slightly acidic, moist, well drained soil. The soil must always remain just wet, never soaked; it tolerates short periods of drought. The following practical experiences are divided according the physical plants while each of them are described temporally from their building up to present.

5.1 *Carex Morrowii* - Gregory

This plant is the *Carex Morrowii* and it was bought and planted on 11/07/2018. As explained in [5, p.65], a new configuration is created through which improve and stabilize the energy production. It has been proved how setting the open circuit voltage V_{OC} , it is possible reach the MPP. However the electrons extraction could not be constant, since the extraction and the setting must be alternate thus to get through this problematic is being proposed a configuration with double anodes in which one is used to record the V_{OC} and the second one is employed to extract the electrons, according the MPP derived from the first. The plant was kept indoor and it has been daily irrigated with tap water.

5.1.1 Plant structure

The pot is made of glass with a wooden slab inside to divide the two anodes and it is siliconed to avoid connections through infiltrations of water in the wood. The wooden slab is 13 cm high and 0.5 cm thick. Starting from the bottom it is composed by:

- a layer of 3 cm of expanded clay to drain the water (Figure 5.10a)
- 3 cm of universal soil for compacted repottings (Figure 5.10b)
- 0.5 cm recycled felt electrode [57] (anode) sold in 100 % recycled carbon fiber mats (Figure 5.10c). In order to connect the anode, it is made to pass through a 0.05 cm titanium wire "like a seam" and the rest of the cable is made to arrive outside and is covered by a heat-shrinking sheath to insulate it. The anode has a diameter of 10 cm but is to be considered only half per part and then from a surface of:

$$A_{ANODE} = \frac{1}{2} \frac{\pi D^2}{4} = \frac{1}{2} \frac{\pi (10 \text{ cm})^2}{4} = 39.27 \text{ cm}^2 \quad (5.1)$$

- 9 cm of universal soil for repotting compacted with the plant inside with its roots (Figure 5.10d). The plant is divided into two parts: one on the left and one on the right. The left plant is 41 cm long and a weight of 116.4 g while the right one is 42 cm long and a weight of 120.49 g.
- 1 cm of polyethylene (PET) membrane (Figure 5.10e) for electrical insulation between anode and cathode. On the side in the picture, you can see the two connectors of the two anodes (one for the left one and the other for the right one). The dimensions of the membrane are: outer diameter of 14 cm and inner diameter (part removed to make the plant stand) of 5 cm

- 0.5 cm recycled felt electrode [57] (cathode) sold in 100 % recycled carbon fiber mats (Figure 5.10f). In order to connect the cathode, as for the anode, it is made to pass through a 0.05 cm titanium wire "like a seam" and the rest of the cable is made to arrive outside and is covered by a heat-shrinking sheath to insulate it. The cathode has an external diameter of 10 cm and an internal diameter (of part removed to make the plant stand) of 4 cm.

$$A_{\text{CATHODE}} = \frac{\pi(D_{\text{EXT}}^2 - D_{\text{INT}}^2)}{4} = \frac{\pi[(10 \text{ cm})^2 - (4 \text{ cm})^2]}{4} = 65.97 \text{ cm}^2 \quad (5.2)$$

Usually in different papers, the electrode area is the anode area but one can think that also the cathode one influences the amount of energy that can be reached so a general, though lower, assumption can be to consider the electrode area as the minimum between the two:

$$A_{\text{ELECTRODE}} = \min(A_{\text{CATHODE}}, A_{\text{ANODE}}) = \min(65.97 \text{ cm}^2, 39.27 \text{ cm}^2) = 39.27 \text{ cm}^2$$

5.1.2 Open circuit voltage measurements

Once the P-MFC system is created, its open circuit voltages (from the cathode and the first anode (C-A1) but also from the cathode and the second anode (C-A2)) were monitored (Figure 5.9) by measuring them with a digital multimeter UT33D [58] and with Agilent 34401A [55]. The monitoring period starts on 26/07/2018 and the measurements are acquired daily. Related on the availability of the instruments, on the graph are shown two curves with different colors depending on the instrument used. Iron deficiency is a limiting factor of plant growth. Iron is present at high quantities in soils, but its availability to plants is usually very low, and therefore iron deficiency is a common problem. In different dates, iron acetate is added to try to improve the soil quality. During this monitoring phase, the voltage measured has large fluctuations also in the polarity. The curves show a temporary voltage increasing after the addition of the iron acetate. An important consideration is that the voltages measured from the cathode and the two anodes have the same trend thus despite the wooden separator, the chemical soil conditions are related. Because of the fall and breakage of the pot that contained the plant on 17/08/2018, first there was a repotting maintaining the same soil and the same plant. Unfortunately, on 08/09/2018 the plant died probably because of the stress produced by the indoor life since it prefers to live outside. An important aspect is related its reuse: when the plant dies, the P-MFC components (electrodes and membrane) can be reused for another system so replacing only the dead plant.

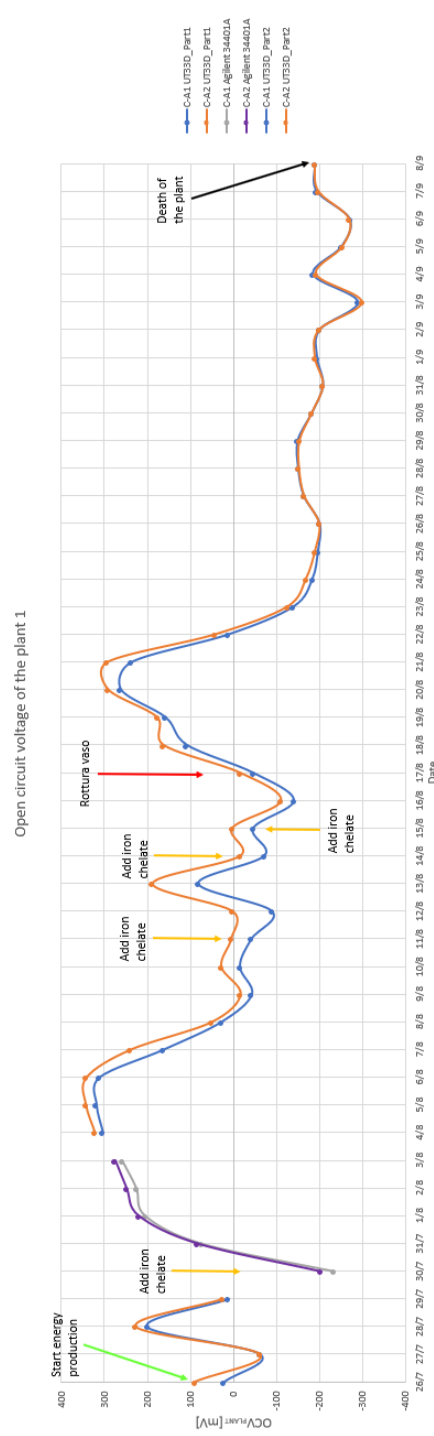


Figure 5.9: Open circuit voltage measurements of *Carex Morrowii*



(a) Top view after a layer of clay



(b) Top view after a layer of universal soil



(c) Recycled felt anode with wire



(d) Plant inserted into the vase



(e) Recycled PET membrane



(f) Recycled felt cathode with wire

Figure 5.10: Pictures of *Carex Morrowii* - Gregory

5.2 *Carex Hachijoensis* - James and Jason

These two plants are the *Carex Hachijoensis* and they were bought and planted on 2/10/2018. In this section, the P-MFCs are implemented with terrestrial plants with a single anode structure [5, p.62]. Since the previous experience (Gregory) gave a large voltage and polarity fluctuation, it was thought to change something in the P-MFC structure. The necessity of the membrane has been questioned: the membrane could act as an insulator because it does not allow the closure of the current loop thus it has been removed. This assumption will be contradicted during the measurements. A lot of considerations will be done about the use of terrestrial plants so plants that are not able to live in a waterlogged conditions. These couple of P-MFC systems are used to allow the comparison between them that have very similar structure. The plants have been daily irrigated with tap water and, learning from the previous example, were kept outdoor to avoid their death.

5.2.1 Plant structure

The pots are made of glass and, unlike the previous one, there is no wooden slab inside but they are completely empty. Starting from the bottom, they are composed by:

- a layer of 2 cm of expanded clay to drain the water
- 2 cm of universal soil for compacted repottings
- 0.4 cm recycled felt electrode (anode) sold in 100 % recycled carbon fiber mats [57]. In order to connect the anode, it is made to pass through a 0.05 cm titanium wire "like a seam" and the rest of the cable is made to arrive outside and is covered by a heat-shrinking sheath to insulate it. The anode has a diameter of 10 cm so with a surface of:

$$A_{\text{ANODE}} = \frac{\pi D^2}{4} = \frac{\pi (10 \text{ cm})^2}{4} = 78.54 \text{ cm}^2 \quad (5.3)$$

- 12 cm of universal soil for repotting compacted with the plant inside with its roots.
- 0.4 cm recycled felt electrode (cathode) sold in 100 % recycled carbon fiber mats [57]. In order to connect the cathode, as for the anode, it is made to pass through a 0.05 cm titanium wire "like a seam" and the rest of the cable is made to arrive outside and is covered by a heat-shrinking sheath to

insulate it. The cathode has an external diameter of 14.5 cm and an internal diameter (of part removed to make the plant stand) of 6 cm.

$$A_{\text{CATHODE}} = \frac{\pi(D_{\text{EXT}}^2 - D_{\text{INT}}^2)}{4} = \frac{\pi[(14.5 \text{ cm})^2 - (6 \text{ cm})^2]}{4} = 136.86 \text{ cm}^2 \quad (5.4)$$

Usually in different papers, the electrode area is the anode area but one can think that also the cathode one influences the amount of energy that can be reached so a general, though lower, assumption can be to consider the electrode area as the minimum between the two:

$$A_{\text{ELECTRODE}} = \min(A_{\text{CATHODE}}, A_{\text{ANODE}}) = \min(136.86 \text{ cm}^2, 78.54 \text{ cm}^2) = 78.54 \text{ cm}^2$$

5.2.2 Open circuit voltage measurements

Once the P-MFC systems are created, their open circuit voltage will be monitored from cathode to anode. These voltages are measured with a digital multimeter UT33D [58]. The Figure 5.15 shows the voltage measurements. The monitoring period starts on 10/10/2018 and the measurements are acquired periodically. The graph shows a red curve that represents the open circuit voltage of James while the blue one of Jason. Initially the voltages are both positive while after few days they became negative so invert their polarity. Differently from the previous experiment (Gregory), once the polarity is reversed, it does not change anymore but the voltage is not constant.

Limit due to power availability

Another consideration must be done about the voltage measurements: once the multimeter is connected to the P-MFC, the voltage readings drop rapidly. This behavior is due to the power availability from the P-MFC; during the voltage measurements, the load effect due to the multimeter connection, place its impedance (about 10 MΩ [58]) in parallel to the P-MFC so it creates a current flowing. The small amount of current needed for the voltage measurement produce a fast reduction of the open circuit voltage due to the limit in power generation.

5.2.3 The absence of the membrane

From the open circuit voltage graph, the considerations about the limit of power generation could be due to the absence of the membrane. The membrane acts as a insulator for the electrons but not for the protons. Its removal produces

that both electrons and protons generated by the microorganisms can reach the cathode passing through the the soil thus reducing the available power at the connected external load. This means a wrong hypothesis about the presence of membrane: the membrane is essential because his absence causes a short-circuit between cathode and anode. After that proof, one tried to insert the membrane between the cathode and the anode but the measurements are still similar and an hypothesis is that leaving the cathode in contact to the soil, the bacteria have colonized its bottom side and also the chemical conditions of the cathode is equal to the anode one taking very long time to come back to the correct ones.

5.2.4 Waterlogged condition

The hypothesis to be proved in this section is the voltage inversion of the P-MFC due to the dry condition of the soil. The presence of the water in the soil ensures the anaerobic condition at the anode chamber. Without the water that acts as a shield, the oxygen can reach the anode: its presence in the soil produces the oxygen reduction at the anode so the anode potential becomes higher with respect to the cathode producing the voltage inversion. There is a role switching between anode and cathode. The *Carex Hachijoensis* is a terrestrial plant so it should not be able to live in a waterlogged condition but can survive for a not too long period. Leading the dry P-MFC in wet condition, it should be measured a positive voltage between cathode and anode. Initially, the pot containing the P-MFC system was filled up with tap water. The voltage V_{PLANT} across the P-MFC was monitored and the measurements are shown in Figure 5.11.

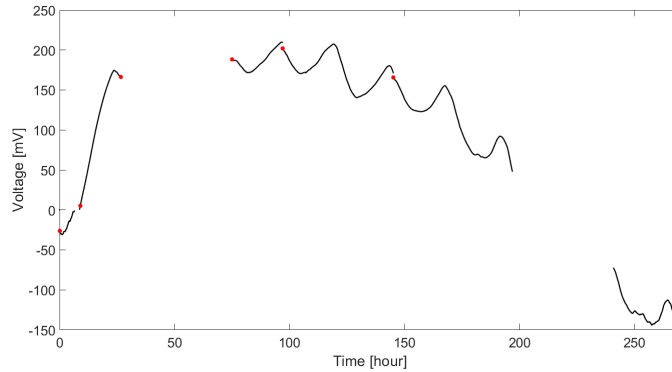


Figure 5.11: Waterlogged condition voltage measurements of the P-MFC

The whole analysis lasts for more than one week (about 200 h). The red points represents the time instant in which the pot is filled up. These voltage measurements were between cathode and anode and they were acquired without absorbing

current from the P-MFC (open circuit voltage condition $V_g = 0$ V). At the beginning, the P-MFC voltage is negative (anode potential higher with respect to the cathode one). The waterlogged condition produce an initial voltage reduction during the first hour but after that one can notice its rising trend. The voltage increased slowly but after about 10 h it became positive and then it kept rising up to reach about 180 mV. Once it reaches this point, there was a sort of voltage ringing (Figure 5.12). These oscillations were due to the environmental condition:

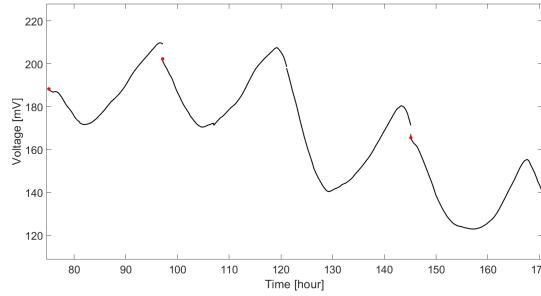


Figure 5.12: Voltage measurements oscillations of the P-MFC

the temperature (Figure 5.14) and the solar radiation (Figure 5.13) during the day produced an increasing in electrons and protons generation with respect to the night period. Higher electrons generation means high current in the P-MFC thus a voltage reduction due to the P-MFC losses. Another consideration can be

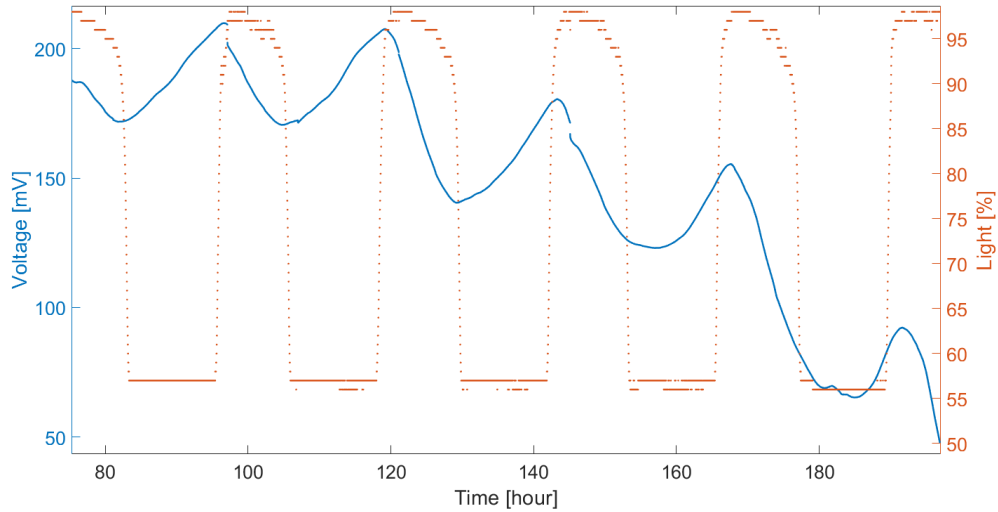


Figure 5.13: Voltage oscillations with respect to the light intensity

made about the water filling operation: once the cathode was kept under waterlogged condition, the daily water filling does not produce relevant voltage changes.

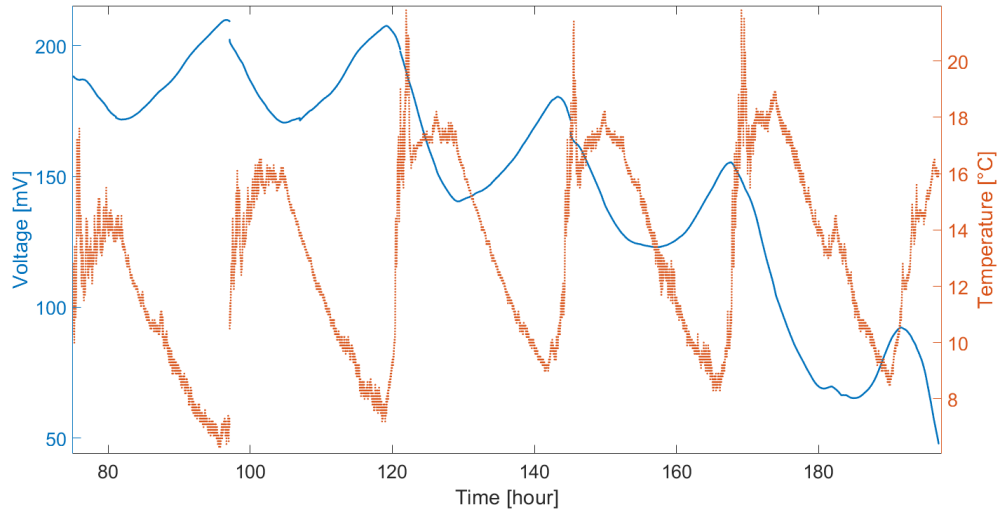


Figure 5.14: Voltage oscillations with respect to the temperature

For 6 d the pot is daily filled. To ensure that the hypothesis is correct, the stop in water filling brings the system back in dry conditions so the voltage measured should come back negative. As shown in Figure 5.11, after few days without filling the pot with water, the P-MFC voltage becomes negative so the assumption was correct. One can notice that also when the voltage become negative, the daily voltage oscillations can be observed. The graph holes are the non monitored periods due to the non possibility to access to the lab during the weekend.

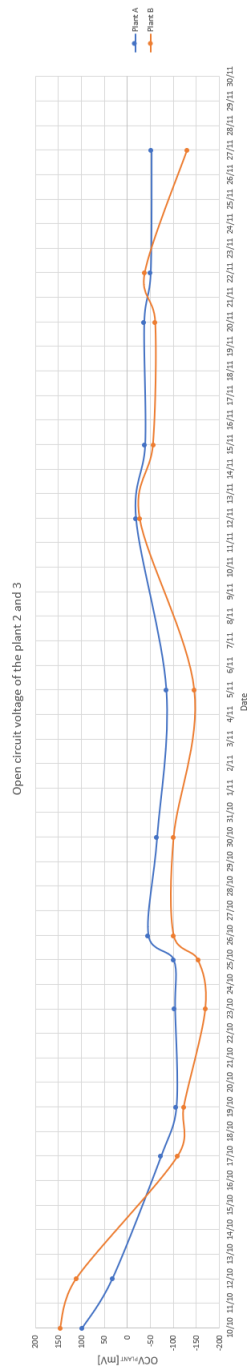
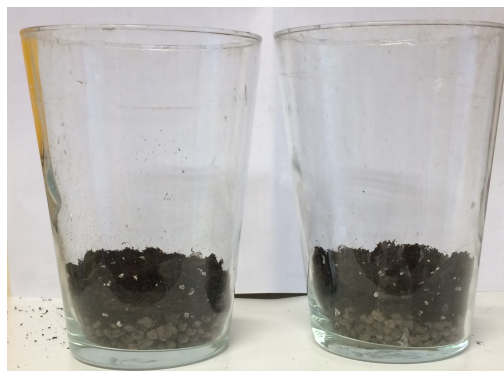


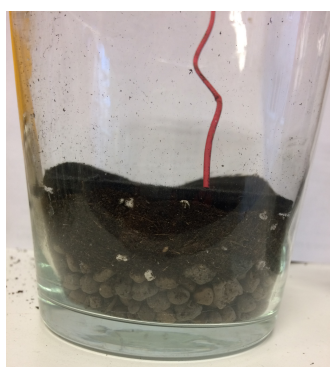
Figure 5.15: Open circuit voltage measurements of carex hachijoensis



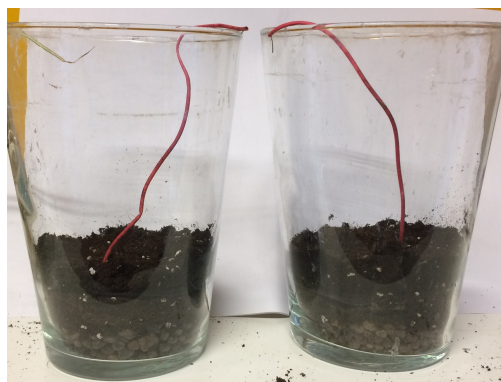
(a) Side view after a layer of clay



(b) Side view after the first layer of universal soil



(c) Recycled felt anode with wire



(d) Side view after the second layer of universal soil



(e) Plant inserted into the vase



(f) Recycled felt cathode with wire

Figure 5.16: Pictures of *Carex Hachijoensis* - James and Jason

5.3 Carex Hachijoensis - Loria

The plant is the *Carex Hachijoensis* and it was bought on 2/10/2018 but planted on 08/01/2019. For this plant, it is used a DIY product Sprout 'n Spark [59] of a Dutch company Plant-e. The kit provides everything one needs (without the plant) to build the P-MFC such as plastic planters (Figure 5.30a), titanium wires, carbon granulates for the anode, carbon felts as cathode, blue-white cloth as membrane and so on. The main difference with the previous systems discussed is that circular carbon felt anode is replaced by carbon granulates.

5.3.1 Plant structure

The process is described point by point providing also some pictures (Figure 5.30):

- Put 1 cm of carbon granules inside the pot (Figure 5.30b).
- Bend about $\frac{2}{3}$ of the longest titanium wire in a ring shape. The ring should be the size of the bottom of the pot. Wrap the end of the wire around itself to secure the ring. Slide the insulation tube around the titanium wire up to the ring. Bend the end of the wire 90°. Place the black plug on the end of the long titanium wire and tighten the screw of the plug with a screwdriver. Place this wire in the pot. (Figure 5.30c).
- Place the plant (Figure 5.30d) in the pot with some of the soil that comes with the plant. Then add the whole bag of the granulates around the roots of the plant.
- Cut the carbon felt (cathode) and the blue-white cloth (membrane) from the edge to the middle. Cut a circle in the middle of the fabrics. Make sure that the stem of the plant will fit through the hole. Weave half of the short titanium wire through the cathode and make sure that the end of the wire does not stick out the bottom (weave it inside the felt or let it end on top of the felt). Bend the end of the wire 90°. Place the red plug on the end of the short titanium wire and tighten the screw of the plug with a screwdriver. Place the membrane and cathode around the plant on the top of the carbon grains (Figure 5.30e). In this case the area of the P-MFC is computed considering only the cathode surface because the anode is all the soil. The cathode has an external diameter of 14.5cm and an internal diameter (of part removed to make the plant stand) of 6cm.

$$A_{\text{CATHODE}} = \frac{\pi(D_{\text{EXT}}^2 - D_{\text{INT}}^2)}{4} = \frac{\pi[(12 \text{ cm})^2 - (8.5 \text{ cm})^2]}{4} = 56.35 \text{ cm}^2 \quad (5.5)$$

Usually in different papers, the electrode area is the anode area but one can think that also the cathode one influences the amount of energy that can be reached so a general, though lower, assumption can be to consider the electrode area as the minimum between the two. For this purpose, the anode is the carbon granulates so the anode could be considered the surface in contact with the membrane that is also equals to the cathode area:

$$A_{\text{ELECTRODE}} = A_{\text{CATHODE}} = 56.35 \text{ cm}^2$$

The P-MFC system (Figure 5.30f) is ready to be connected to the sensing system to be analyzed and characterized.

5.3.2 Negative voltages with electronic load board

Once the P-MFC system is created, the open circuit voltage between cathode and anode was -0.422 mV measured with the digital multimeter MT-1132 [60]. The negative voltage creates a problem in the use of the designed circuit (Figure 6.1). Considering negative V_{OC} , the voltage drop across the transistor M_1 becomes too

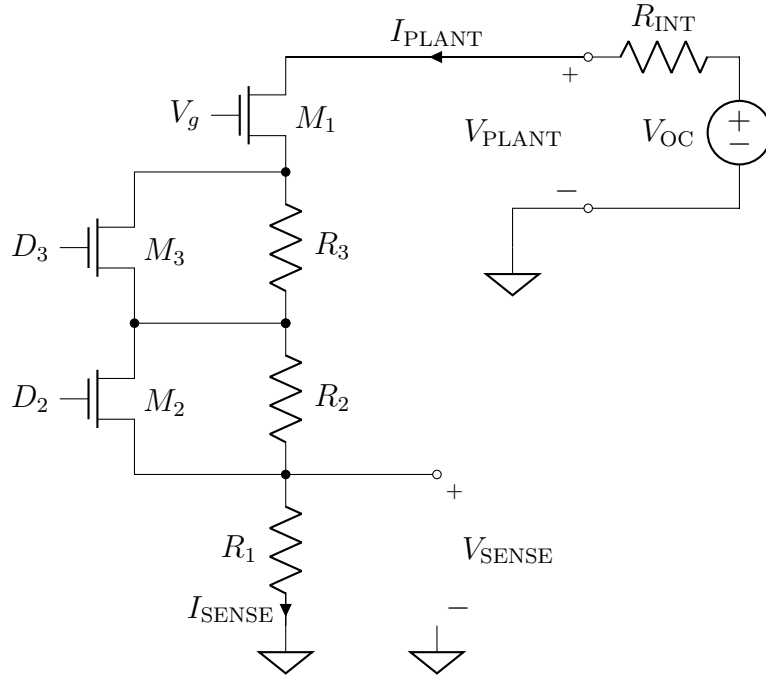


Figure 5.17: Proposed circuit solution

low (also negative) meaning that it is no longer able to impose the desired current. This problem was solved inverting the wire connection between cathode and anode:

this allows the plant characterization but one has to pay attention that all the future considerations must be done remembering the voltage inversion.

5.3.3 Current range identification

The system start to produce immediately probably due to the fact that during the transfer into the P-MFC pot, the soil close to the roots of the plant is hold the same: this means that the microorganisms are still present so the energy generation can directly start. Before to perform a static analysis, a roughly evaluation of the current range that the system is able to generate must be done. To find the upper limit in current range, two values are tested. The duration of each current value is an important parameter because it must be higher with respect to the transient time. Initially all this info are unknown so the analysis start absorbing $10\text{ }\mu\text{A}$ for 10 h and then $20\text{ }\mu\text{A}$ for other 10 h. This analysis was made on 15/01/2018. The Figure 5.18 shows the current (blue) and the voltage (red) measurements.

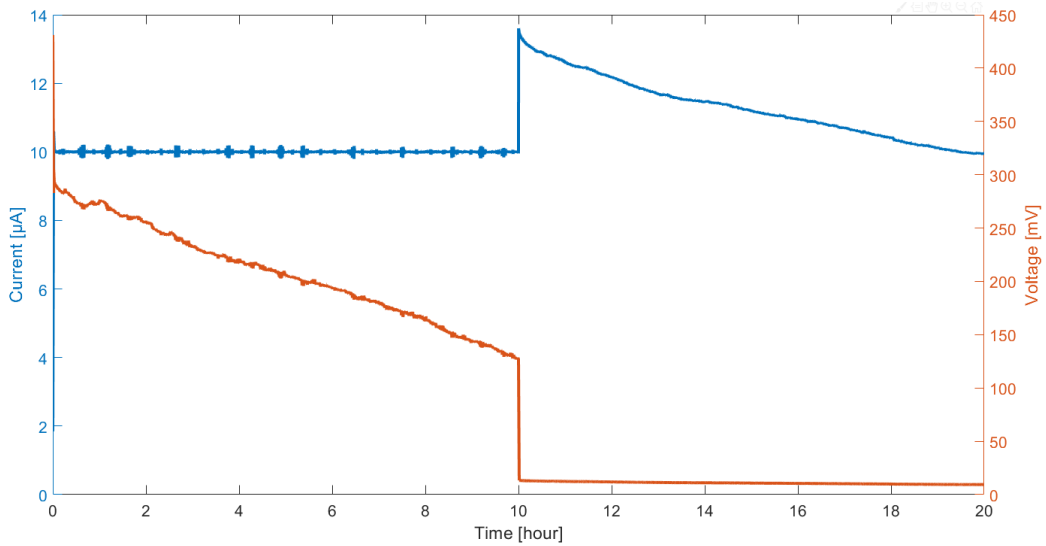


Figure 5.18: Current and voltage of P-MFC for current range identification

The first 10 h impose a constant current absorption of $10\text{ }\mu\text{A}$ and the voltage measured shows an initial instantaneous drop of 140 mV and then this voltage slowly tries to goes in a constant operating point. What is noticed, after this duration, the voltage does not reach the operation point meaning that for this large current step, the transient takes very long time. For the second 10 h the current should reach $20\text{ }\mu\text{A}$ but the current curve shows that initially increases but at a certain point, the curve change slope and the voltage drops to about 12 mV: this behavior means that the system composed by the P-MFC and the electronic load board connected

creates a current limitation of about $14\mu\text{A}$ and the very low voltage across the plant switch off the transistor of the electronic load that sets the current absorbed.

5.3.4 Environment influence

Once the upper current limit is defined, it is possible to check the influences due to the environmental parameters. This analysis is performed on 17/01/2018 setting a constant current absorption of $1\mu\text{A}$ for 7 h. The Figure 5.19 shows the current (blue) and the voltage (red) measurements.

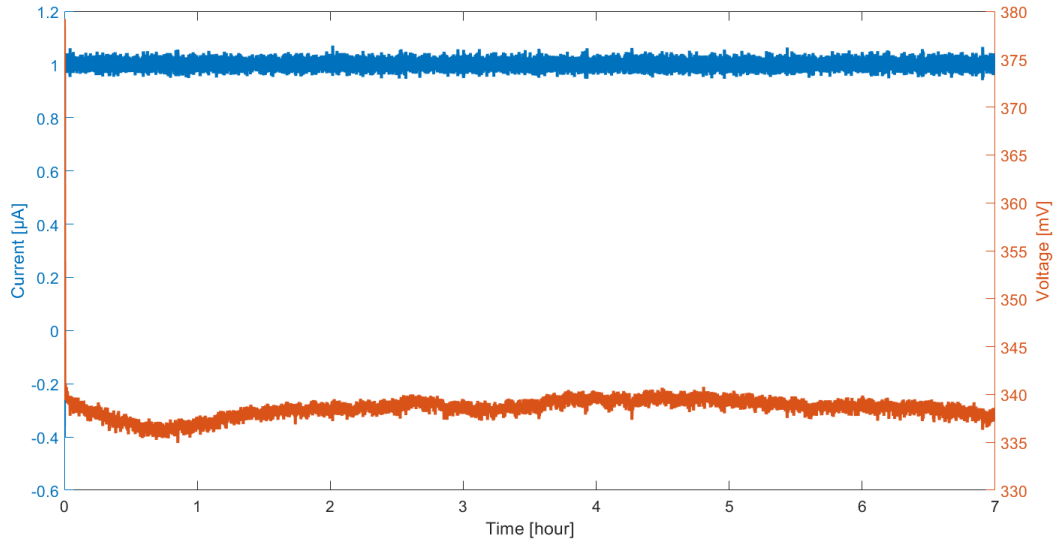


Figure 5.19: Voltage and current of P-MFC in steady state conditions

One can note that the transient is faster due to a smaller current step ($1\mu\text{A}$): to start from the initial voltage (379 mV) up to the stable operation point (337 mV) it takes about 1 h. After this initial period, the voltage is quite constant across this operating point for all the time. During this interval, the light intensity and the temperature are monitored. The Figures 5.20 shows the voltage with respect to the light intensity. From this graph, the influence of the solar radiation seems to be not so influential in the voltage generation. A more interesting effect can be seen from the temperature measurements. The Figure 5.21 shows the positive correlation between the voltage and the temperature: an increasing of 4°C produces an increasing of about 4 mV. This behavior confirms the considerations made in the state of art chapter. It is possible to define a roughly temperature sensitivity of this P-MFC:

$$S_V^T = \frac{\Delta V}{\Delta T} = \frac{4\text{ mV}}{4^\circ\text{C}} = 1 \frac{\text{mV}}{^\circ\text{C}}$$

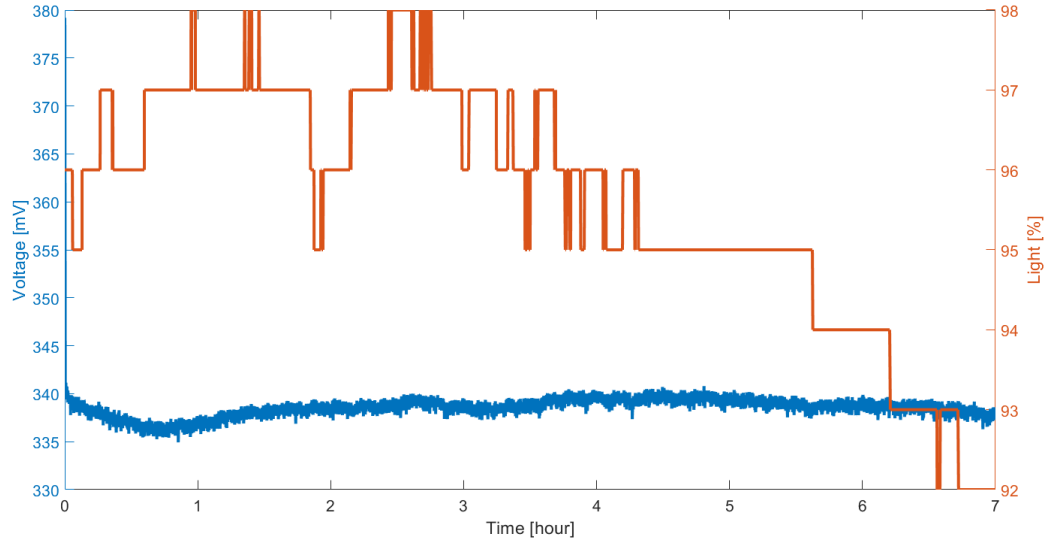


Figure 5.20: Light intensity and the measured voltage of the P-MFC

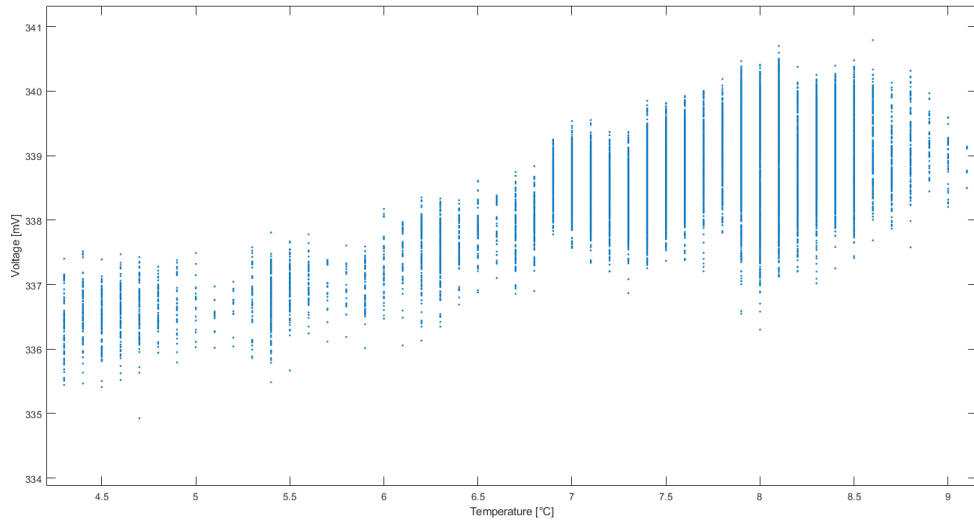


Figure 5.21: Correlation between temperature and the measured voltage of the P-MFC

5.3.5 Static analysis

At this point, one has enough information to perform a static analysis. This analysis allows to estimate the static parameters (open circuit voltage V_{OC} and internal resistance R_{INT}) of the P-MFC equivalent model (Figure 5.22). From the previous measurements, the upper current limit was founded at about $14\mu A$

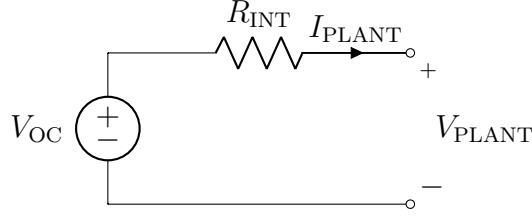


Figure 5.22: Equivalent electronic circuit to model the P-MFC

and with a current step of $1\mu\text{A}$, the transient is extinguished after about 1 h. These information are useful to define the parameters for the static analysis. The current interval is defined from $0.1\mu\text{A}$ up to $12\mu\text{A}$. In this interval are taken 10 equally spaced points and each current absorbed is taken for 1 h30 min so the whole analysis lasts $1\text{ h}30\text{ min} \cdot 10\text{ points} = 15\text{ h}$. The Figure 5.23 represents the static analysis from the measurements on 23/01/2019.

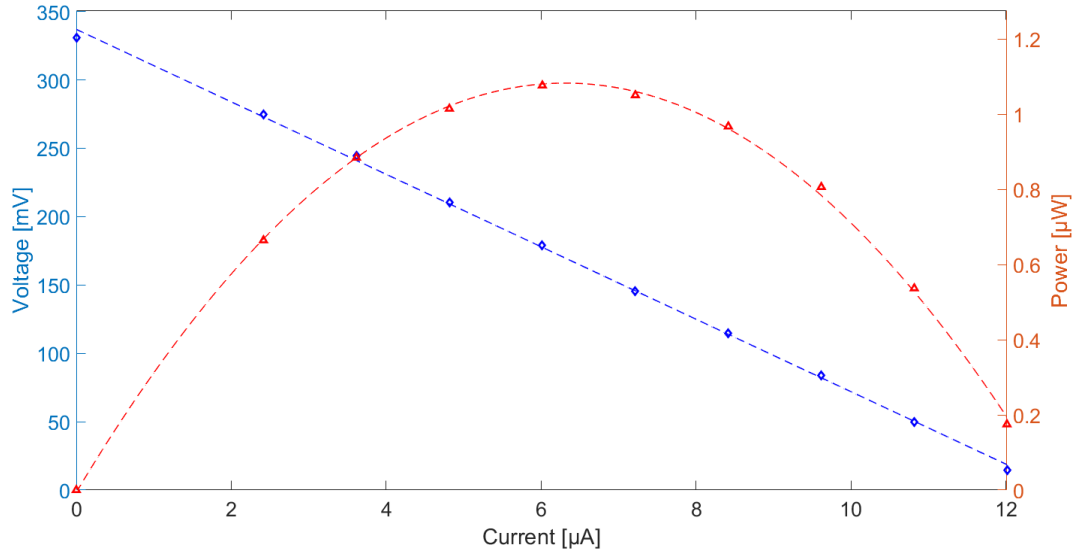


Figure 5.23: Polarization curve and power curve of the P-MFC

The blue curve represents the polarization curve while the red one the power curve. Each point of the curve is computed averaging the last 30 min of each current interval so the measurements after each voltage transient. The open circuit voltage V_{OC} is computed as the intersection of the curve with the voltage axis:

$$V_{OC} = V(I = 0\text{ A}) = 336.3\text{ mV}$$

while the internal resistance R_{INT} from the slope of the curve:

$$R_{\text{INT}} = \left\| \frac{310.2 \text{ mV} - 71.83 \text{ mV}}{1.01 \text{ } \mu\text{A} - 10 \text{ } \mu\text{A}} \right\| = 26.515 \text{ k}\Omega$$

The maximum power generated is about $1.07 \text{ } \mu\text{W}$ when the absorbed current is $I_{\text{MPP}} = 6.3 \text{ } \mu\text{A}$ so across the plant the voltage is $V_{\text{MPP}} = 170.3 \text{ mV}$.

5.3.6 Dynamic analysis

After the static, performing the dynamic analysis allows to increase the information about this P-MFC. This analysis allows to estimate the dynamic parameters (series resistances R_s , R_1 and the capacitance C_1) of the impedance of the P-MFC model (Figure 5.24). The impedance defines the value of the P-MFC resistance for a

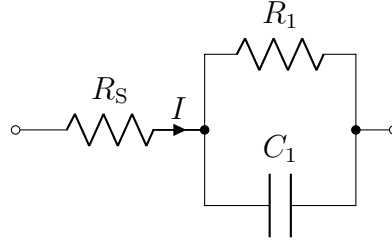


Figure 5.24: Impedance of the P-MFC model

frequency band. To reduce the duration of the analysis, the Welch method is applied so a white noise current signal is superimposed to a bias current and by comparing the spectra of this current injected and the voltage of the P-MFC measured, it is possible to obtain the impedance information. For this purpose, the bias current is chosen near to the MPP thus $8 \text{ } \mu\text{A}$ with a white noise signal with a maximum amplitude of 200 nA and the analysis duration is defined of 14 h . The Figure 5.25 shows the results of the dynamic analysis performed on 24/01/2019. This graph is obtained using the Welch method implementing the Blackman-Harris window with a width of $10\,000 \text{ s}$ and an overlap between adjacent windows of 90% . The sample frequency is 1 Hz so according the Nyquist theorem, the maximum frequency f_{MAX} that can be analyzed is:

$$f_{\text{MAX}} = \frac{f_{\text{SAMPLE}}}{2} = \frac{1 \text{ Hz}}{2} = 500 \text{ mHz}$$

The minimum frequency is defined not only by the number of samples N but also by the windowing function. This frequency axis of this graph starts from 4 mHz up to 500 mHz . The blue dots represent the results of the dynamic analysis from the measurements on the P-MFC. Simulating the behavior of the P-MFC model, it is possible to find out some components values that better approximate

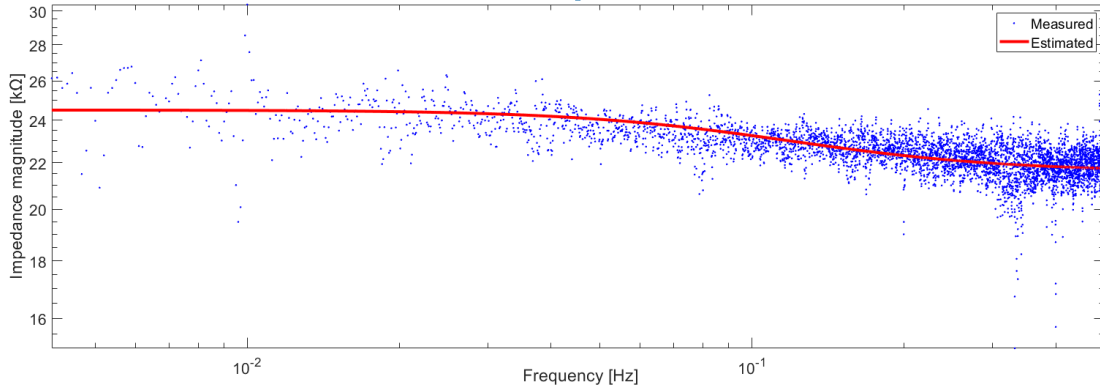


Figure 5.25: Impedance in frequency

the P-MFC results. The red curve represents the impedance obtained from the estimation parameters. The results behavior can be approximated with 1-time constant equivalent impedance. At low frequency, the capacitor C_1 is an open circuit so the resistance seen is the summation of R_S and R_1 while when the frequency is far higher than the pole, the capacitor C_1 is a short-circuit thus the resistance seen is only R_S . The red curve is obtained simulating the equivalent model of the P-MFC in the frequency range with $R_S = 21.6 \text{ k}\Omega$, $R_1 = 2.9 \text{ k}\Omega$ and $C_1 = 493 \text{ }\mu\text{F}$. With this values, the frequency pole f_P is:

$$f_P = \frac{1}{2\pi R_1 C_1} = \frac{1}{2\pi \cdot 2.9 \text{ k}\Omega \cdot 493 \text{ }\mu\text{F}} = 111.32 \text{ mHz}$$

At low frequency the resistance seen should be equal to the internal resistance R_{INT} computed during the static analysis. From the dynamic analysis, this resistance $R_{\text{INT}_{\text{DYN}}}$ is the summation of R_S and R_1 :

$$R_{\text{INT}_{\text{DYN}}} = R_S + R_1 = 21.6 \text{ k}\Omega + 2.9 \text{ k}\Omega = 24.5 \text{ k}\Omega$$

The comparison between this two resistances gives not a perfect matching but they are quite similar meaning that the dynamic analysis gives a rather accurate results. The main cause of this difference could be the difficulty to hold the P-MFC system in a perfect constant environmental conditions for all the duration of the analysis: the plant was left outdoor and in 14 h the temperature, the solar intensity and also the soil humidity can vary widely.

5.3.7 The need of the plant

Once all these results are reached, one could ask if they were due to the new Plant-e structure and not due to the presence of the plant. This is a good question thus

a verification was made measuring the electrical parameters without the plant. Similar results means the plant could be not necessary. Two different experiments are performed in order to check this assumption: the structure is always the same but in the first case the soil is composed only by topsoil while in the second one only by carbon granulates as in the Plant-e kit. Since the plant is removed, the systems can be named only microbial fuel cells (MFCs).

P-MFC with only topsoil

This set up experiment uses the Plant-e cathode, membrane and wires but the carbon granulates are replaced by the topsoil. The Figure 5.26 shows this MFC structure in practice. The analysis performed is the connection of the electronic



Figure 5.26: P-MFC with only top soil structure

load between cathode and anode of this structure, set the current absorption of $2\text{ }\mu\text{A}$ and monitor the voltage across this MFC. An important consideration is that before to start the measurements, the cathode must be wet in order to promote the protons exchange with the soil through the membrane. The Figure 5.27 shows the voltage and current behavior of this analysis performed on 07/02/2019.

What one notices is that the absorbed current oscillates up to 50 nA without never reaching $2\text{ }\mu\text{A}$ and the voltage starts from about 33 mV but after only 10 s it drops to 0.3 mV . The meaning of this graph is that there is a small energy production due to the microorganisms naturally present in the soil but they are not able to provide sufficiently energy as in the previous cases due to the absence of the plant. The plant provides continuously the fuel for the microorganisms to increase the maintain the energy production.

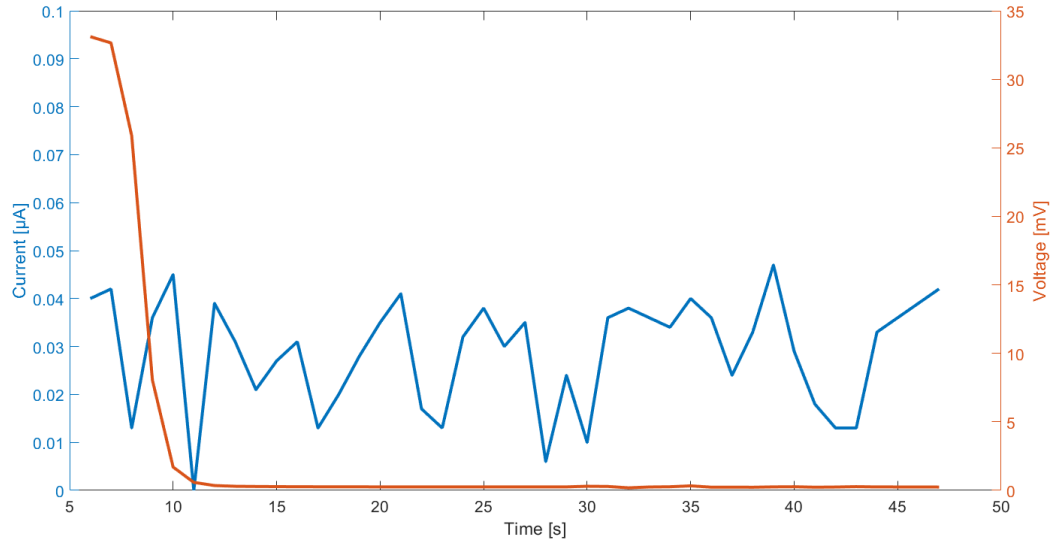


Figure 5.27: Voltage and current for MFC with only topsoil

P-MFC with only carbon granulates

This set up experiment uses the Plant-e cathode, membrane, wires and the carbon granulates. The Figure 5.28 shows this MFC structure in practice. The analysis is



Figure 5.28: P-MFC with only carbon granulates structure

performed connecting cathode and anode of this structure at the electronic load, setting the current absorption of $2\ \mu\text{A}$ and monitoring the voltage across this MFC. An important consideration is that before to start the measurements, the cathode must be wet in order to promote the protons exchange with the soil through the

membrane. The Figure 5.29 shows the voltage and current behavior of this analysis performed on 07/02/2019.

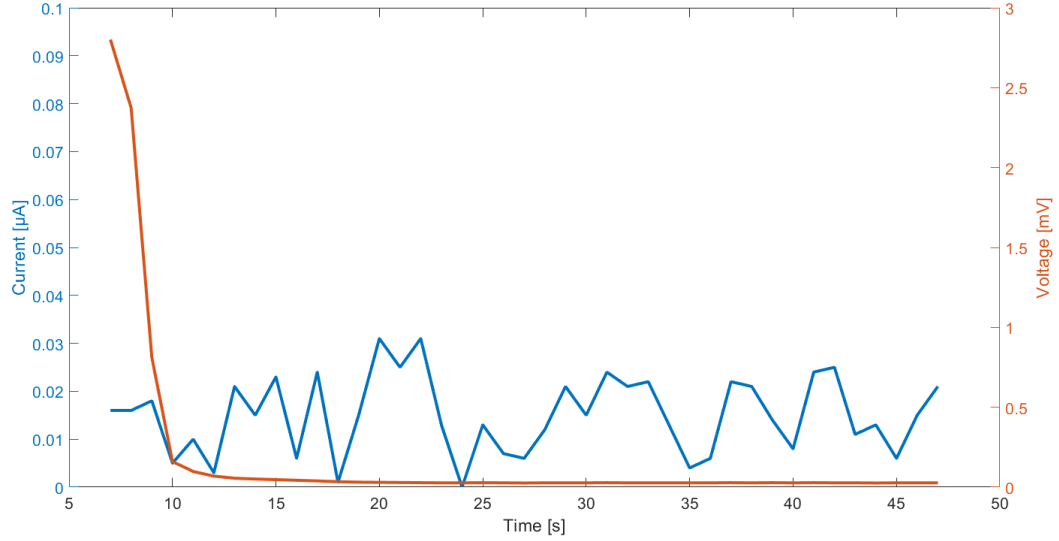


Figure 5.29: Voltage and current for MFC with only carbon granulates

What one notices is that the absorbed current oscillates up to 40 nA without ever reaching 2 μA and the voltage starts from about 3 mV but after only 10 s it drops to 0.03 mV. The meaning of this graph is as for the topsoil, there is a small energy production due to the microorganisms naturally present in the carbon granulates but they are not able to provide sufficiently energy as in the previous cases due to the absence of the plant.



(a) Top view of the plastic pot



(b) Top view after a first carbon granules layer



(c) Inserting the titanium wire



(d) Plant *Carex Hachijoensis*



(e) Top view of cathode and membrane



(f) Complete P-MFC with *Carex Hachijoensis*

Figure 5.30: Pictures of *Carex Hachijoensis* - Loria

Chapter 6

Conclusions

After these months of research, our understanding of the possibilities of the P-MFC has increased. Part of the black box was turned into grey. In this final chapter, one can find an overview of the results obtained with a low cost automatized sensing system evaluating the influence that the external world has on the P-MFC energy generation and how the sensing system can measure them. According to this measurements experience, some future prospective and improvements are proposed both on P-MFC design and mainly on electronic point of view. This thesis is focused on sensing system design and the P-MFC characterization.

6.1 Summary

This thesis starts from the necessity to find out some sustainable energy source to feed some IoT nodes spread in several application fields. The possibility to replace the batteries with the plant technology opens a wide research field and allows to optimize what the nature gives. The use of a new technology means an accurate characterization and study to understand how it works but also how to improve efficiency in the energy extraction. An entire chapter is dedicated on the explanation of what the current state of art of the P-MFC technology offers. It describes in detail all the components needed for its creation and also the internal mechanisms which allow the energy production. These studies do not have to stop to an ideal behavior but they have to analyze the losses due to non idealities and how the surrounding environment acts on them. Since this technology is used to extract electric energy, an electric characterization must be performed. One starts from a black box so without any information. The two main described in this thesis are the static and the dynamic analysis. They are linked because they give complementary information about the P-MFC: related to the steady state behavior (static) and to the transient behavior (dynamic). Both are described

proved, the electronic load system is implemented on a PCB. At this point, the known load can be replaced with the P-MFC for its characterization. Different systems are created but with the same family Carex plant. For each system, the structure and the performed analysis are described in details.

6.2 Results

The P-MFCs which implement the Carex family plant, in outdoor conditions during the winter (January and February) period, produces the results depicted in Figure 6.2.

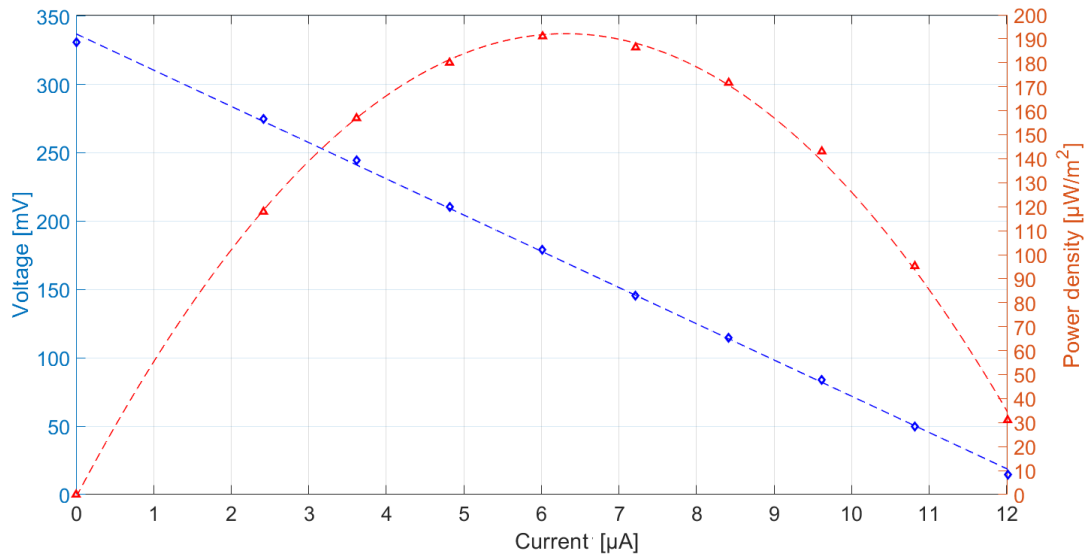


Figure 6.2: Polarization curve and power density of P-MFC (Loria)

This graph shows the polarization curve (in blue) and the power density (in red) with respect to the current. The maximum voltage generated was around 350 mV with the Plant-e P-MFC structure. The power density generated is about $192 \frac{\mu\text{W}}{\text{m}^2}$ when the system produces a current of $6.5 \mu\text{A}$ and the voltage across cathode and anode is 170 mV. If the connected load works close to these electrical conditions, it is able to maximize the energy production. These information are obtained performing a static analysis with the P-MFC (Loria) connected to the electronic load board. This is a terrestrial plant so it is not recommended to fill the pot with water. These results show how, also if the anode is not in an anaerobic condition, the system generates energy. Probably, there was a reduction in energy production with respect to its maximum due to the fact that a large number of electrons are used to reduce the oxygen in the soil and not for the energy harvesting. Using

terrestrial plants, it produces a polarity inversion in the P-MFC due to the presence of the oxygen in the anode chamber. To perform this analysis, the anode was connected to the positive terminal of the electronic load board and the cathode to the negative terminal. The solution that can be used to overcome this polarity problem is to invert the electrode role: the polarity inversion means that also the chemical reaction that occur are overturned so an appropriate solution due to their potential could be to name cathode the electrode in the soil and anode the electrode in contact with the air. From the dynamic analysis (Figure 6.3), one is able to see the steady state resistance of $24.5\text{ k}\Omega$ but most important to notice is that increasing the frequency of the current signal that is sinked, the resistance decreases to $21.6\text{ k}\Omega$: lower resistance means an higher output voltage so lower losses and higher power generation. This kind of analysis allows to choose how

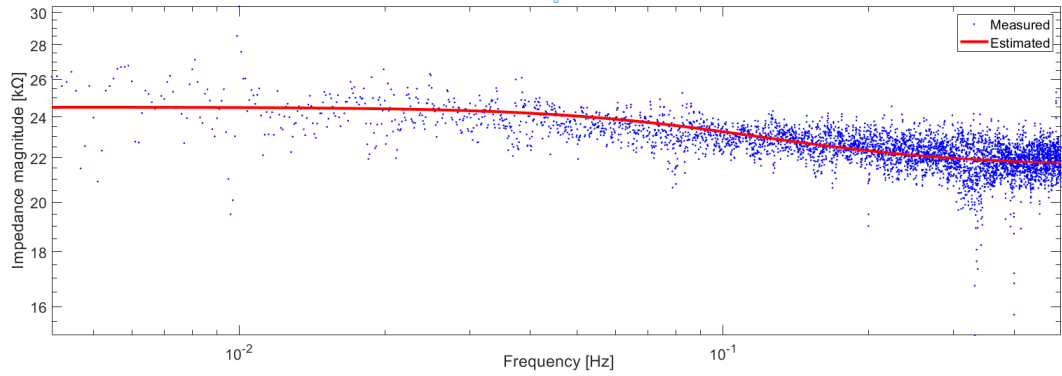


Figure 6.3: Dynamic analysis results for Loria

the energy harvester has to work in order to optimize the energy extraction from the P-MFC: if the harvester extract energy with frequency of 300 mHz, the resistance is lower and the energy extraction is optimized. Another interesting aspect is related to the correlation between the temperature and the voltage generation (Figure 6.4). This behavior recommends to use this kind of systems in warmer area because it can increase the voltage generation with an increasing of temperature.

6.3 Future prospective and applications

6.3.1 Possible future P-MFC researches

For this thesis, only one family plant is used in order to do not insert too many variables in the characterization. Some improvements can be applied referring to the components material, structure direction or adding other sensors. First,

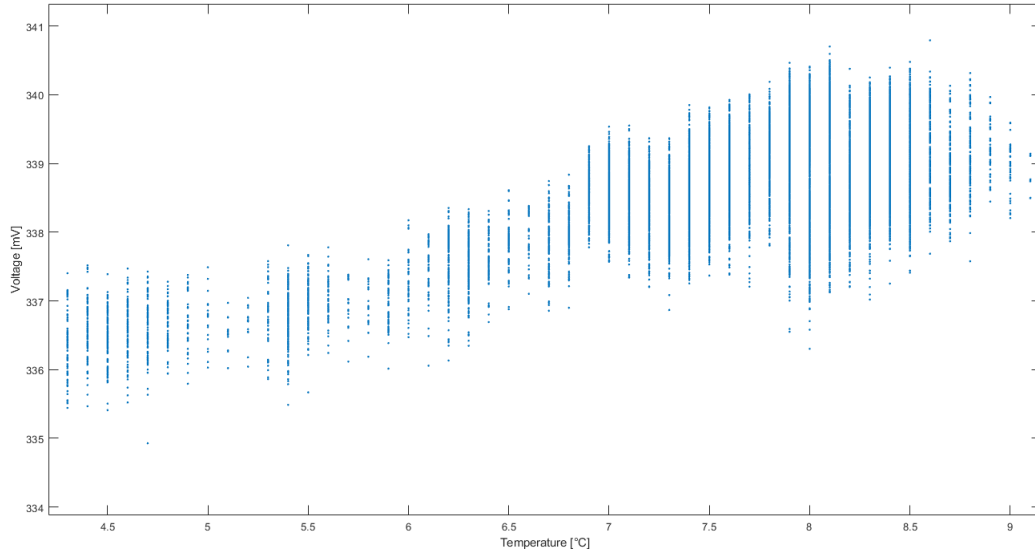


Figure 6.4: Temperature influences on the voltage generation

different plants can be used to compare their energy generation and not only with planter plants but also with trees so the system has to be adapted for probably higher energy generation but also the structure can be different due to the larger roots. Different researches treat the components material choice trying to find a material with good performance, reliable and also not expensive. Some papers talk about P-MFC with horizontal structure so also this system can be better studied: when the plant is a tree, dig under the plant roots could be difficult so this horizontal structure can be a good solution. Implementing terrestrial plants, the humidity sensor problem must be solved in order to increase the knowledge of the energy generation with respect to the soil humidity. Moreover, other kind of sensors can be used (e.g. soil pH sensor) to understand how these parameters influence the system.

6.3.2 Electronic circuit improvements

In order to create an as general as possible circuit able to characterize the connected load, the proposed solution can be improved.

Independence from the load voltage polarity

The voltage polarity inversion can create some problems to the electronic load. When V_{PLANT} is very low or also negative means that the transistor M_1 is no longer able to set the desired current flowing through. In this situation, the measurements

of the ADC keep to be valid because it is able to measure also the negative voltages (± 625 mV) even if they do not exceed the voltage range $||625 \text{ mV}||$. Using the same circuit idea, a possible solution that can solve this problem is to keep the electronic load circuit and, using some switches, reverse the positive and negative terminals depending on their polarity (Figure 6.5). This solution introduces some systematic

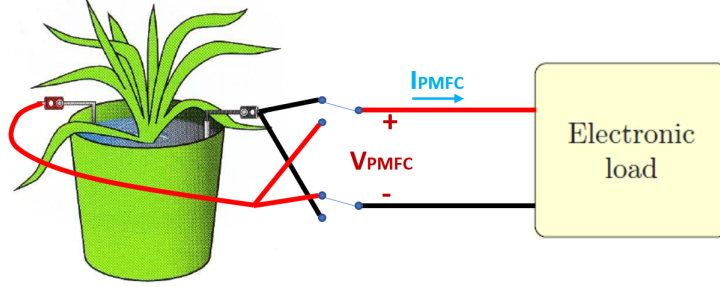


Figure 6.5: Solution improvement for polarity problem

effects due to the insertion of the switches but allows, in principle, to solve the polarity problem.

Electrode potential with respect to a reference

The P-MFC voltage E_{CELL} is the difference between the cathode E_{CATHODE} and the anode E_{ANODE} potential:

$$E_{\text{CELL}} = E_{\text{CATHODE}} - E_{\text{ANODE}}$$

For this purpose, the anode is connected to the ground reference of the electronic load board and the cathode voltage is measured by the input of the ADC. This allows to monitor the cell voltage E_{CELL} but limits the knowledge of what happen at each electrode. As different papers shows, the measured cathode E_{CAT} and the measured anode E_{AN} potential are measured with respect to a voltage reference E_{REF} .

$$E_{\text{CATHODE}} = E_{\text{CAT}} - E_{\text{REF}} \quad E_{\text{ANODE}} = E_{\text{AN}} - E_{\text{REF}}$$

The cell voltage E_{CELL} , of course, is computed as usual:

$$E_{\text{CELL}} = E_{\text{CATHODE}} - E_{\text{ANODE}} = E_{\text{CAT}} - E_{\text{REF}} - (E_{\text{AN}} - E_{\text{REF}}) = E_{\text{CAT}} - E_{\text{AN}}$$

but in this case it is possible to monitor the cell voltage variation understanding which produces this variation: for example, an increasing in cell voltage could be due to an increasing in cathode potential or in a decreasing in anode potential or also both together.

Waterlogged condition avoid voltage inversion

In this thesis, the P-MFC systems are implemented using terrestrial plants. As largely explained, the absence of water in the soil allows the intrusion of the oxygen in the anode chamber. The hypothesis that the voltage inversion of this terrestrial P-MFC is due to the absence of waterlogged condition is demonstrated: the pot of one P-MFC system is filled up with tap water and the voltage across it changes polarity becoming positive (Figure 6.6). The red points on the graph represent the

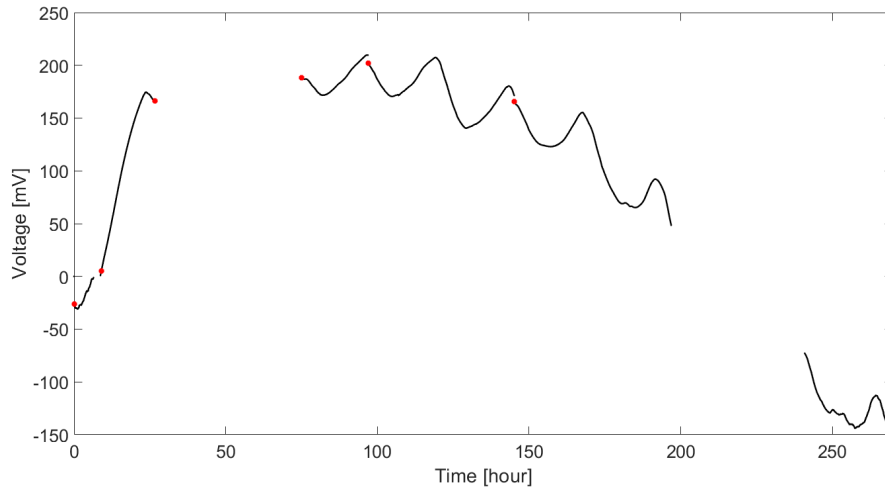


Figure 6.6: Waterlogged condition voltage measurements of the P-MFC

instant in which the pot is water filled. The system starts with a negative polarity but after a couple of days after the water filling, the voltage becomes positive reaching a value of about 180 mV. For few days the system is daily water filled and the voltage holds positive. One important aspect is related to the voltage oscillations in these days due to the effect that temperature and solar radiation have on the electrons generation. A final proof is to stop the water filling and, how the graph shows, the P-MFC voltage comes back negative. The daily oscillations are present also during the negative polarity.

Software improvements

Not only the hardware part can be improved but also the software. The algorithm implemented on the RPi board can be modified in order to optimize the sensing system management. For the data, they can be stored not only at the end of the analysis but at each sample time: this prevents the lost of data (e.g. due to power supply disconnection, program break). For the calibration phase, it can be performed on-board without connecting other instruments or components

at the electronic load board (simpler calibration procedure). The current region transition can be optimized analyzing in real-time the measurement trend and understand automatically how and when change region. Another improvement can be done removing the user interface on the PC but using an interface directly on the RPi board (simpler system).

6.4 Applications

The final use of these P-MFCs could be the power generation for IoT nodes. Each node can be equipped with different electronic components that act as a load for the system. Depending on the amount of power generated from the P-MFC, different kind of loads can be powered. In table 6.1, different sensors and their energy requirements are investigated in order to understand which one can be connected to the P-MFC used for this thesis. Supposing to have the electrode area of 1 m^2 ,

Name	Voltage [V]	Current [mA]	Power[mW]	Price [€]
TEMPERATURE				
LM335	5	5	25	0.76
LM35	5	0.131	0.655	3.50
DS18B20	3.3	1.5	4.95	2.90
MCP9700A	3.3	0.012	0.04	1.50
SOIL HUMIDITY				
Moisture	5	51	255	4.05
TEMP/HUM				
DHT11	3.3	2.5	8.25	5.40
DHT22	3.3	1.5	4.95	9.00
Termoigrosense	3.3	2	6.6	10.00

Table 6.1: Different sensors for the P-MFC application

the maximum generated power P_{PMFC} is $192 \text{ } \mu\text{W}$. From this table, only one sensor can be connected to the P-MFC (from power point of view): the temperature sensor MCP9700A because it consumes continuously $P_{\text{MCP9700A}} = 40 \text{ } \mu\text{W}$. The smart idea to duty cycling the use of the load allows to connect sensors that consumes an higher power but infrequently. For example, the temperature sensor LM35 consumes continuously $P_{\text{LM35}} = 655 \text{ } \mu\text{W}$ but using it with a duty cycle DC it is possible to connect it to the P-MFC. The average consumed power \bar{P} from the sensor is computed as:

$$\bar{P} = P_{\text{SENSOR}} \cdot \text{DC}$$

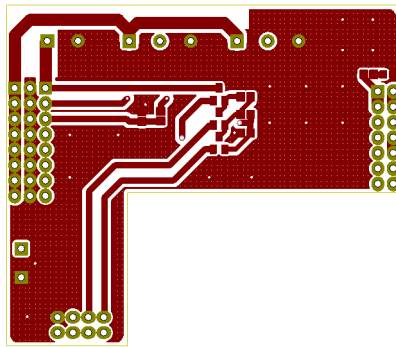
and it must be lower than the P_{PMFC} :

$$\bar{P} < P_{\text{PMFC}} \rightarrow P_{\text{LM35}} \cdot \text{DC} < P_{\text{PMFC}} \rightarrow \text{DC} < \frac{P_{\text{PMFC}}}{P_{\text{LM35}}} = \frac{192 \mu\text{W}}{655 \mu\text{W}} \approx 0.3$$

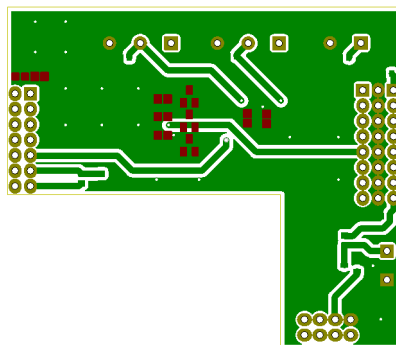
This means that the power generated by the P-MFC can be harvested and switching on the LM35 with a DC lower than 0.3, the P-MFC is able to feed it. For the rest of the cycle, the energy harvester accumulate the energy from the P-MFC. The energy harvester has to increase also the voltage to be sufficient for the load application.

Appendix A

Schematic, PCB layers, 3D viewer and prototype



(a) Front layer



(b) Back layer

Figure A.1: PCB layers

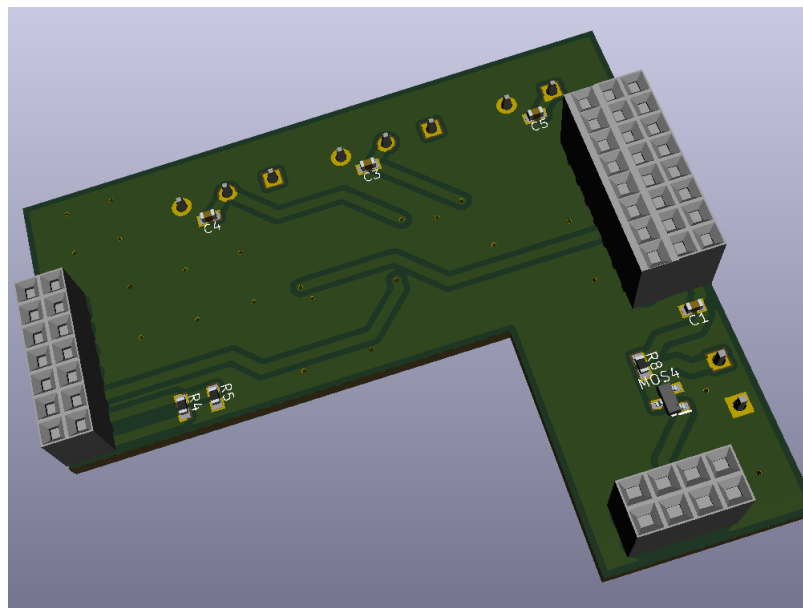
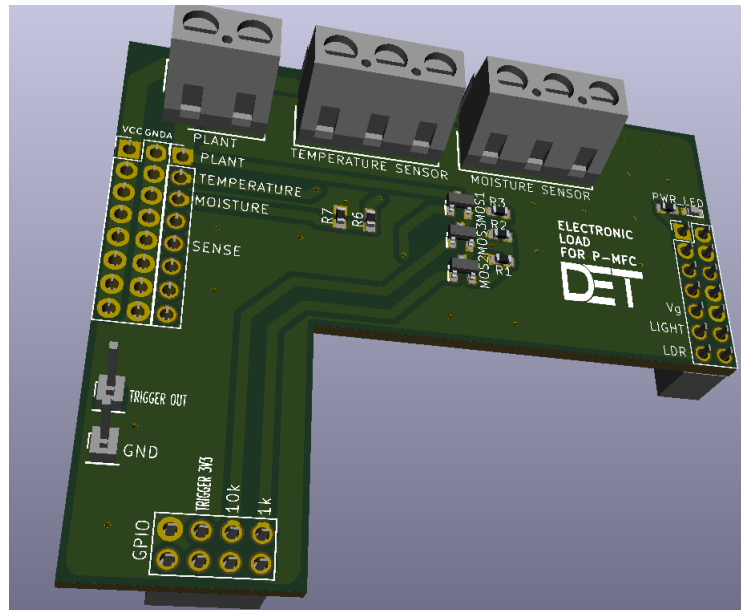
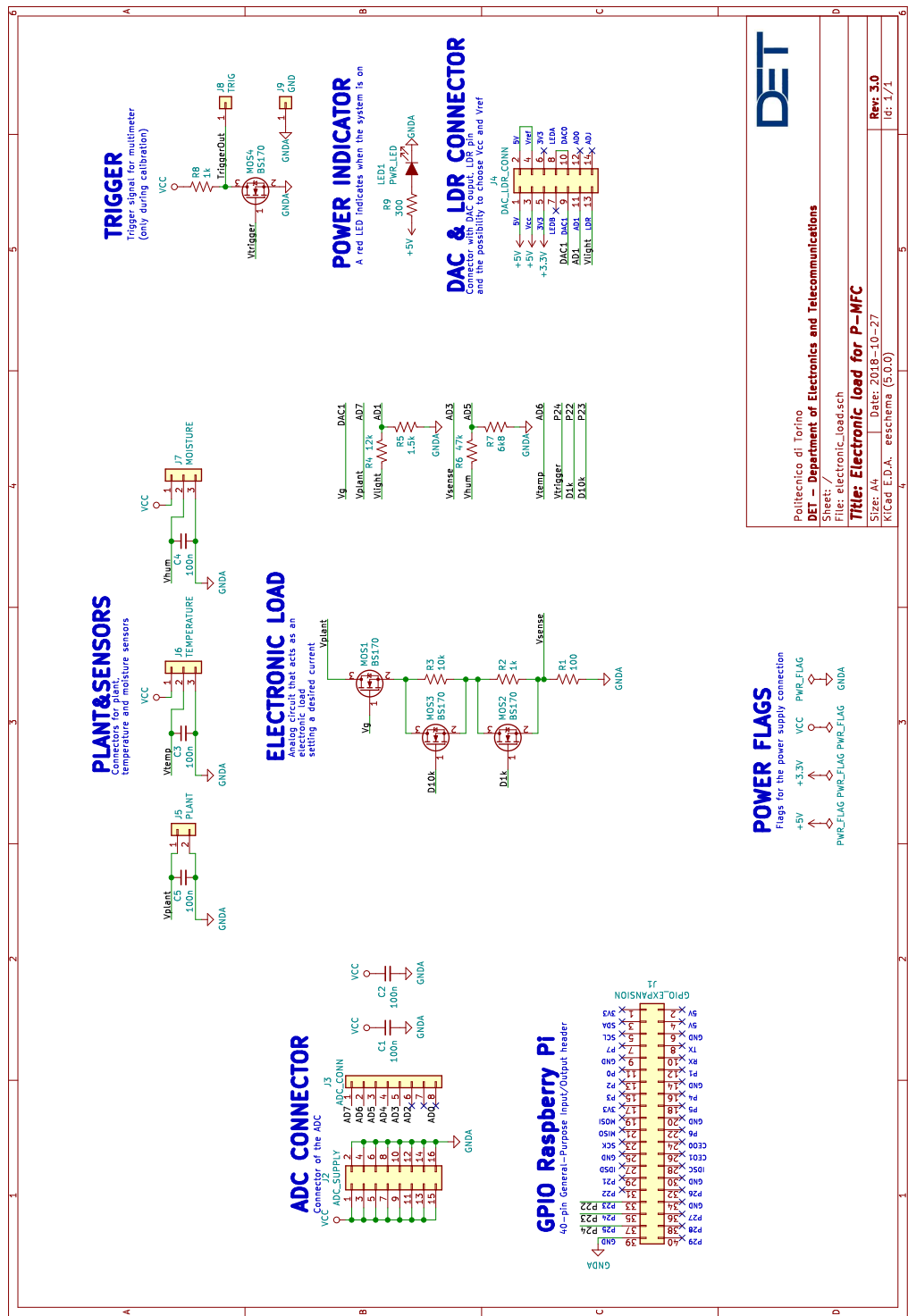


Figure A.2: 3D viewer PCB



Appendix B

User interface application and Raspberry Pi algorithm: code

B.1 User interface application: main functions

```
1 %% MATHEMATICAL FUNCTIONS
2 %% -----> Fast Fourier Transform
3 function [mag, ph, f_range] = FFT(app, signal, Fs)
4 %Fast Fourier Transform: FFT
5 % Samples a signal over a periof of time
6 % and divides it into its frequency components.
7
8 % Length of signal
9 if mod(length(signal),2) == 0 % if length(signal)
    is divisible by 2
10     L = length(signal);
11 else
12     L = length(signal)+1;
13 end
14
15 % Compute the Fast Fourier Transform of the signal
16 Y = fft(signal);
17 % Compute the two-sided spectrum
18 % Magnitude
19 M2 = abs(Y/L);
20 % Phase
21 P2 = angle(Y);
22 % Compute the single-sided spectrum P1 based on P2
```

```

23     % and the even-valued signal length L
24     % Magnitude
25     M1 = M2(1:L/2+1);
26     % Phase
27     P1 = P2(1:L/2+1);
28     % Results
29     mag = M1; % Magnitude of FFT
30     P1(abs(P1) < 0.1) = 0;
31     ph = rad2deg(P1); % Phase of FFT
32     f_range = Fs*(0:(L/2))/L; % Frequency domain
33
34 end
35
36 %% -----> Inverse Fast Fourier
    transform
37 function [y] = IFFT(app, MAG, PH, f)
38
39     L = 2*(length(f)-1);
40     Ymag = ones(1,L); Yph = ones(1,L);
41     Ymag(1:L/2+1) = MAG(1:end).*L;
42     Ymag(L/2:end) = MAG(end:-1:1).*L;
43     Yph(1:L/2+1) = PH(1:end);
44     Yph(L/2:end) = PH(end:-1:1);
45
46     Ymag(2:end) = Ymag(2:end)/2;
47
48     Y = Ymag.*exp(1j.*deg2rad(Yph));
49
50     y = ifft(Y, 'symmetric');
51
52 end
53 %% KIND OF ANALYSIS
54 %% -----> Calibration analysis
55 function CalibrationAnalysis(app)
56     global calibDes calibSense
57     global calibPlant
58     global calibIsense calibIplant calibt
59     global GainError OffsetError DNL INL
60

```

```
61 [t, Ides, RPiCurrent, ~, ~, ~, ~] = ReadFileResults(app
    );
62 [Iplant] = ReadFileCalibration(app);
63 Isense = RPiCurrent(2:end);
64 error = Isense - Iplant;
65 calibIsense = Isense;
66 calibIplant = Iplant;
67 calibt = t(1:end-1);
68 f = 1; j = 1;
69 for i=1:length(Isense)
70     CurrentDes(f,j) = Ides(1,i);
71     CurrentPlant(f,j) = Iplant(1,i);
72     CurrentSense(f,j) = Isense(1,i);
73     if(Ides(i+1)~=Ides(i))
74         f = f+1;
75         j = 0;
76     end
77     j = j+1;
78 end
79
80 CurrentDes(end,end) = CurrentDes(end,end-1);
81 CurrentPlant(end,end) = CurrentPlant(end,end-1);
82 CurrentSense(end,end) = CurrentSense(end,end-1);
83
84 lastSec = 15;
85 for i=1:f
86     calibDes(i) = sum(CurrentDes(i,end-lastSec+1:end))/
        lastSec;
87     calibPlant(i) = sum(CurrentPlant(i,end-lastSec+1:
        end))/lastSec;
88     calibSense(i) = sum(CurrentSense(i,end-lastSec+1:
        end))/lastSec;
89 end
90 %% STATIC PARAMETERS
91 INL = max(calibSense - calibPlant);
92 Ad(:) = calibPlant(2:end)-calibPlant(1:end-1);
93 Ad1(:) = calibSense(2:end)-calibSense(1:end-1);
94 DNL = max(Ad-Ad1);
95 pSense =polyfit(calibDes,calibSense,1);
96 pPlant =polyfit(calibDes,calibPlant,1);
```

```
97     GainMolt = pPlant(1)/pSense(1); % Fattore
        moltiplicativo per aggiustare il guadagno
98     GainError = pSense(1)/pPlant(1);
99     OffsetError = pPlant(2)-pSense(2);
100    app.GainErrorLabel_calibration.Text = [ 'Gain error = '
        num2str(GainError) ];
101    app.OffsetErrorLabel_calibration.Text = [ 'Offset error
        = ' num2str(OffsetError) ' A ' ];
102    app.INLLabel_calibration.Text = [ 'INL = ' num2str(INL)
        ' A ' ];
103    app.DNLLabel_calibration.Text = [ 'DNL = ' num2str(DNL)
        ' A ' ];

104
105    close all;
106    ShowResults_calib(app);
107 end

108
109 %% -----> Static analysis
110 function StaticAnalisis(app)
111     if isfile('PMFC_Results.csv')
112         [~, Ides, Isense, Vplant, Light, Temp, Hum] =
            ReadFileResults(app, 'PMFC_Results.csv');
113     else
114         [~, Ides, Isense, Vplant, Light, Temp, Hum] =
            ReadFileResults(app, 'previous_results_static.
            csv');
115         app.SavedLabel_dynamic.Text = '';
116     end
117
118     f = 1; j = 1; Ides(end+1) = Ides(end);
119     for i=1:length(Isense)
120         CurrentDes(f,j) = Ides(1,i);
121         CurrentSense(f,j) = Isense(1,i);
122         VoltagePlant(f,j) = Vplant(1,i);
123         LightEnv(f,j) = Light(1,i);
124         TempEnv(f,j) = Temp(1,i);
125         HumPlant(f,j) = Hum(1,i);
126         if (Ides(i+1)~=Ides(i))
127             f = f+1;
128             j = 0;
```

```
129         end
130         j = j+1;
131     end
132
133     CurrentDes(end,end) = CurrentDes(end,end-1);
134     VoltagePlant(end,end) = VoltagePlant(end,end-1);
135     CurrentSense(end,end) = CurrentSense(end,end-1);
136     LightEnv(end,end) = LightEnv(end,end-1);
137     TempEnv(end,end) = TempEnv(end,end-1);
138     HumPlant(end,end) = HumPlant(end,end-1);
139
140     lastSec = app.LastTimeAverageEditField_static.Value;
141     for i=1:f
142         staticDes(i) = sum(CurrentDes(i,end-lastSec+1:end))
143             /lastSec;
144         staticPlant(i) = sum(VoltagePlant(i,end-lastSec+1:
145             end))/lastSec;
146         staticSense(i) = sum(CurrentSense(i,end-lastSec+1:
147             end))/lastSec;
148         staticPower(i) = staticPlant(i)*staticSense(i);
149         staticLight(i) = sum(LightEnv(i,end-lastSec+1:end))
150             /lastSec;
151         staticTemp(i) = sum(TempEnv(i,end-lastSec+1:end))/
152             lastSec;
153         staticHum(i) = sum(HumPlant(i,end-lastSec+1:end))/
154             lastSec;
155     end
156 end
157
158 %% -----> Dynamic analisys
159 function DynamicAnalisys(app)
160     Fs = 1/app.TimeintervalEditField_dynamic.Value;
161     if isfile('PMFC_Results.csv')
```

```
162         [t, ~, isense, vplant, Light, Temp, Hum] =  
            ReadFileResults(app, 'PMFC_Results.csv');  
163     else  
164         [t, ~, isense, vplant, Light, Temp, Hum] =  
            ReadFileResults(app, 'previous_results_dynamic.  
            csv');  
165         app.SavedLabel_dynamic.Text = '';  
166     end  
167  
168     if app.MethodDropDown_dynamic.Value == "FFT"  
169         % FFT  
170         transient = app.TransientEditField_dynamic.Value;  
171         [Iplant_mag, Iplant_ph, ~] = FFT(app, isense(  
            transient:end), Fs);  
172         [Vplant_mag, Vplant_ph, fx] = FFT(app, vplant(  
            transient:end), Fs);  
173  
174         Z = Vplant_mag./Iplant_mag;  
175         Zplant_ph = Vplant_ph - Iplant_ph;  
176         ShowResults_dynamic(app, t(transient:end), isense(  
            transient:end), vplant(transient:end), ...  
177             Light(transient:end), Temp(transient:end), Hum(  
                transient:end), fx, abs(Z));  
178     elseif app.MethodDropDown_dynamic.Value == "Welch"  
179         % Welch method with zero padding  
180         lwin = app.WindowLengthEditField_dynamic.Value;  
181         switch app.WindowDropDown_dynamic.Value  
182             case 'Blackman-Harris'  
183                 window_filter = window(  
                    @blackmanharris, lwin);  
184             case 'Flat top'  
185                 window_filter = window(@flattopwin,  
                    lwin);  
186             case 'Hamming'  
187                 window_filter = window(@hamming,  
                    lwin);  
188             case 'Hanning'  
189                 window_filter = window(@hann, lwin)  
190                 ;  
191         end  
192     end
```



```
191         nfft = lwin;
192         Noverlap = lwin*app.OverlapEditField_dynamic.Value
            /100;
193         [pvi, ~] = cpsd(vplant, isense, window_filter,
            Noverlap, nfft, Fs);
194         [pii, fx] = pwelch(isense, window_filter, Noverlap,
            nfft, Fs);
195         Z = pvi./pii;
196         ShowResults_wdynamic(app, t, isense, vplant, Light,
            Temp, Hum, fx, abs(Z));
197     end
198
199     if isfile('PMFC_Results.csv')
200         SaveResults_dynamic(app, fx, abs(Z));
201     end
202
203 end
204
205 %% -----> Start calibration
    procedure to communicate with Agilent multimeter
206 function calibAgilent(app)
207     %% Simulation parameters
208     t_sample = 1;
209     t_end_sim = app.NumberofpointEditField_calibration.
        Value * app.TimeintervalEditField_calibration.
        Value;
210     current = zeros(1,t_end_sim/t_sample);
211     voltage = zeros(1,t_end_sim/t_sample);
212     %% Instrument Connection
213
214     % Create a GPIB object.
215     interfaceObj = instrfind('Type', 'gpib', '
        BoardIndex', app.BoardindexEditField_calibration
        .Value, 'PrimaryAddress', app.
        PrimaryAddressEditField_calibration.Value, 'Tag'
        , '');
216
217     % Create the GPIB object if it does not exist
218     % otherwise use the object that was found.
219     if isempty(interfaceObj)
```

```

220         interfaceObj = gpib('KEYSIGHT', app.
                BoardindexEditField_calibration.Value, app.
                PrimaryAddressEditField_calibration.Value);
221     else
222         fclose(interfaceObj);
223         interfaceObj = interfaceObj(1);
224     end
225
226     % Create a device object.
227     deviceObj = icdevice('agilent_34401a.mdd',
                interfaceObj);
228
229     % Connect device object to hardware.
230     connect(deviceObj);
231
232     type = 'c';
233     %% ----- CURRENT MEASUREMENTS
234     if type == 'c'
235         set(deviceObj, 'MeasurementType', 'dcurrent');
236         set(deviceObj, 'Range', 'max');
237         disp('Now you can start the Raspberry Pi
                program – Current meas');
238         % ----- Reading
239         t = 0;
240         for i=1:t_sample:t_end_sim
241             t = t + t_sample;
242             % Configure property value(s).
243             set(deviceObj.Trigger(1), 'Source', '
                external');
244             set(deviceObj.Trigger(1), 'Delay', 0.0)
                ;
245             current(1,i)=str2double(invoker(
                deviceObj, 'measure'))*1e6;
246         end
247         % Disconnect device object from hardware.
248         disconnect(deviceObj);
249         % ----- Writing results
250         disp('Writing on file the results..please
                wait just a moment');

```

```
251         fileID = fopen('Agilent34401A_current.txt',
252                        'w');
253         fprintf(fileID, 'Current[uA]\n');
254         for i=1:t_sample:t_end_sim
255             fprintf(fileID, '%.3f\n', current(1,i));
256         end
257         fclose(fileID);
258     %% ----- VOLTAGE MEASUREMENTS
259
260     else
261         set(deviceObj, 'MeasurementType', 'dcvolts');
262         set(deviceObj, 'Range', 'max');
263         disp('Now you can start the Raspberry Pi
264              program – Voltage meas');
265         % ----- Reading
266         t = 0;
267         for i=1:t_sample:t_end_sim
268             t = t + t_sample;
269             % Configure property value(s).
270             set(deviceObj.Trigger(1), 'Source', '
271                external');
272             set(deviceObj.Trigger(1), 'Delay', 0.0)
273             ;
274             voltage(1,i)=str2double(invoker(
275                deviceObj, 'measure'))*1e6;
276         end
277         % Disconnect device object from hardware.
278         disconnect(deviceObj);
279         % ----- Writing results
280         disp('Writing on file the results..please
281              wait just a moment');
282         fileID = fopen('Agilent34401A_voltage.txt',
283                        'w');
284         fprintf(fileID, 'Voltage[uV]\n');
285         for i=1:t_sample:t_end_sim
286             fprintf(fileID, '%.3f\n', voltage(1,i));
287         end
288         fclose(fileID);
289     end
290 end
```

```
283     disp('You can read the results on the file');
284     disp('See you later ');
285 end
```

B.2 Raspberry Pi algorithm: main function

```
1  /*
2  * pmfc.c:
3  *   Program for characterization of the plant microbial fuel cell
4  *   Main board: Raspberry Pi 3 Model B
5  *   Add boards: High-Precision AD/DA Board – WaveShare
6  *               ADC: ADS1256
7  *               DAC: DAC8532
8  *               Library: bcm2835-1.45 (only this one works!)
9  *                       wiringPi
10 *               Electronic load for P-MFC
11 *
12 *   Alessandro Rizzo – 243924
13 *   DET – Politecnico di Torino
14 *   2018/12/11
15 */
16
17 // Libraries
18 #include <wiringPi.h>
19 #include <bcm2835.h>
20 #include <stdio.h>
21 #include <unistd.h>
22 #include <string.h>
23 #include <math.h>
24 #include <errno.h>
25 #include <sys/time.h>
26 #include <time.h>
27 #include <stdlib.h>
28 #include "ADDAlib.h"
29 #include "filesReadWrite.h"
30
31 int main()
32 {
33     // Library initialization
34     bcm2835_initialization();
35     wiringPi_initialization();
36
37     // Current profile
38     float t_sample = 0, t_end_sim = 0;
39     readCurrentProfile(&t_sample, &t_end_sim);
40     // Calibration parameters for adjustment
41     readCalibrationParameters();
42 }
```

```
43 // Simulation parameters
44 int N = t_end_sim/t_sample; // Number of samples
45 struct timeval t_start, t_stop;
46 float t_total = 0, t_loop = 0, elapsedTime = 0;
47 double_t sim_time[N];
48 // Isense
49 double Inom; //uA
50 double_t Ides[N], Isense[N], Rsense;
51 // Vplant
52 double_t Vplant[N];
53 // Temperature
54 double_t T[N];
55 // Humidity
56 double_t RH[N];
57 // Dark & Light intensity
58 int8_t DI[N], LI[N], LFS = 100; // LFS = Light Full-Scale
59 // DAC parameters
60 float V_DAC = 0;
61
62 // _____ ALGORITHM _____
63 Rsense = 100; // ohm
64 boardSetting();
65 ADCsetting();
66 ledOff();
67 int i = 0, meas = 0;
68
69 // DAC starts from V_DAC
70 V_DAC = 1.08; //V : voltage Vg to switch on the MOSFET
71 writeVg(V_DAC);
72
73 printf("\nSTART SIMULATION...\n");
74
75 do{
76     Inom = current_vector[i];
77     t_loop = 0;
78     do{
79
80         gettimeofday(&t_start, NULL); // Start timer
81
82         V_DAC = settingCurrentCorrection(Inom, V_DAC);
83         trigger();
84
85         // Measurements from ADC
86         for(int b = 1; b<9; b++)
87             measure();
88
89         // Desired current [uA]
90         Ides[meas] = Inom;
91         // Plant voltage [mV]
```

```

92     Vplant[meas] = voltage [pin_Vplant_ADC]*1e-6;
93     // Light intensity [%]
94     DI[meas] = voltage [pin_light_ADC]*1e-9/(2*Vref/PGA)*LFS;
95     LI[meas] = LFS-DI[meas];
96     // Temperature [ C ]
97     T[meas] = voltage [pin_Vt_ADC]*1e-6/10 - 1.2;
98     // Relative humidity [%]
99     RH[meas] = voltage [pin_Vh_ADC]*1e-6/(Vcc/PGA*1e3)*100;
100    // Isense [uA]
101    Isense [meas] = voltage [pin_Vsense_ADC]/Rsense*1e-3;
102    Isense [meas] = Isense [meas]*FC+Ioffset;
103    // Adjust the Vg in order to have the desired Vg
104    V_DAC = adjustVg ( Isense [meas] , Inom , V_DAC );
105
106    gettimeofday(&t_stop , NULL);           // Stop timer
107    elapsedTime = (t_stop.tv_sec-t_start.tv_sec); //s
108    elapsedTime += (t_stop.tv_usec-t_start.tv_usec)/1e6; //s
109
110    do{
111        gettimeofday(&t_stop , NULL);           // Stop timer
112        elapsedTime = (t_stop.tv_sec-t_start.tv_sec); //s
113        elapsedTime += (t_stop.tv_usec-t_start.tv_usec)/1e6; //s
114    }while (elapsedTime < t_sample);           // Repeat if this is
true
115
116    t_loop += elapsedTime;
117
118    gettimeofday(&t_start , NULL);           // Start timer
119
120    //————— Results
121    printOnScreen ( Ides [meas] , Isense [meas] , Vplant [meas] , LI [meas] , T
[meas] , RH[meas] );
122
123    gettimeofday(&t_stop , NULL);           // Stop timer
124    elapsedTime = (t_stop.tv_sec-t_start.tv_sec); // s
125    elapsedTime += (t_stop.tv_usec-t_start.tv_usec)/1e6; //us→s
126    t_total +=t_loop+elapsedTime;
127    t_total = floor(t_total);
128    sim_time[meas] = t_total;
129    t_loop = 0;
130
131    meas++;
132
133    }while (t_total < time_vector [i+1]);
134
135    i++;
136
137    }while (current_vector [i] != 0);
138    printf ("SIMULATION COMPLETE!\n\n");

```

```
139     printf("Wait the copy of the results on the file...\n");
140
141     writeResultsOnFile(N, sim_time, Ides, Isense, Vplant, LI, T, RH);
142
143     printf("WRITING COMPLETE!\n\n");
144
145     ledOn();
146
147     // Closing SPI and library
148     bcm2835_spi_end();
149     bcm2835_close();
150
151     printf("END PROGRAM! BYE BYE!\n");
152
153     return 0;
154 }
```


Bibliography

- [1] K. Ashton, "That 'Internet of Things' Thing", RFID Journal, <https://www.rfidjournal.com/articles/view?4986>, Jun. 2009.
- [2] M. Alioto, *Enabling the Internet of Thing - From Integrated Circuits to Integrated Systems*, Springer, Italy, 2017.
- [3] dr.ir. DPBTB Strik David. <https://www.wur.nl/en/show/Plants-create-energy.htm>. Wageningen university.
- [4] R.A. Timmers, D.P.B.T.B. Strik, H.V.M. Hamelers, C.J.N. Buisman, "Characterization of the internal resistance of a plant microbial fuel cell", *Electrochimica Acta*, Apr 2012.
- [5] G. Daga, "Plant microbial fuel cell: research, analysis and design proposal for future application", MSc thesis, Dipartimento di Architettura e Design, Politecnico di Torino, Turin, Italy, Sep 2017.
- [6] D.P.B.T.B. Strik, H.V.M. Hamelers, J.F.H. Snel and C.J.N. Buisman, "Green electricity production with living plants and bacteria in a fuel cell", *International Journal of Energy Research*, Jan 2008.
- [7] Senseable City Laboratory, "Treepedia", <http://senseable.mit.edu/treepedia>, Massachusetts Avenue Cambridge, Ma, USA.
- [8] CalFire, "Fire statistics", .
- [9] Wageningen University, "Spin-off: Electricity from living plants", <https://www.wur.nl/en/newsarticle/Spin-off-Electricity-from-living-plants-.htm>, Wageningen University and Research, May 2017.
- [10] Wageningen University, "A living, breathing building", <https://nioo.knaw.nl/en/about-nioo/living-breathing-building>, Wageningen University and Research.
- [11] M. Helder, "Design criteria for the Plant-Microbial Fuel Cell: Electricity generation with living plants – from lab to application", PhD thesis, Wageningen University, Wageningen, The Netherlands (2012).
- [12] L. Rosén, S. Samimi, "Small Electronic Load: Design and analysis of a small electronic load for testing on-board DC/DC converters", MSc thesis, Chalmers University Of Technology, Sweden, 2012.
- [13] A. Bouaicha, H. Allegui, A. Rouane, E.H. Aglzim, A. Mami, "Design and

- Realization of an Electronic Load for a PEM Fuel Cell", World Academy of Science, Engineering and Technology International Journal of Electronics and Communication Engineering Vol:8, No:1, 2014.
- [14] R. Piyare, A.L. Murphy, P. Tosato, D. Brunelli, "Plug into a Plant: Using a Plant Microbial Fuel Cell and a Wake-Up Radio for an Energy Neutral Sensing System", ResearchGate, Oct 2017.
 - [15] M. Rossi, P. Tosato, L. Gemma, L. Torquati, C. Catania, S. Camalò, D. Brunelli, "Long range wireless sensing powered by plant-microbial fuel cell", IEEE, 2017.
 - [16] N. Degrenne, "Power Management for Microbial Fuel Cells", Biotechnology, Ecole Centrale de Lyon, 2012, English. <tel-00757996>.
 - [17] T. Esram ; P.L. Chapman, "Comparison of Photovoltaic Array Maximum Power Point Tracking Techniques", IEEE Transactions on Energy Conversion, Vol. 22, Issue 2, Jun 2007.
 - [18] J. Sankman, D. Ma, "A 12 μ W to 1.1 mW AIM Piezoelectric Energy Harvester for Time-Varying Vibrations With 450 nA I_Q ", IEEE Transactions on Power Electronics, Vol. 30, Issue 2, Feb 2015.
 - [19] A. Kadier, Y. Simayi, P. Abdesahian, N.F. Azman, K. Chandrasekhar, M.S. Kalil, "A comprehensive review of microbial electrolysis cells (MEC) reactor designs and configurations for sustainable hydrogen gas production", Alexandria Engineering Journal (2016) 55, 427–443.
 - [20] "3D Micro and Nano Technologies for Improvements in Electrochemical Power Devices".
 - [21] J. Ran, L. Wu, Y. He, Z. Yang, Y. Wang, C. Jiang, L. Ge, E. Bakangura, T. Xu, "Ion exchangemembranes: New developments and applications", Journal of Membrane Science 522 (2017) 267–291.
 - [22] D.P.B.T.B. Strik, R.A. Timmers, M. Helder, K.J.J. Steinbusch, H.V.M. Hamelers, C.J.N. Buisman, "Microbial solar cells: applying photosynthetic and electrochemically active organisms", Trends in Biotechnology January 2011, Vol. 29, No. 1.
 - [23] F. Fischer, "Photoelectrode, photovoltaic and photosynthetic microbial fuel cells", Renewable and Sustainable Energy Reviews 90 (2018) 16–27.
 - [24] R. Nitisoravut, R. Regmi, "Plant microbial fuel cells: A promising biosystems engineering", Renewable and Sustainable Energy Reviews 76 (2017) 81–89.
 - [25] Y. Kuzyakov, "Priming effects: Interactions between living and dead organic matter", Soil Biology & Biochemistry 42 (2010) 1363–1371.
 - [26] R.A. Timmers, M. Rothballer, D.P.B.T.B. Strik, M. Engel, S. Schulz, M. Schlöter, A. Hartmann, B. Hamelers, C. Buisman, "Microbial community structure elucidates performance of *Glyceria maxima* plant microbial fuel cell", Appl Microbiol Biotechnol (2012) 94:537–548.

- [27] B.R. Maricle, R.W. Lee, "Aerenchyma development and oxygen transport in the estuarine cordgrasses *Spartina alterniflora* and *S. anglica*" *Aquatic Botany*, 2002;74(2):109-20.
- [28] R.A. Rozendal, H.V.M. Hamelers, K. Rabaey, J. Keller, C.J.N. Buisman, "Towards practical implementation of bioelectrochemical wastewater treatment", *Trends in Biotechnology*, Sep 2008.
- [29] J. Larminie, A. Dicks, "Fuel cell systems explained", JohnWiley Sons, 2nd edition, 2003.
- [30] A. Larrosa-Guerrero, K. Scott, I. Head, F. Mateo, A. Ginesta, C. Godinez, "Effect of temperature on the performance of microbial fuel cells", *Fuel*, 89(June):3985–3994, 2010.
- [31] H.N. Hayhoe, D. Balchin, "Time-domain reflectometry and electrical conductance measurements during seasonal soil frost", *Cold Regions Science and Technology* 1988;15:195.
- [32] L.C. Lundin, H. Johnsson, "Ion dynamics of a freezing soil monitored in situ by time domain reflectometry", *Water Resources Research* 1994;30:3471.
- [33] R. Regmi, R. Nitorisavut, J. Ketchaimongkol, "A decade of plant-assisted microbial fuel cells: looking back and moving forward", *Biofuels*, 9:5, 605-612, 2018.
- [34] Y. Ahn, F. Zhang, B.E. Logan, "Air humidity and water pressure effects on the performance of air-cathode microbial fuel cell cathodes", *J Power source*, 247:665-659, 2014.
- [35] F. Harnisch, U. Schröder, "From MFC to MXC: Chemical and biological cathodes and their potential for microbial bioelectrochemical systems", *Chemical Society Reviews* 2010, 39:4433-4448.
- [36] S. Kerzenmacher, K. Mutschler, U. Kräling, H. Baumer, J. Ducrée, R. Zengerle, F. Stetten, "A complete testing environment for the automated parallel performance characterization of biofuel cells: design, validation, and application", *Journal of Applied Electrochemistry*, 39(9):1477–1485, 2009.
- [37] P.S. Bonanni, G.D. Schrott, L. Robuschi, J.P. Busalmen, "Charge accumulation and electron transfer kinetics in *Geobacter sulfurreducens* biofilms", *Energy Environmental Science*, 5(3):6188, 2012.
- [38] Gamry Instruments, "Basics of Electrochemical Impedance Spectroscopy", Application note, 734 Louis Drive, Warminster PA 18974, www.gamry.com.
- [39] A.P. Borole, D. Aaron, C.Y. Hamilton, C. Tsouris, "Understanding Long-Term Changes in Microbial Fuel Cell Performance Using Electrochemical Impedance Spectroscopy", *Environ. Sci. Technol.* 2010, 44, 2740–2745.
- [40] N. Sekar and R.P. Ramasamy, "Electrochemical Impedance Spectroscopy for Microbial Fuel Cell Characterization", *Microbial & Biochemical Technology* 2013, S6.

- [41] A.K. Manohar, O. Bretschger, K.H. Neelson, F. Mansfeld, "The use of electrochemical impedance spectroscopy (EIS) in the evaluation of the electrochemical properties of a microbial fuel cell", *Bioelectrochemistry* 72 (2008) 149–154.
- [42] H. Piret, P. Granjon, V. Cattin, N. Guillet, "Online Estimation of Electrical Impedance", 7th International Workshop on Impedance Spectroscopy (IWIS 2014), Sep 2014, Chemnitz, Germany, 2014.
- [43] P.-D. Welch, "The use of fast fourier transform for the estimation of power spectra: a method based on time averaging over short, modified periodograms," *IEEE Trans. on Audio Electroacoustics*, Vol. AU-15, pp. 70–73, 1967.
- [44] Raspberry Pi, "Raspberry Pi Compute Module", Raspberry Pi board datasheet, Oct. 2016 [Revised Jun 2018].
- [45] Texas Instruments, "ADS1256 - Very Low Noise, 24-Bit Analog-to-Digital Converter", SBAS288D. Jun 2003. Rev. Aug 2004. Copyright 20032004, Texas Instruments Incorporated.
- [46] Texas Instruments, "DAC8532 - Dual Channel, Low Power, 16-Bit, Serial Input Digital-to-Analog Converter", SBAS246A. Dec 2001. Rev. May 2003. Copyright 20012003, Texas Instruments Incorporated
- [47] Raspberry Pi High-Precision AD/DA Expansion Board. <https://www.waveshare.com/High-Precision-AD-DA-Board.htm>. WaveShare.
- [48] Motorola, "LM285 - Micropower Voltage Reference Diodes". LM285/D. 1996 Rev. 2. Motorola, Inc.
- [49] Semiconductor Components Industries, "BS170 - Small Signal MOSFET 500 mA, 60 Volts". BS170/D. Rev 7 - Nov 2017. Semiconductor Components Industries, LLC, 2011.
- [50] Adafruit, "DHT11, DHT22 and AM2302 Sensors". Adafruit.
- [51] Texas Instruments, "LMx35, LMx35A Precision Temperature Sensors". SNIS160E. Rev. Feb 2015. 1999–2017, Texas Instruments Incorporated
- [52] Texas Instruments, "LM35 Precision Centigrade Temperature Sensors". SNIS159H. Rev. Dec 2017. 1999–2017, Texas Instruments Incorporated
- [53] Broadcom Corporation, "BCM2835 ARM Peripherals", BCM2835 manual, Feb. 2012.
- [54] Rigol Technologies, "DP800 Series Programmable Linear DC Power Supply - Rigol User's Guide". UGH04109-1110. 2014. 2012 RIGOL TECHNOLOGIES, INC
- [55] Keysight Technologies, "Agilent 34401A 6½ Digit Multimeter". 34401-90004. Edition 10, Aug 2014. 1991-2014, Keysight Technologies, 1400 Fountaingrove Parkway, Santa Rosa, CA 95403
- [56] Keysight Technologies, "GPIB, USB and Instrument Control for Easy PC-to-Instrument Connections". 5989-1889EN. Dec 2017. Keysight Technologies, 2011 - 2017.

- [57] "Carbiso M, recycled carbon fiber - nonwoven mats". Rev. 3. ELG Carbon Fibre Ltd. Cannon Business Park, Gough Road, Coseley, West Midlands
- [58] UT33D manual, https://www.tme.eu/html/IT/multimetri-universali-uni-t-serie-ut33/ramka_10187_IT_pelny.html. UNI-T.
- [59] Plant-e Spark of nature, "Sprout 'n Spark", <https://www.plant-e.com/en/product/sprout-n-spark/>, Wageningen, Holland.
- [60] Prokit's Industries Co., "Pro'skit MT-1132 3-1/2 digital multimeter", user's manual, 1st edition 2012.